The role of dynamic interfacial phenomena in marine crude oil spill dispersion

A DISSERTATION
SUBMITTED TO THE FACULTY OF THE
UNIVERSITY OF MINNESOTA
BY

David Riehm

IN PARTIAL FULFILLMENT OF THE REQUIREMENTS
FOR THE DEGREE OF
DOCTOR OF PHILOSOPHY

Alon McCormick, Advisor

December 2016

Acknowledgements

I would like to acknowledge the support and guidance of my advisor, Alon McCormick, as well as support from Han Seung Lee, my immediate predecessor in the McCormick group. Thanks are also due to Profs. Joe Zasadzinski and David Morse of CEMS for their helpful scholarly feedback, and to Wieslaw Suszynski (CPFP director), Chris Frethem (CharFac staff), and Bob Hafner (CharFac staff) for getting me access to and training on all of the equipment I have needed. I am grateful for financial support from the Nanostructured Materials and Processes (NMP) program of UMN IPRIME, as well as from the Sebastian C. Reyes Fellowship.

I am also grateful for two grants from the Gulf of Mexico Research Initiative in support of our work: First, through the Consortium for the Molecular Engineering of Dispersant Systems (C-MEDS) headed by Prof. Vijay John (Tulane), and second, to study "Molecular Engineering of Food-Grade Dispersants as Highly Efficient and Safe Materials for the Treatment of Oil Spills" through Prof. Srinivasa Raghavan at the University of Maryland. Discussions with GoMRI collaborators, including Vijay John, Srinivasa Raghavan, Geoff Bothun, Lynn Walker, Shelley Anna, and Ron Larsen, have been invaluable.

Finally, my undergraduate assistants David Rokke, Prakash Paul, Brent Vizanko, and Sarah Downey have made indispensable contributions to my work over the past 2-3 years, with support from the UMN Undergraduate Research Opportunities Program (UROP). Without them as collaborators, and without the love and support of my family and friends, I likely would not be where I am today.

Dedication

This thesis is dedicated to

My parents, Stephen and Mary, without whom I could not have started

And my someone, Adriana, without whom I could not have finished

Thank you

Abstract

Marine oil spill dispersants containing the surfactants Tween 80, Span 80, and dioctyl sodium sulfosuccinate (DOSS) have been widely used for decades, but their environmental impact remains controversial. The interfacial science behind their formulation has been studied in this work in order to develop new, equally effective dispersants using nontoxic components.

The effectiveness of dispersants containing different Tween 80-Span 80-DOSS (T-S-D) blends was measured using a Stirred Flask Test and correlated with the dynamic oil-water interfacial tension (IFT) produced by each dispersant (Chapter 3). Very low IFT ($<10^{-4}$ mN/m) was produced by both DOSS-rich dispersants and Span 80-rich dispersants, but DOSS-rich dispersants were significantly more effective and adsorbed to the oil-water interface faster than Span 80-rich dispersants. In order to investigate whether T-S-D dispersants form water-in-oil microstructures which influence dispersants' interfacial adsorption rates, T-S-D blends were added to a transparent, low-viscosity model crude oil and studied using cryo-transmission electron microscopy and dynamic light scattering (Chapter 4). T-S-D blends formed spherical water-in-oil microstructures in the oil, and the microstructures formed by DOSS-rich T-S-D blends were much smaller than those formed by Span 80-rich T-S-D blends. This may explain why DOSS-rich T-S-D blends adsorb to the interface faster, and thus are more effective, than Span 80-rich T-S-D blends.

Blends of Tween 80 and lecithin (L), a biosurfactant which also forms water-in-oil microstructures, were investigated as a substitute for T-S-D dispersants (Chapter 5). The most effective L-T dispersants performed comparably to the most effective T-S-D dispersants in the Baffled Flask dispersant effectiveness test. However, lecithin-rich L-T dispersants were significantly more effective than Tween 80-rich L-T dispersants which produced lower or comparable IFT, even though interfacial adsorption rates of L-T dispersants did not vary as a function of lecithin:Tween 80 ratio. This suggests that interfacial phenomena other than dynamic IFT influence L-T dispersants' effectiveness. The interface between seawater and crude oil treated with L-T dispersants was therefore studied using light microscopy, cryogenic scanning electron microscopy, and droplet

coalescence tests (Chapter 6). Tween 80-rich L-T dispersants caused oil-into-water spontaneous emulsification, indicating rapid dispersant leaching from oil into water. This may explain why Tween 80-rich L-T dispersants are less effective than lecithin-rich L-T dispersants which produce similar IFTs. Conversely, lecithin-rich L-T dispersants exhibited water-into-oil emulsification, indicating that such surfactant blends are stable in the oil and perhaps explaining why some lecithin-rich L-T dispersants are as effective as T-S-D dispersants which produce much lower IFT. Possible mechanisms for the spontaneous emulsification induced by L-T dispersants are discussed, based on images of the spontaneously emulsifying L-T dispersant-treated oil-water interfaces.

Table of Contents

List of Tables

List of Figures

Chapter 1. Introduction

1.1 Motivation

In April 2010, the Deepwater Horizon drilling rig exploded and sank in the Gulf of Mexico, causing a three-month subsea oil blowout which ultimately released 150 million gallons of crude oil into the ocean (see Figure 1.1). As part of efforts to mitigate the spill's environmental impact, 1.8 million gallons of the marine oil dispersant Corexit 9500 were applied to surface slicks and to the oil geyser at the sea floor.[9] While this was by far the largest application of dispersants to an oil spill in history, it was unfortunately neither the first nor the last. From 1968-2007, marine oil spill dispersants were applied to 213 oil spills worldwide—an average of one spill every two to three months, with a median spill volume of ~150,000 gallons (equivalent to a moderately-sized backyard pool).[4] Moreover, as of 2013, more than 1 million gallons of oil dispersants have been stockpiled worldwide[10], for application to the spills of tomorrow.

Figure 1.1 The Deepwater Horizon surface slick on May 24, 2010. NASA analysis of this image estimates the slick's volume at 2-10% of the total volume of oil discharged during the blowout.[4] Image credit: NASA

The development of specialized dispersants for oil slicks first began in the early 1970s, in the wake of the disastrous *Torrey Canyon* spill in 1968 off the coast of the U.K.[11] 10,000 tons of toxic industrial detergents were applied to disperse the spill, thoroughly poisoning that coastal ecosystem. In response to this catastrophe, oil companies began developing more concentrated and less toxic dispersants to apply to future spills, which eventually gave rise to the proprietary formulations (Corexit, Finasol, Dasic, etc.) commonly applied to spills around the world today. Many authors[11-14] assert that modern dispersants' toxicity is no longer an issue, as numerous studies[14-18] have found modern oil dispersants to be considerably less toxic than dispersed crude oil, and

they are applied to spills at relatively low dispersant:oil ratios (typically 1:20 to 1:100)[11]. Others,[15, 16, 19] however, express concern at introducing any oil dispersant which is not completely nontoxic into the environment. It is therefore important to develop an understanding of why existing dispersants are effective, in order to develop new, equally effective dispersants using entirely nontoxic components.

Unfortunately, despite their widespread use, the proprietary nature of oil dispersants' development and composition means that there is little published work on the interfacial science underlying their formulation and action. It is generally understood[4] that dispersants are mixtures of surfactants and solvents which are applied to marine oil slicks in order to lower their oil-water interfacial tension (IFT), enabling waves or other

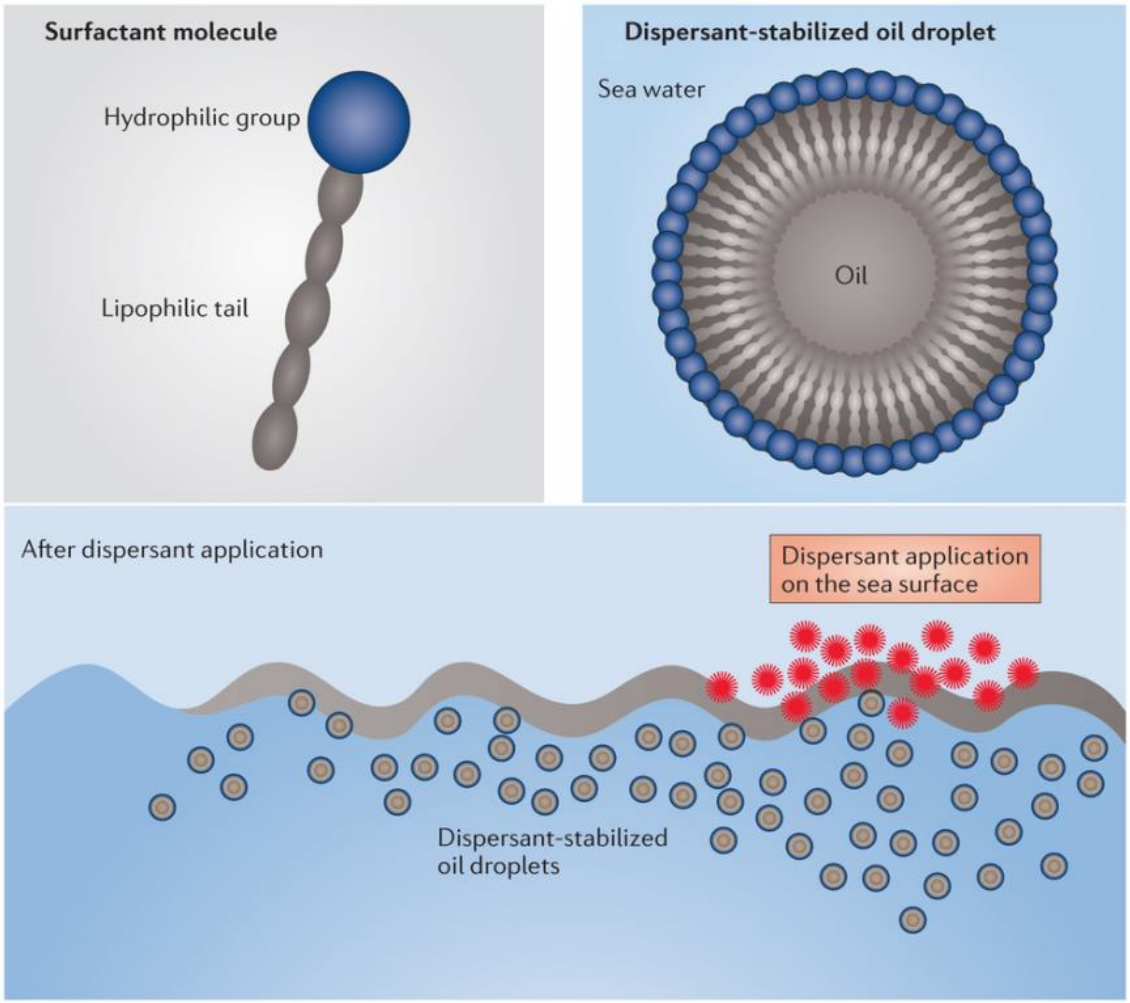

Figure 1.2 Schematic of dispersant application to a marine crude oil spill and subsequent dispersion of crude oil into seawater by waves.
Image adapted with permission from Kleindienst et al.[7]

turbulence to emulsify the oil into the water (see Figure 1.2). To date, however, most published work on dispersants consists of empirical oil dispersion tests: A dispersant is agitated together with crude oil and seawater in a flask according to a reproducible protocol, and then the fraction of the oil dispersed into the seawater at the end of the test is reported as the dispersant's "effectiveness". Moreover, due to the proprietary nature of most dispersants, only a few authors[3, 23] report the compositions of the dispersants which they evaluate. To the best of our knowledge, no prior work has developed explanations for observed compositional trends in effectiveness by correlating them with more fundamental data, such as the dynamic IFT or water-in-oil microstructures produced by different dispersants.

1.2 Thesis Outline

Chapter 2 is an overview of the surfactants and experimental techniques employed in this work. Chapters 3 and 4 focus on dispersants containing blends of Tween 80, Span 80, and dioctyl sodium sulfosuccinate (DOSS), three surfactants commonly used in modern oil dispersants such as Corexit.[24] Chapter 3 relates compositional trends in crude oil-seawater dynamic IFT produced by these dispersants to compositional trends in their effectiveness. It has largely been adapted from the publication

> Riehm, D.; McCormick, A. The role of dispersants' dynamic interfacial tension in effective crude oil spill dispersion. *Mar Poll Bull* **2014**, 84, 155-163.

Chapter 4 characterizes water-in-oil microstructures formed by these dispersants in a model crude oil, and relates them to the dynamic IFT and effectiveness data from Chapter 3. It has largely been adapted from the publication

> Riehm, D.; Rokke, D.; McCormick, A. Water-in-oil microstructures formed by marine oil dispersants in a model crude oil. *Langmuir* **2016**, 32, 3952-3962.

Chapters 5 and 6 focus on dispersants which are composed of blends of the nontoxic surfactants lecithin and Tween 80. Chapter 5 compares the effectiveness and IFT of lecithin-Tween 80 dispersants with that of Tween 80-Span 80-DOSS dispersants. It has been adapted in part from the publication

Riehm, D.; Neilsen, J.; Bothun, G.; John, V.; Raghavan, S.; McCormick, A. Efficient Dispersion of Crude Oil by Blends of Food-Grade Surfactants: Toward Greener Oil-Spill Treatments. *Mar Poll Bull* **2015**, 101, 92-97.

Chapter 6 reveals the spontaneous emulsification caused by lecithin-Tween 80 dispersants at crude oil-seawater interfaces, and relates it to the effectiveness and IFT data (for lecithin-Tween 80 dispersants) discussed in Chapter 5. It has largely been adapted from the publication

Riehm, D; Rokke, D.; Paul, P.; Vizanko, B.; Lee, H; McCormick, A. Dispersion of oil into water using lecithin-Tween 80 blends: The role of spontaneous emulsification. *J Colloid Interface Sci* **2017**, 487, 52-59.

Finally, Chapter 7 lays out possible directions for future work.

Chapter 2: Background and Methodology

2.1 Dispersant Components

Surfactants are molecules with both hydrophilic ("water-loving") and hydrophobic ("water-hating") moieties. When dissolved in oil-water systems, surfactants accumulate at oil-water interfaces and prevent water and oil from coming into direct contact. This lowers oil-water interfacial tension (IFT), a force which resists stretching and expansion of the interface, and facilitates emulsification of oil into water or vice versa. Surfactants can also self-assemble within bulk oil or water to form various microstructures, which in turn can swell with water (in oil) or with oil (in water) to form "water-in-oil" (W/O) or "oil-in-water" (O/W) microstructures (Figure 2.1).

Dispersants are composed of blends of surfactants in one or more solvents. The solvents' role is (a) to solubilize hydrophilic and hydrophobic surfactants into a single phase with sufficiently low viscosity (<100 cSt) to be sprayed onto a marine oil slick, and

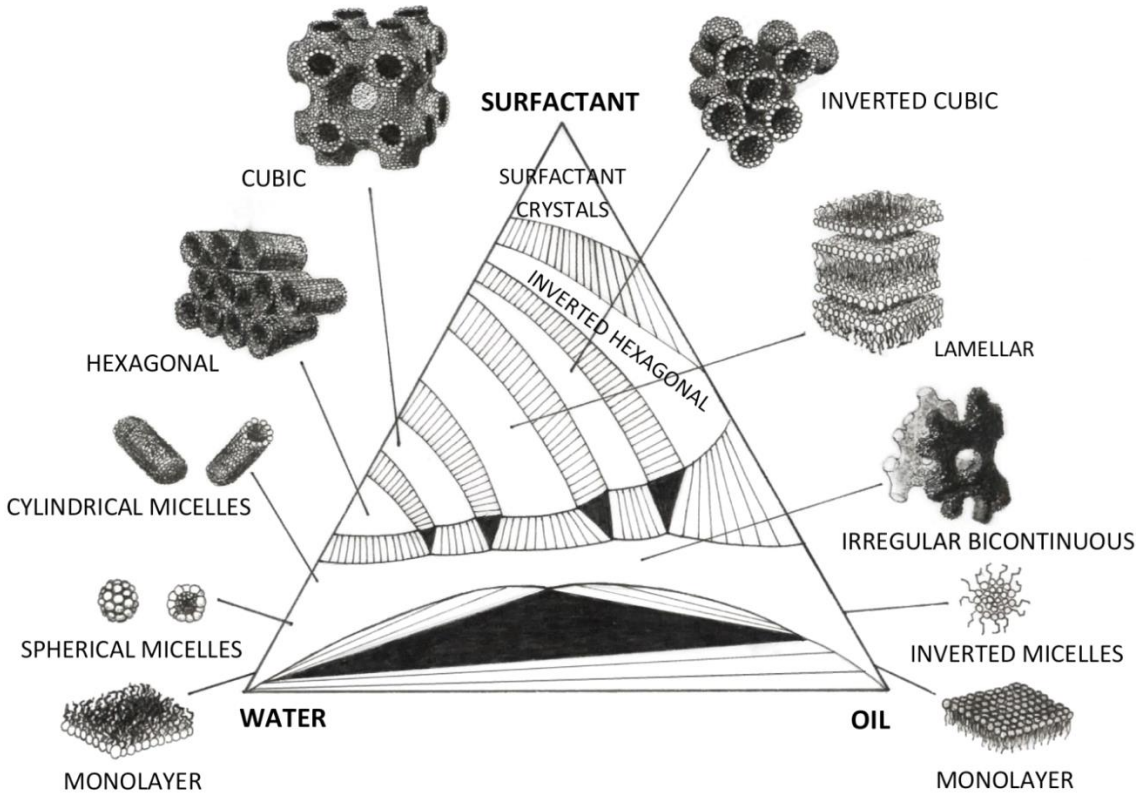

Figure 2.1 Generic surfactant-oil-water ternary diagram of the microstructural morphologies which surfactants typically take on at various surfactant:oil:water ratios.
Image adapted with permission from J. Bellare.[2]

(b) to solubilize these surfactants into the crude oil slick upon dispersant-oil contact. Most commonly, a mixture of dearomatized kerosenes (light petroleum distillates with relatively low toxicity, such as Isopar M or Exxsol D80) and glycol ethers (e.g. propylene glycol) is employed.

A wide variety of surface-active materials have been evaluated for use in dispersants, including small-molecule surfactants,[11, 13, 24] biomolecules,[25, 26] nanoparticles,[27-29] and block copolymers.[30] However, dispersants composed of readily available small-molecule surfactants produced in industrial quantities dominate the market.[11, 24] In particular, the surfactants Tween 80 (polyoxyethylenated sorbitan monooleate), Span 80 (sorbitan monooleate) and DOSS (dioctyl sodium sulfosuccinate) are used in numerous dispersants around the world, [11, 13, 31] including the Corexit family of dispersants, which dominate the dispersant market in the United States.[32]

The high dispersion effectiveness of blends of Tween 80, Span 80, and DOSS has been well-established in prior work.[3, 23] Additionally, Tween 80 (EC_{50} > 100 mg/L, *Daphnia magna* (96 h))[33] and Span 80 (LC_{50} > water solubility limit, *Salmo gairdneri* (96 h))[34] are desirable in environmental applications for their exceptionally low toxicity. Unfortunately, DOSS does exhibit some marine toxicity (Maggi and Cossa[35] found 96-hr LC_{50} values ranging from 3 to >100 mg/L for 13 different marine organisms). However, DOSS is also well-known to be capable of forming reverse micelles without a cosurfactant, above a critical micelle concentration of ~1 mM, in a wide range of hydrophobic solvents,[36-38] and readily incorporates nonionic surfactants, including Tween 80 and Span 80, into its reverse micelles.[39] In this way, therefore, DOSS is potentially capable of solubilizing a blend of surfactants containing various hydrophilic moieties into a hydrophobic medium, such as a dispersant solvent or a crude oil slick.

In recent years (and concurrently with much of the work in this thesis), lecithin (phosphatidtylcholine) has attracted interest as a possible substitute for DOSS in marine oil dispersants.[40-42] Lecithin is a biosurfactant and nutrient which is typically refined from soy or eggs (20-25 wt% of a solid/dry egg yolk is composed of lecithin)[43] and is used extensively in food and pharmaceutical products. Lecithin is also well known to form water-in-oil microstructures both on its own[44, 45] and with other surfactants.[46, 47]

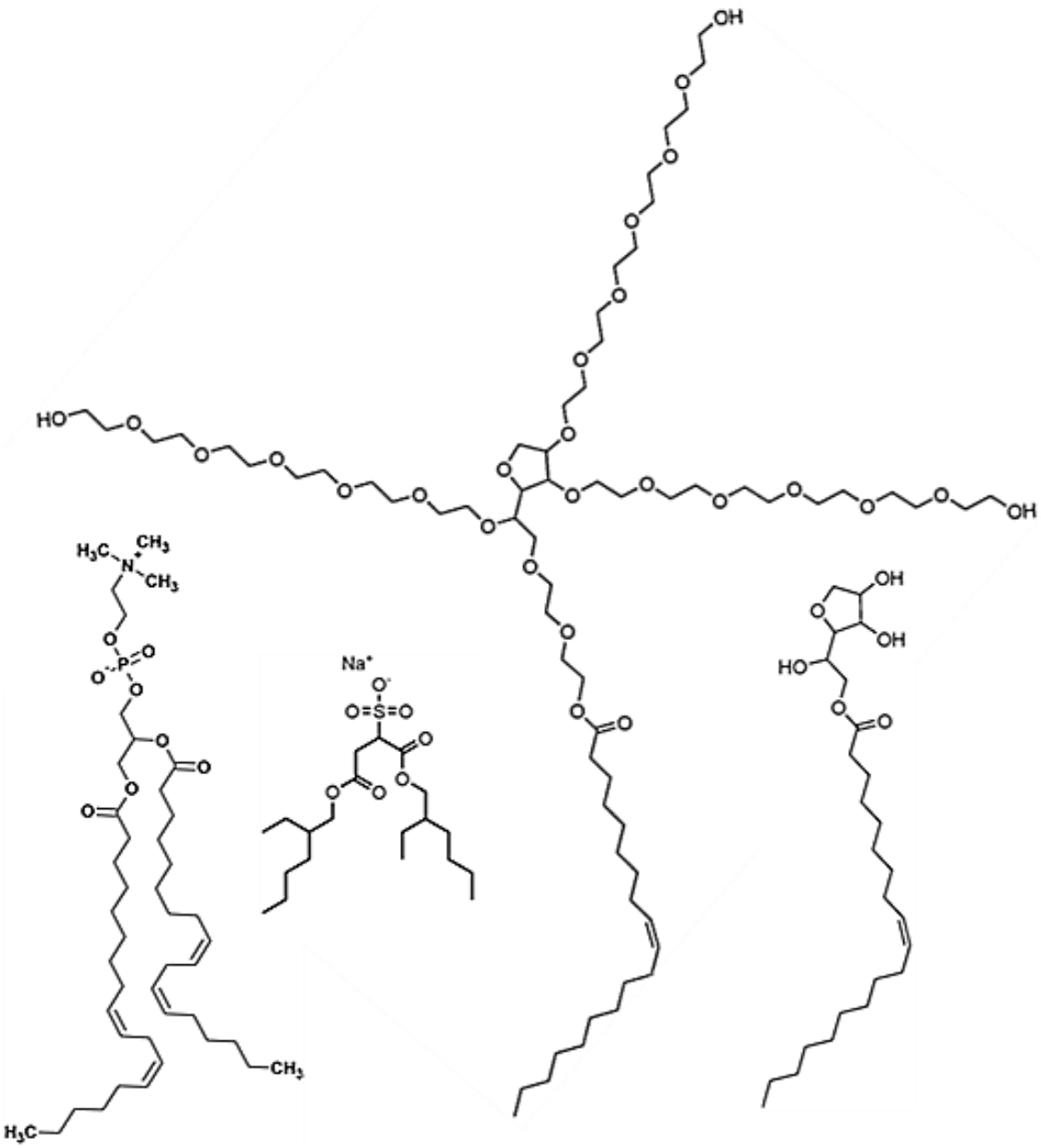

Figure 2.2 From left to right, the surfactants lecithin; DOSS; Tween 80; and Span 80, to scale. Surfactants' hydrophilic moieties are at the top and their hydrophobic moieties are at the bottom.

2.2 Dispersant Effectiveness Testing

Numerous tests for dispersant effectiveness, with a variety of mixing energies and total dispersion volumes, have been developed.[48] Typically, initial screening of new dispersant formulations is conducted using a bench-scale agitation protocol in a flask, at a total oil-water dispersion volume of ~0.1 L.[49, 50] Successful formulations are then tested in larger wave tanks, such as the 11,000 L wave tank operated by SL Ross Environmental Research Ltd.,[51, 52] or the 10,000,000 L wave tank at the National Oil Spill Response Research & Renewable Energy Test Facility (OHMSETT),[53] before being subjected to sea trials. Our work, however, has exclusively employed bench-scale tests.

In our early work,[54] dispersant effectiveness was measured using a modified version of the Swirling Flask test, dubbed the "Stirred Flask Test". The Swirling Flask test was originally developed by Fingas et al[49] and is currently the standard testing protocol used by the U.S. EPA to determine whether a dispersant is "effective" enough for use in U.S. territorial waters.[55] In the "Stirred Flask Test", we scaled down the volumes of oil and water involved in the procedure, and replaced the shake table with a stir bar in order to increase the mixing energy imparted to the dispersant-treated oil. In brief, the Stirred Flask test involves (1) filling a 50 mL Erlenmeyer flask with 50 mL seawater and stirring it at 140 RPM; (2) premixing crude oil and dispersant at a dispersant:oil volume ratio of 1:20, then adding 105 μL of this oil:dispersant mixture to the surface of the swirling salt water; (3) allowing the oil to disperse for 20 minutes, then ceasing to stir the flask so that the oil could settle for 5 minutes; and finally (4) extracting the remaining, dispersed oil from a sample of the dispersion using dichloromethane, and employing spectrophotometry to quantify the extracted oil. A more detailed description of the test methodology is found in Chapter 3.

The Baffled Flask Test was developed by Sorial et al[50], and improves on the original Swirling Flask test by imparting a much higher and more uniform mixing energy to the oil-water dispersion without resorting to a stirbar, as in the Stirred Flask test. This is accomplished in part by increasing the shake table speed to 200 RPM, from 140 RPM in the Swirling and Stirred Flask tests, and in part by using a much larger flask (250-300 mL total volume) with ½"-deep baffles in it., This larger flask is only 40-50% full during

the test, which allows a much larger, deeper standing wave to form than the 80-90% full flask in the Swirling Flask test does. All of this allows for far more vertical turbulence, uniform mixing, and reproducibility in the Baffled Flask test than in the original Swirling Flask test,[50] which is why the EPA plans to make the Baffled Flask test their official effectiveness test in the near future.

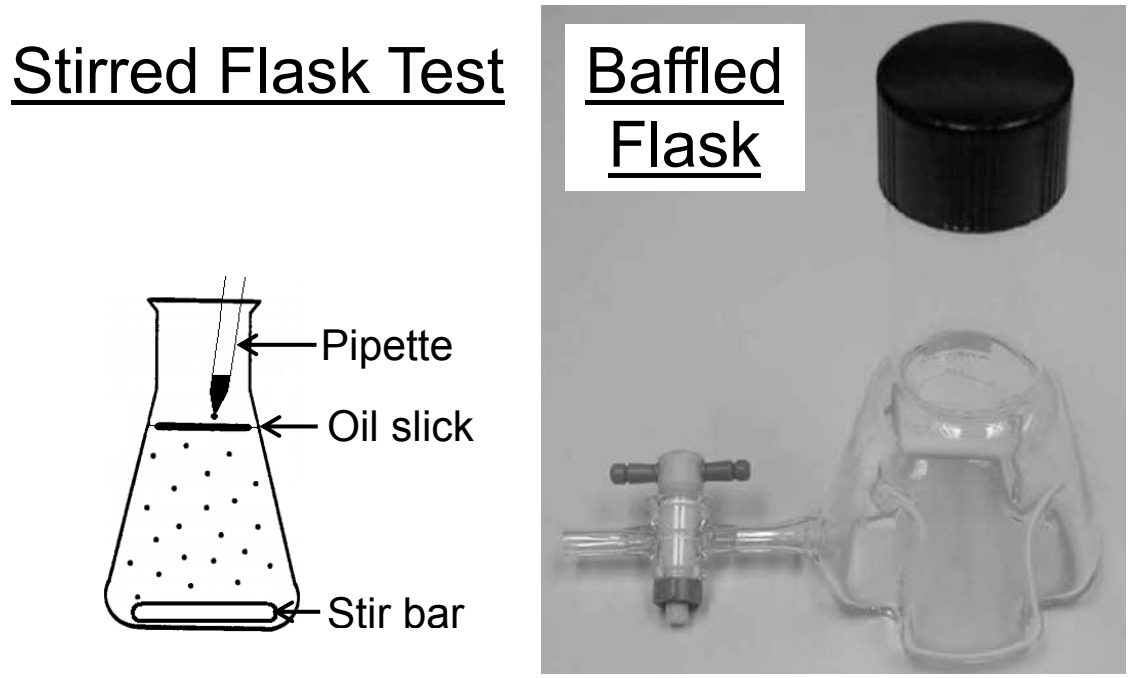

Figure 2.3 (Left) Schematic of Stirred Flask Test in a 50 mL Erlenmeyer flask.
(Right) Schematic of a 150 mL Wheaton baffled trypsinizing flask used in the Baffled Flask test, modified with a stopcock at its base for sample withdrawal.
Flasks are depicted approximately to scale.

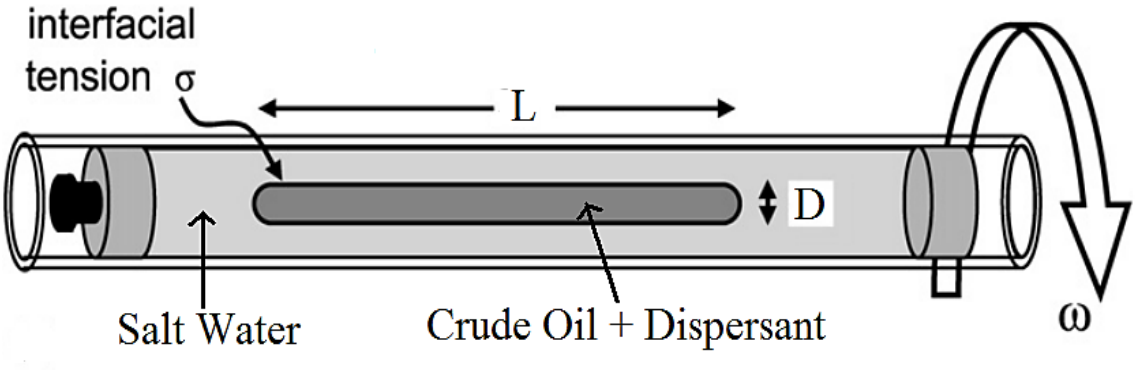

Figure 2.4 Schematic of spinning drop tensiometer, showing a droplet of dispersant-crude oil mixture suspended in a tube filled with seawater. The tube is plugged at both ends and spun about its longitudinal axis at angular velocity ω. Using the length L and diameter D of the droplet, the density difference between the dispersant-oil mixture and seawater, and ω, it is possible to calculate[5] the oil-water interfacial tension σ. Image adapted with permission from Martin and Velankar.[8]

2.3 Spinning Drop Tensiometry

As discussed in Chapter 1, despite clear importance of dynamic interfacial tension in the effective dispersion of marine oil spills, only one prior publication, by Brochu et al.[3], has studied oil-water interfacial tension as a function of dispersant composition. There are a wide variety of techniques for measuring dynamic interfacial tension, from pendant drop tensiometry to capillary drop tensiometry[56] to a simple du Nuoy ring or Wilhelmy plate. For our dispersant-oil-seawater system, however, spinning drop tensiometry is the clear choice for a number of reasons. In spinning drop tensiometry (Figure 2.4, previous page), a glass tube is filled with a droplet of a less dense phase, such as dispersant-oil mixture, suspended in a denser phase such as seawater. When the tube is sealed and spun about its longitudinal axis, the droplet is centered and elongated by centripetal force. The interfacial tension of the droplet can be calculated using the length and diameter of the droplet, the angular velocity of the tube, and the difference in density between the droplet and the bulk phase.

A major advantage of spinning drop tensiometry is that it does not involve solid-liquid contact, and intrinsically damps interfacial oscillation, so it is widely used to measure "ultralow" IFT (< 1 mN/m) such as that commonly observed at dispersant-treated oil-water interfaces. Moreover, once a droplet has reached mechanical equilibrium at a particular rotation rate and its initial IFT has been recorded, it is straightforward to continue to monitor its dynamic IFT for minutes or even hours using this technique. An important deviation from typical spinning drop tensiometry protocols in this work was the large sample tube employed, with a volume of ~20 mL. This large tube enabled very high water:oil ratios (1000:1 to 100000:1 for oil droplet volumes ranging from 0.1-10 μL) which better approximated the tremendous body of aqueous diluent surrounding a chemically dispersed droplet of oil in the ocean. A more detailed description of the tensiometer and of a typical experimental procedure may be found in Chapters 3 and 5.

2.4 Microstructure Characterization

Prior to this work, there have been no studies of water-in-oil microstructures formed by marine oil dispersants specifically, despite calls for such work to be conducted.[13] There have, however, been extensive studies of microstructures formed by individual components (esp. DOSS[36-38] and lecithin[44-47]), as well as of the solubility of water in solutions of DOSS-Span 80 and DOSS-Tween 80 in nonaqueous solvents.[39] In this work, two complementary techniques are employed to characterize dispersant water-in-oil microstructures: cryogenic electron microscopy and dynamic light scattering.

2.4.1 Cryogenic Electron Microscopy

Electron microscopy (EM) is widely used to image nanoscale (<100 nm) structures, as the minimum theoretical resolution for light microscopy is ~200 nm (half the wavelength of violet light). Unfortunately, high-quality EM imaging requires that the sample be subjected to an ultra-high vacuum—a major obstacle to resolving nanoscale features in volatile soft matter or liquid systems. The solution to this, first pioneered in the 1980s by Dubochet[57] and others, is to rapidly immerse the liquid sample into a cryogen, so that the water in it is not able to form ice crystals before it is immobilized in an amorphous "vitrified" state. This prevents destruction of the microstructures present in the sample at room temperature, while still reducing sample volatility enough to enable EM imaging under high vacuum. In this work, both cryogenic scanning electron microscopy (cryo-SEM) and cryogenic transmission electron microscopy (cryo-TEM) are employed to characterize water-in-oil microstructures formed by dispersants.

To prepare a sample for cryo-SEM (Figure 2.5), it is first sandwiched within a cylindrical cavity formed between two planchets, typically a few millimeters in diameter and 0.1-1 mm in height. The sample is cryogenically fixed by immersing the sandwich in a cryogen such as liquid nitrogen or ethane, often within a "high pressure freezer" to lower the freezing point of water in the sample (according to Le Chatelier's principle). The planchets are cut apart either under liquid nitrogen or in a cryogenic stage at high vacuum to expose a cross-section of the vitrified sample, which is then prepared for imaging by coating the sample with a few nanometers of platinum to prevent sample charging and/or by sublimating volatile components under high vacuum to create

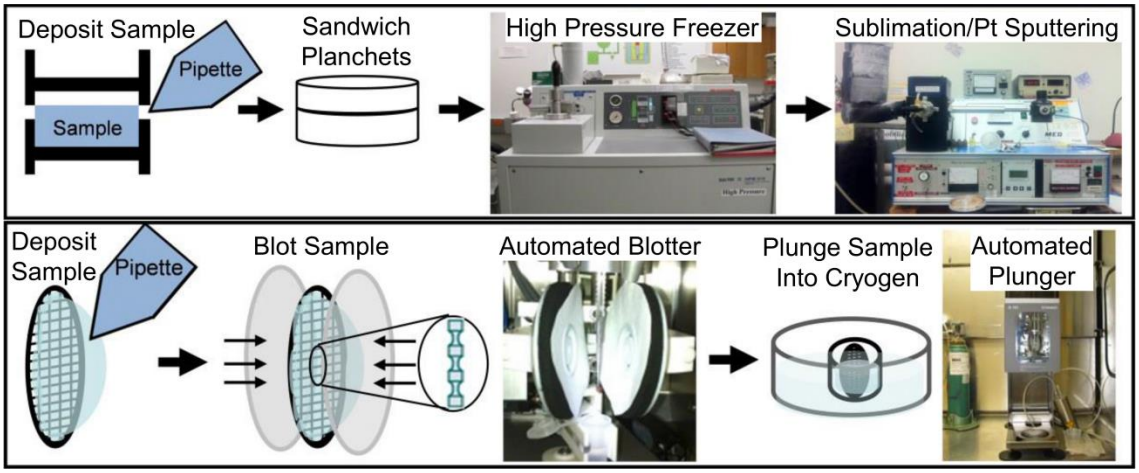

Figure 2.5 Schematic of sample preparation procedures for cryo-SEM (top) and cryo-TEM (bottom). Adapted with permission from Lee.[1]

topographical contrast. Finally, the sample is imaged on a cryogenic stage in a scanning electron microscope, which shows topographical contrast using backscattered electrons and elemental sample compositions using characteristic X-rays (energy-dispersive x-ray spectroscopy). The main advantage of this technique is the ability to visualize nanoscale (<100 nm) features of microscale (>100 nm) structures (see Chapter 6), which are accommodated by the planchet cavity, though SEM resolution is typically not as high as TEM resolution.

Cryo-TEM sample preparation (Figure 2.5) involves pipetting the sample onto a TEM grid with a nano-perforated backing (e.g., holey Formvar or lacey carbon) and then blotting enough sample away to leave a <200 nm thick film across the nanoperforations, thin enough to be penetrated by the electron beam in the microscope. The sample must then be rapidly plunged into a cryogen (liquid ethane for aqueous samples, liquid nitrogen for samples in nonpolar solvents) before liquid can evaporate out of or condense into the films. The blot and plunge are typically automated for the sake of reproducible sample preparation. The sample is then imaged on a cryogenic stage in a transmission electron microscope, which (for an amorphous, non-diffracting sample) shows differences in electron density caused by mass or phase changes. For microstructures small enough to fit into a <200 nm thick film (see Chapter 4), cryo-TEM enables higher resolution imaging than cryo-SEM, but larger microstructures risk being distorted by shear or removed from the TEM grid entirely during blotting.

2.4.2 Dynamic Light Scattering

Light scattering complements and validates cryo-electron microscopy, because microscopy produces detailed images of a few hundred microstructures and light scattering produces average dimensions for a macroscopic volume of microstructures. The diameters of the dispersant microstructures observed in this work are as small as 20 nm, which makes them isotropic Rayleigh scatterers of 400-700 nm visible light (particles are Rayleigh scatterers if $d < \lambda/10$, where d = particle diameter and λ = wavelength of light).[58] Thus, it was not possible to determine their average size using static light scattering, which relies on the angular dependence of anisotropic scattering intensity to determine particle size or shape.

Instead, dispersant microstructures were characterized using dynamic light scattering, in which a diffusion coefficient for the microstructures is calculated from the characteristic decay time of an exponential function fitted to autocorrelation data for fluctuations in scattered light intensity over time (Figure 2.6).[59] These autocorrelation data quantify correlation between scattered light intensity at a given time t_0 and scattered light intensity at later times ($t_0 + t$), as a function of "delay time" t. A longer exponential decay time corresponds to a longer characteristic timescale for fluctuations in scattered light intensity, yielding a smaller average diffusion coefficient and, therefore, a larger average diameter for the particles. It is particularly important to validate dynamic light scattering data with cryo-microscopy, as an average particle diameter can only be calculated from the diffusion coefficient if the particles are known to be spheres.

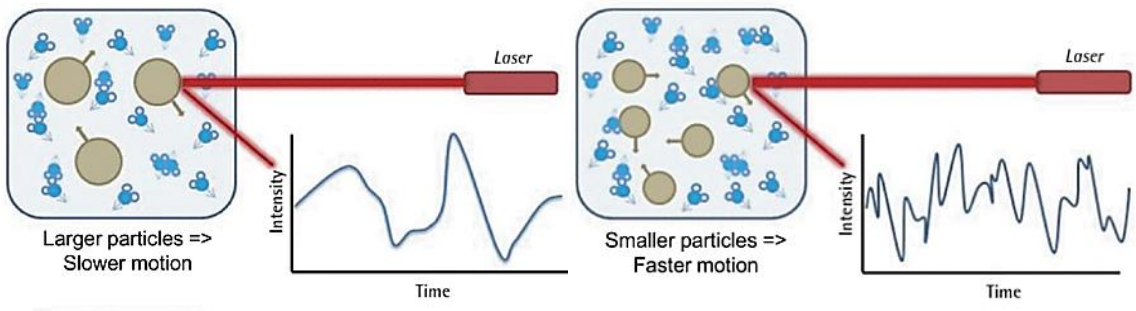

Figure 2.6 Schematic illustrating the principle behind dynamic light scattering. This figure has been adapted from Kim et al.[6] under the terms of the Creative Commons Attribution Non-Commercial License (http://creativecommons.org/licenses/by-nc/3.0/). Some of the original text has been removed, and alternate text added.

2.5 Summary

There is a great deal of prior work on the effectiveness of various surfactant blends as marine oil dispersants, and on the self-assembly of individual surfactants used in those dispersants. However, there is very little prior work on the interfacial phenomena underlying dispersant effectiveness, such as dispersants' oil-water dynamic interfacial tension and water-in-oil microstructure formation. The goal of this thesis is to use the techniques discussed in this section to gain a better understanding of the relationship between these interfacial phenomena and dispersant effectiveness, both for traditional dispersant formulations based on DOSS-Tween 80-Span 80 blends and for the relatively new dispersants containing blends of lecithin and Tween 80.

Chapter 3. The role of dispersants' dynamic interfacial tension in effective crude oil spill dispersion*

3.1 Introduction

Oil dispersants have been employed as a component of marine oil spill responses around the world for decades.[13] In spite of their widespread use, though, the published literature exploring the fundamental interfacial science of dispersants' formulation and action is underdeveloped. Much of the dispersant literature has focused on empirical characterizations of dispersants, such as dispersion effectiveness,[48] and/or on the study of proprietary dispersant formulations, of unknown composition. A few authors[3, 60] have directly measured the initial interfacial tension (IFT) upon application of various dispersants to a crude oil-salt water interface and attempted to correlate these values with the results of effectiveness tests on those dispersants, but have met with limited success. Of particular note is a paper by Brochu et al.,[3] who measured both initial oil-water IFT and dispersion effectiveness for 49 different surfactant mixtures at a crude oil-salt water interface. Their data showed some correlation between these properties, but also contained a great deal of unexplained variation in dispersion effectiveness. Thus, it seems natural to propose that other, more dynamic interfacial phenomena also control the breakup of oil slicks into seawater by dispersants.

One potential influence on the effectiveness of Tween 80-Span 80-DOSS dispersants is the differing rates at which these three surfactants have each been observed to leach out of dispersant-treated crude oil into surrounding seawater. Knudsen et al.,[61, 62] found that Tween 80 exhibits a very low leaching rate from crude oil into synthetic seawater, more than an order of magnitude lower than that of DOSS. Similar studies[20, 63] have failed to confirm this observation, though this is due at least in part to the challenge of distinguishing Tween 80 from other water-soluble components of crude oil. Reichert

* This chapter was adapted from the publication: Riehm, D.; McCormick, A. The role of dispersants' dynamic interfacial tension in effective crude oil spill dispersion. *Mar Poll Bull* **2014**, 84, 155-163. DOI: 10.1016/j.marpolbul.2014.05.018

The underlying raw data is publicly available through GRIIDC (DOI: 10.7266/N7B56GQQ).

and Walker[64] and Kirby et al. [65] found that Tween 80 adsorbing from aqueous solution to a squalane-seawater interface forms an insoluble monolayer, whereas DOSS adsorbing to the same interface from aqueous solution readily desorbs back into water when the aqueous concentration of DOSS is reduced. Since Span 80 is hydrophobic (HLB = 4.3) and leaches more slowly than either Tween 80 (HLB = 15) or DOSS,[63] DOSS is therefore expected to partition from dispersant-treated crude oil into seawater much faster than either Tween 80 or Span 80.

The aim of this chapter is to better understand the role of dynamic IFT in the dispersion effectiveness of mixtures of sorbitan monooleate (Span 80), $(PEO)_{20}$ sorbitan monooleate (Tween 80), and dioctyl sodium sulfosuccinate (DOSS). These three surfactants (Figure 3.1) have been widely used for decades as primary surface active agents in oil dispersants around the world,[11, 13, 31] and exhibit high dispersion effectiveness when mixed.[3, 23] Tween 80 and Span 80 are also desirable in environmental applications for their exceptionally low toxicity, [33, 34] though DOSS does exhibit marine toxicity to some extent.[35] However, DOSS is also well-known to be capable of forming reverse micelles without a cosurfactant, above a critical micelle concentration of ~1 mM, in a wide range of hydrophobic solvents,[36-38] and has been found to readily incorporate nonionic surfactants, including Tween 80 and Span 80, into its reverse micelles.[39] In this

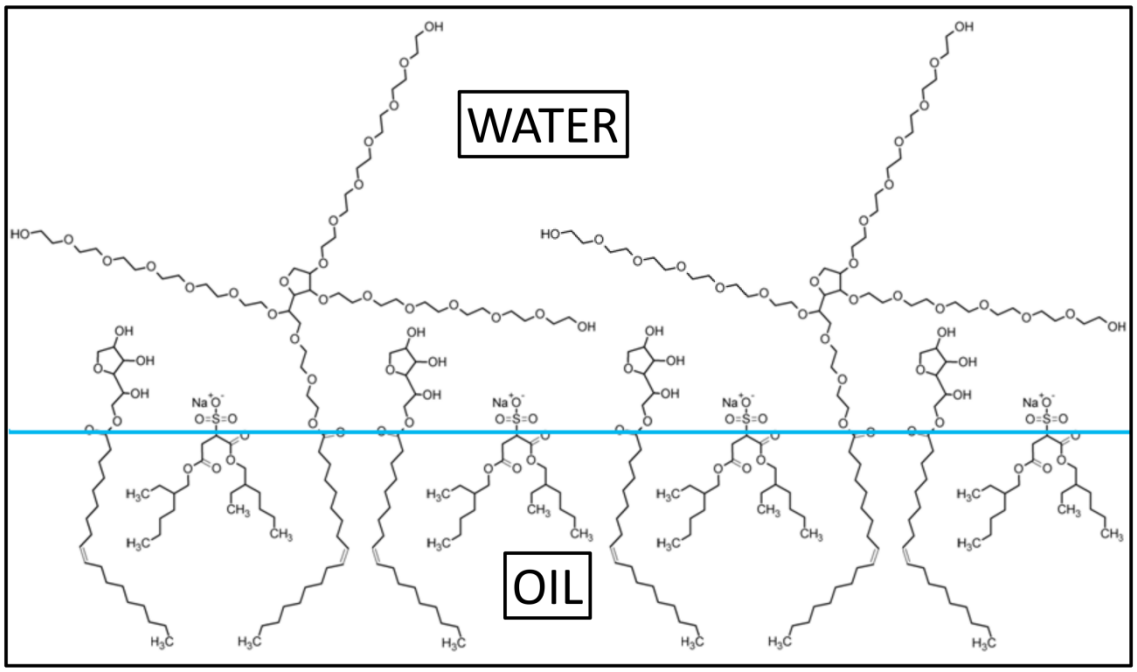

Figure 3.1 Sketches of Span 80, Tween 80, and DOSS at an oil-water interface.

way, therefore, DOSS is potentially capable of solubilizing a blend of surfactants containing various hydrophilic moieties into a hydrophobic medium, such as a dispersant solvent or a crude oil slick. In order to understand the role (if any) of these microstructures in effectiveness, however, it is first necessary to map out trends in interfacial tension as a function of dispersant composition which these microstructures may be responsible for.

3.2 Experimental

3.2.1 Experimental Design

Brochu et al.[3] reported qualitative, visually-assessed estimates of dispersion effectiveness across the full Tween 80-Span 80-DOSS compositional space (Figure 3.2). Their results were used to identify compositional lines in Tween 80-Span 80-DOSS compositional space along which dispersion effectiveness exhibited large, rapid changes. Then, both dispersion effectiveness and IFT were measured as a function of composition along those lines, with the aim of correlating changes in effectiveness with changes in either initial IFT or in trends in dynamic IFT. As shown in Figure 3.2, the Tween 80-DOSS edge ("Region A") and the 40 wt% Tween 80 compositional line ("Region B")

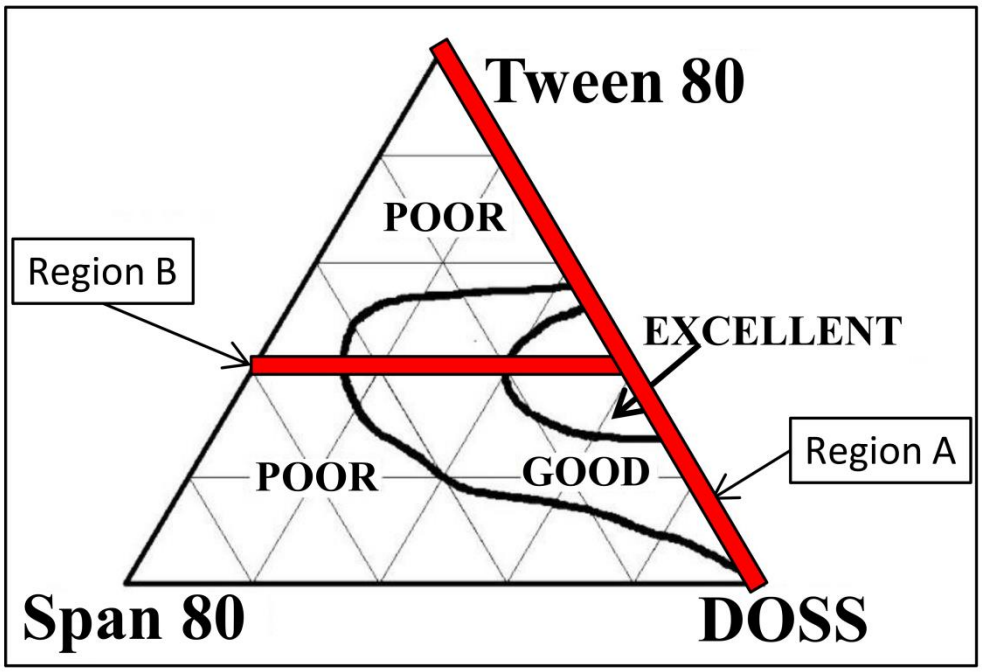

Figure 3.2 Qualitative dispersion effectiveness of DOSS-Tween 80-Span 80 mixtures (in a cyclohexanone solvent) as reported by Brochu et al.[3] Compositional regions of interest for this work are highlighted in red. Figure adapted from Brochu et al.[3]

were reported to traverse large changes in dispersion effectiveness, and were therefore selected for detailed characterization.

3.2.2 Materials

Sodium chloride (BDH Chemicals), magnesium chloride (Sigma), sodium sulfate (Macron Chemicals), dichloromethane (Sigma-Aldrich), Tween 80 (Sigma-Aldrich), Span 80 (Sigma), dioctyl sodium sulfosuccinate (98%, Aldrich), ethanol (AAPER Alcohol and Chemical Co.), and Isopar M (Seacole Chemical) were used as received. It was important to use Tween 80 which had been purchased within the past year, as the periodic exposure of Tween 80 to air and light, over the course of months, degraded it enough to alter oil-dispersant mixtures' observed behavior. Deionized water was obtained using a Milli-Q purification system (18.2 MΩ·cm at 25 °C). The crude oil employed in these experiments was a South Louisiana crude selected by BP as a surrogate for the MC252 crude oil spilled in the Gulf of Mexico in 2010. The oil was shipped on ice, and was subsequently stored in a freezer at -5 °C until use. At 20 °C, its density was 0.842 g/cm^3 and its viscosity was 10 cSt. Artificial seawater was prepared according to a modified version of the formulation reported by Kester et al.[66] 427 mM NaCl, 55 mM $MgCl_2$, and 27 mM Na_2SO_4 were added to deionized water (Millipore, 18.2 MΩ*cm) in order of increasing solubility (Na_2SO_4 < NaCl < $MgCl_2$ at 20 ˚C) to speed dissolution.

3.2.3 Dispersant Preparation

The basic formulation of all oil dispersants characterized in this work was adapted from US Patent 3,793,218 (G. Canevari, 1973),[31] the first published formulation for a Tween-Span-DOSS based dispersant. In accordance with Canevari's 1973 patent, DOSS was added to the dispersant as part of a mixture of DOSS, ethanol, and water (75 wt% DOSS, 18.5 wt% H_2O, 6.5 wt% EtOH). This mixture was a replicate of the commercial surfactant "Aerosol OT-75" (AOT-75).[67] Dispersants therefore consisted of blends of Tween 80, Span 80, and AOT-75, dissolved in the paraffinic solvent Isopar M at a total surfactant:solvent volumetric ratio of 13:20 as specified by Canevari. However, the dispersants' surfactant weight ratios, reported in this paper, use only the mass of DOSS they contained, and not the mass of ethanol and water added along with the DOSS as part of AOT-75. An algorithm for calculating the amount of each component required for

dispersants formulated in this manner may be found in Appendix A. It is also important to note that for dispersant surfactant blends containing >50 wt% Tween 80, the dispersant was observed to separate over time into two phases, even after vigorous mixing. Such dispersants were, therefore, only drawn off for mixing with crude oil contemporaneously with sufficiently vigorous stirring to produce a finely and homogeneously emulsified mixture of the two phases.

3.2.4 Stirred Flask Test

Our "Stirred Flask Test" was adapted from the "Swirling Flask Test" used by the US EPA[55] to officially assess dispersant effectiveness (originally developed by Fingas et al.[49]). Experiments were conducted at 20 ± 1 °C. 50.0 mL of artificial seawater was added to each of two 50 mL Pyrex Erlenmeyer flasks, which were each then continuously stirred with a 1-1/2" x 3/8" Fisherbrand Spinbar Octagonal Magnetic Stir Bar (Fisher Scientific) at 140 ± 5 RPM. In a separate container, a chemical surrogate for Macondo crude oil (MC252, South Louisiana Crude) was thoroughly mixed with dispersant at a 1:20 dispersant-to-oil (D:O) volumetric ratio. The container of crude oil was thoroughly stirred before each day's samples were withdrawn, to counteract potential separation of its components. 105 μL of this oil-dispersant mixture was then carefully added dropwise to the surface of the salt water in each flask and allowed to disperse for 20 minutes, after which stirring was halted and the dispersion was allowed to settle for 5 minutes. If a large fraction of the oil settled out of the dispersion and obstructed the air-water interface during this period, it was carefully wicked away with a Kimwipe until the air-water interface had been sufficiently cleared of oil to allow a pipette to sample the oil-water dispersion without having to penetrate through the resurfaced oil. This wicking process was not observed to significantly affect the rate of droplet settling in the sub-surface dispersion, due to the small volumes of fluid being wicked away.

After the settling period was complete, 4.5 mL of oil-water dispersion was carefully drawn off from the bottom of each flask with a glass pipette and transferred to a 60 mL separatory funnel which contained 2 mL of dichloromethane (DCM). The funnel was then stoppered, vigorously shaken for 60 seconds, and allowed to sit long enough for its contents to phase separate. If the dichloromethane phase was persistently cloudy after

30-60 seconds of quiescent settling, the funnel was ultrasonicated until the cloudiness dissipated. 1.5 mL of the oil-DCM phase was then drawn off from the bottom of the funnel, and 1.5 mL of new DCM was added through the top.

This extraction procedure was performed a total of three times on each oil-water dispersion, although only 1 mL of oil-DCM phase was drawn off from the funnel after the third extraction, for a total oil-DCM extract volume of 4 mL. The absorbances of each dispersion's oil-DCM extract were measured with a Thermo Scientific Evolution 60S UV-Vis spectrophotometer at 0.2 nm increments over the range 360-400 nm. In addition, a 100%-dispersion-standard oil-DCM mixture, containing 9.45 µL of oil-dispersant mixture in 4 mL of DCM, was prepared after every extraction, and its absorbances were measured at the same wavelengths. (4.5 mL/50 mL = 18% of the oil-water dispersion was sampled, so 100% dispersion would have put 18% of the original slick, or (105 µL x 0.18) = 9.45 µL, into a 4 mL oil-DCM extract.) The ratios of the absorbances of each sample's extract to the absorbances of the 100% oil-DCM standard at corresponding wavelengths were each interpreted as "percentage of slick dispersed" or "dispersion effectiveness." These values were averaged between 360-400 nm to yield each sample's effectiveness value. If the range of all measured effectiveness values between 360 and 400 nm spanned more than one percentage point of measured effectiveness, the data from that sample were discarded. The validity of approximating dispersant effectiveness as the ratio of the absorbance of an oil-water dispersion sample extract to the absorbance of a 100%-dispersion-standard (described above) was established by constructing a full dispersion-effectiveness calibration curve, as discussed in Appendix A.

3.2.5 Spinning Drop Tensiometry

The spinning drop tensiometer (SDT) employed in this work was originally designed and built by D. Joseph.[68] Experiments were conducted at 20 ± 1 °C. In a typical experiment, the 5/8" ID, 10" long glass sample tube was initially (1) thoroughly scrubbed with soap and DI water, until water fully wetted the tube's interior; (2) rinsed with DI water; and (3) rinsed with salt water. Separately, two cylindrical Teflon plugs were rinsed of crude oil residues in dichloromethane, after which Viton O-rings were inserted into grooves cut in the plugs' circumferences. With the tube wall still wet with salt water, one

of the Teflon plugs was inserted snugly into one end of the tube, and then a volume (typically 2-20 µL) of premixed, degassed crude oil and dispersant (overall density ≈ 0.850 g/cm^3) appropriate to the expected IFT range and corresponding cylindrical droplet radius was deposited onto the wall of the tube. The tube was then held nearly horizontal, gently filled with salt water and sealed via insertion of a second Teflon/O-ring plug into the open end, as the remaining air in the tube was simultaneously removed. This filling method was found to be more conducive to maintaining the initial physical integrity of oil-dispersant mixture in the SDT than the injection of oil-dispersant mixture with a needle into an already filled and sealed tube, as oil-dispersant mixtures were often partially dispersed by needle injection shear at low (<10^{-2} mN/m) IFT. The filling method's effectiveness at purging interfacial contaminants from the tensiometer was verified by filling the tube according to this procedure using pure DI water, and then pouring that water out into a Wilhelmy plate tensiometer and confirming that its surface tension was 72.8 ± 0.5 mN/m (at 20° C).

Upon tube spinup, the oil-dispersant mixture was forced away from the tube wall towards the tube centerline and formed one or more droplets. Dispersants with lower IFT, particularly <10^{-2} mN/m, often broke into tens of droplets during spinup, which then spread out along the length of the tube's centerline. The tube's speed was gently increased over 30-60 seconds to a final speed at which the largest droplet(s) achieved a length:diameter ratio of at least 1.1 (ideally 2-4). Depending on the IFT of the oil-dispersant mixture being characterized, this speed ranged from 500-5000 RPM. Once the droplets had become sufficiently non-spherical, a video capture system was trained on one of them and its radius was recorded continuously, with length measurements taken at regular intervals. IFT was calculated using the methodology of Princen et al.[5] For droplet length:diameter ratios of > 3.5, Princen's exact relation between drop shape and IFT is approximated to within < 1% error by Vonnegut's classic equation, $\sigma = \frac{\Delta\rho\omega^2 D^3}{32}$, in which σ = IFT, D = droplet diameter, $\Delta\rho$ = (density of salt water) – (density of degassed crude oil) = (1.017 g/cm^3) – (0.850 g/cm^3) = 0.174_3 g/cm^3, and ω = angular velocity.

3.3 Results and Discussion

3.3.1 Tween 80-DOSS Mixtures

Observed trends in effectiveness and initial IFT for crude oil treated with DOSS-Tween 80 mixtures (Figure 3.3) are consistent with those reported in prior work. Brochu et al.[3] report peak effectiveness for DOSS-Tween 80 mixtures around 60:40 DOSS:Tween 80; a rapid effectiveness dropoff between 40:60 and 60:40 DOSS:Tween 80; and minimal effectiveness for 100:0 and 0:100 DOSS:Tween 80, consistent with the data in Figure 3.3. Initial IFT measurements carried out by Brochu et al. were more limited in scope than those reported here, but initial IFT produced by 60:40 DOSS:Tween 80 dispersant was found to be much lower than those produced by 100:0 or 0:100 DOSS:Tween 80 dispersants, again consistent with Figure 3.3. Finally, Brandvik and Daling[23] extrapolated the measured effectivenesses of DOSS-Tween 80-Span 80 mixtures to 0 wt% Span 80 using a partial-least-squares (PLS) algorithm, and predicted both peak effectiveness for Tween 80-DOSS mixtures around 60:40 DOSS:Tween 80 and minimal

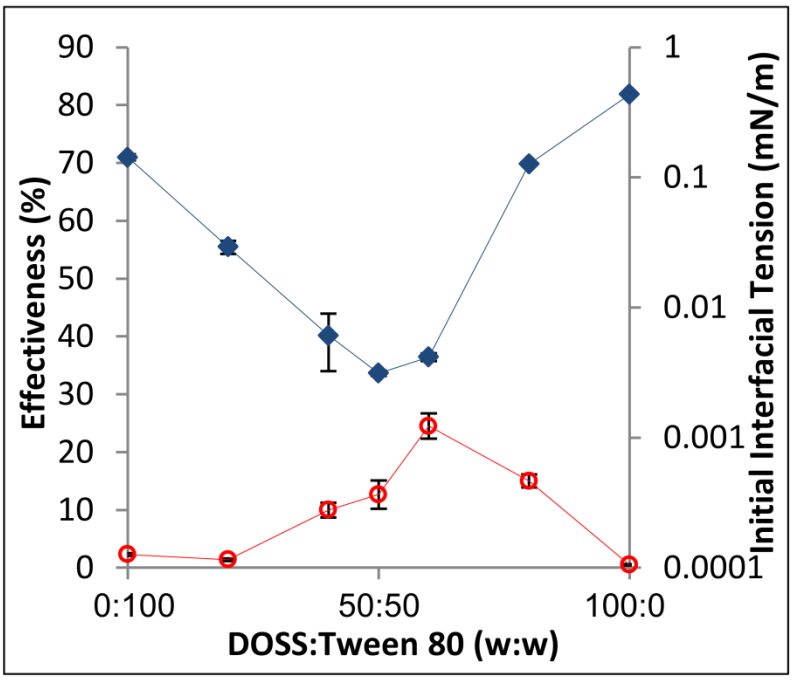

Figure 3.3 Dispersant effectiveness (o) and initial IFT (♦) of dispersant-treated crude oil in seawater as a function of DOSS:Tween 80 weight ratio. Dispersant-treated crude oil contains 2.0-2.3 wt% total surfactant, depending on DOSS:Tween 80 weight ratio. Plotted data points are arithmetic means for effectiveness and geometric means for initial IFT, based on n = 3 repetitions. Error bars extend one standard error above and below each mean.

effectiveness at both 100:0 and 0:100 DOSS:Tween 80. Thus, the compositional trends in Tween 80-DOSS dispersants' properties observed in this work are qualitatively similar to those observed by others using different crude oils and effectiveness testing methods.

Effectiveness of Tween 80-DOSS mixtures was found to be governed by both initial oil-water IFT and by rates of change in oil-water IFT over time. It is clear from Figure 3.3 that initial IFT alone does not determine effectiveness, as compositions with comparable initial IFT yield significantly different dispersion effectiveness. For example, while the initial IFT is approximately 0.1 mN/m for both 0:100 and 80:20 DOSS:Tween 80, the mean dispersion effectivenesses at these compositions are 2.25 ± 0.25% and 15 ± 1%, respectively—a clearly significant difference ($p=0.0003$, 1-tailed Student's t-test, unequal variances). Similarly, while the initial IFTs at 50:50 and 60:40 DOSS:Tween 80 are 0.003 mN/m and 0.004 mN/m, respectively, the corresponding mean dispersion effectivenesses are 12.5 ± 2.5% and 24.5 ± 2.2%—again, a significant difference ($p=0.01$, 1-tailed Student's t-test, unequal variances). These differences likely result from the fact that, as shown in Figure 3.4, the magnitudes and directions of IFT change over time also vary significantly with composition, from an extremely rapid increase at 40:60 DOSS:Tween 80 to a decline of nearly an order of magnitude over three hours at 80:20 DOSS:Tween 80. Strikingly, the changes in IFT characteristic of dispersants containing only Tween 80 or only DOSS are significantly lower in magnitude than the changes characteristic of dispersants containing both surfactants (Figure 3.4). Thus, a more complex interplay between the interfacial dynamics of Tween 80 and DOSS appears to be at work in their mixtures than just a direct transition between the IFT dynamics of Tween 80 and those of DOSS.

It appears that the large swings observed in the magnitudes and directions of IFT change as initial dispersant composition is varied result from the fact that, as reported by Knudsen et al.,[62] DOSS is lost much more rapidly from crude oil into salt water than is Tween 80. Over time, this decreases the DOSS:Tween 80 ratio in dispersant-treated oil, altering the composition of the interfacial surfactant film and, thus, the oil-water IFT. The rate and direction of IFT change for a particular initial dispersant composition is governed by the trend in initial IFT as DOSS:Tween 80 is decreased from that composition (see Figure 3.3). A corollary to this hypothesis is that the initial IFT which is

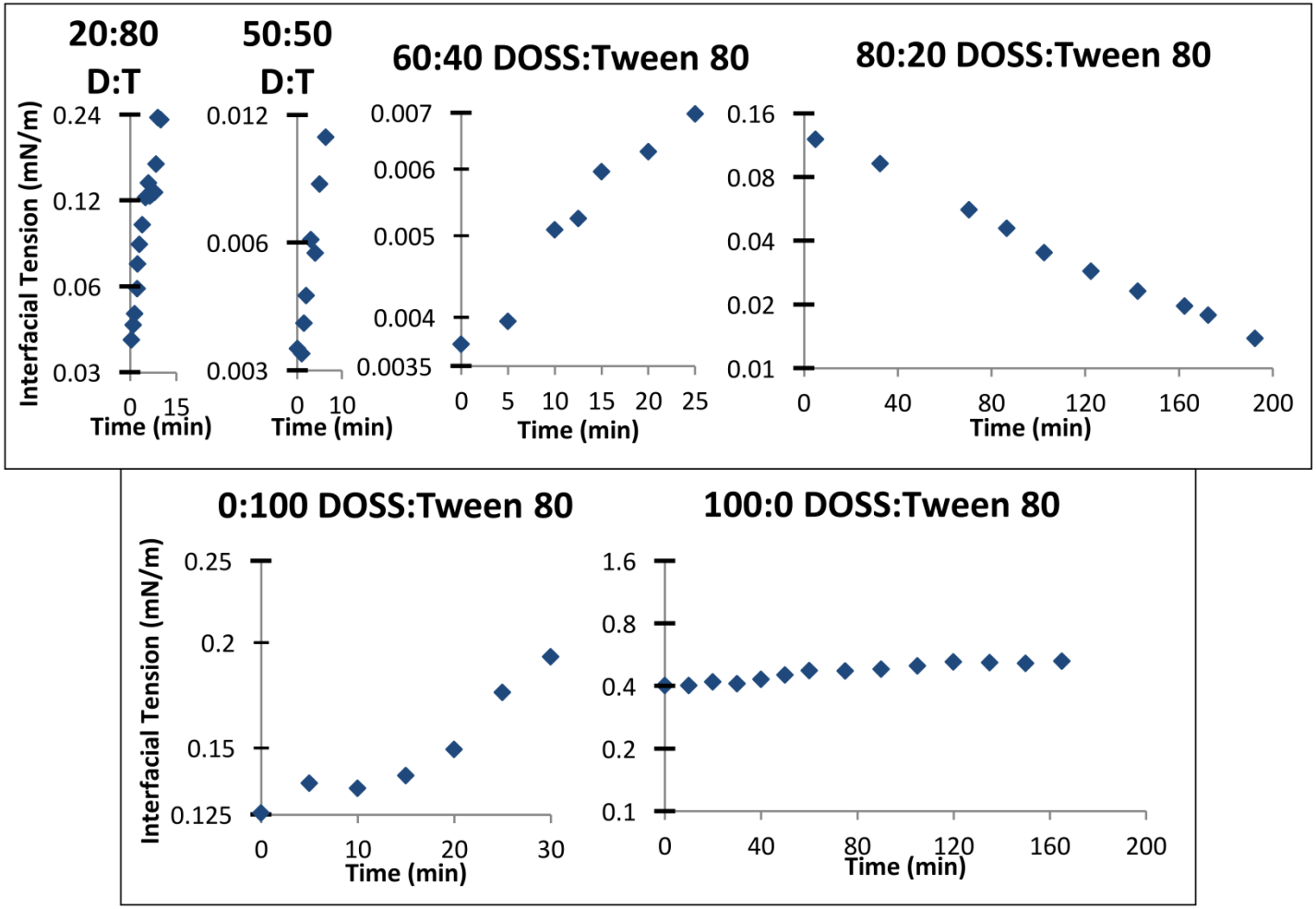

Figure 3.4 IFT of dispersant-treated crude oil droplets in seawater. Dispersant-treated crude oil contains 2.0-2.3 wt% total surfactant, depending on DOSS:Tween 80 weight ratio. t = 0 coincides with the start of image recording for each droplet, immediately following tensiometer spinup. Data could not be collected at 40% DOSS due to rapid IFT increase (droplets became spherical < 1 min after spinup). Droplet volumes ranged from 0.07 µL (50% DOSS) to 0.35 µL (20% DOSS) as necessitated by their differing IFT ranges.

reproducibly observed at each dispersant composition is the "actual" IFT corresponding to that blend of surfactants, before surfactant leaching depletes the dispersed oil of DOSS.

In Figure 3.3, as the DOSS fraction in a dispersant is decreased, its initial IFT declines from a local maximum at 100:0 DOSS:Tween 80 to a minimum (~0.003 mN/m) around 50:50 DOSS:Tween 80, and then rises again to another local maximum at 0:100 DOSS:Tween 80. Thus, our hypothesis predicts that dispersant initially containing 80:20 DOSS:Tween 80 should exhibit decreasing IFT, while dispersant containing 20:80 DOSS:Tween 80 should exhibit increasing IFT, in agreement with the data in Figure 3.4. The slow increase in IFT observed at 60:40 DOSS:Tween 80, despite the fact that initial IFT declines slightly as DOSS:Tween 80 decreases from 60:40 to 50:50, presumably results from leaching-related loss of surfactants from the oil droplet(s) having a greater effect on IFT in this region than compositional changes. Finally, the fact that the 0:100 and 100:0 DOSS:Tween 80 dispersants exhibit the slowest rates of change in IFT over time is as expected, based on the hypothesis that the changes in IFT exhibited by dispersants containing mixtures of Tween 80 and DOSS are driven by a gradual change in interfacial composition as DOSS is lost from the oil faster than Tween 80.

A possible objection to the proposition that the changes in IFT shown in Figure 3.4 influence the effectiveness shown in Figure 3.3 is that the timescales for significant IFT change in Figure 3.4 are longer, in some cases, than the 20 min mixing period of the Stirred Flask Test, as well as the 10-20 min period within which waves have generally been observed[69, 70] to break up an oil slick into dispersed droplets (diameter < 70 um[71]). It is important to recognize, however, that the droplets characterized in the tensiometer have much larger volumes than those dispersed into water during effectiveness testing. As calculated in Appendix A.3, a spherical oil droplet with a volume > $5*10^{-5}$ µL (or, a diameter > 45 µm) would settle out of the dispersion during the Stirred Flask test. In contrast, the droplets characterized via interfacial tensiometry (Figure 3.5) had volumes ranging from 0.07 µL to 0.35 µL, over 1000x higher than the largest possible dispersed droplet volume. As shown in Figure 3.5 (using 80:20 DOSS:Tween 80 dispersant as an

example—similar behavior was observed at other compositions), oil-water IFT deviates from its initial value more rapidly at lower droplet volumes. Presumably, this results from the fact that smaller droplets have higher surface- area-to-volume ratios than larger droplets, which enable interfacial dynamics such as surfactant desorption and loss into the aqueous phase to proceed much more rapidly in smaller droplets. Thus, as oil droplets break apart during oil spill dispersion, the changes in IFT shown in Figure 3.4 are projected to occur increasingly rapidly, and eventually become fast enough to significantly influence dispersant effectiveness, as shown in Figure 3.2.

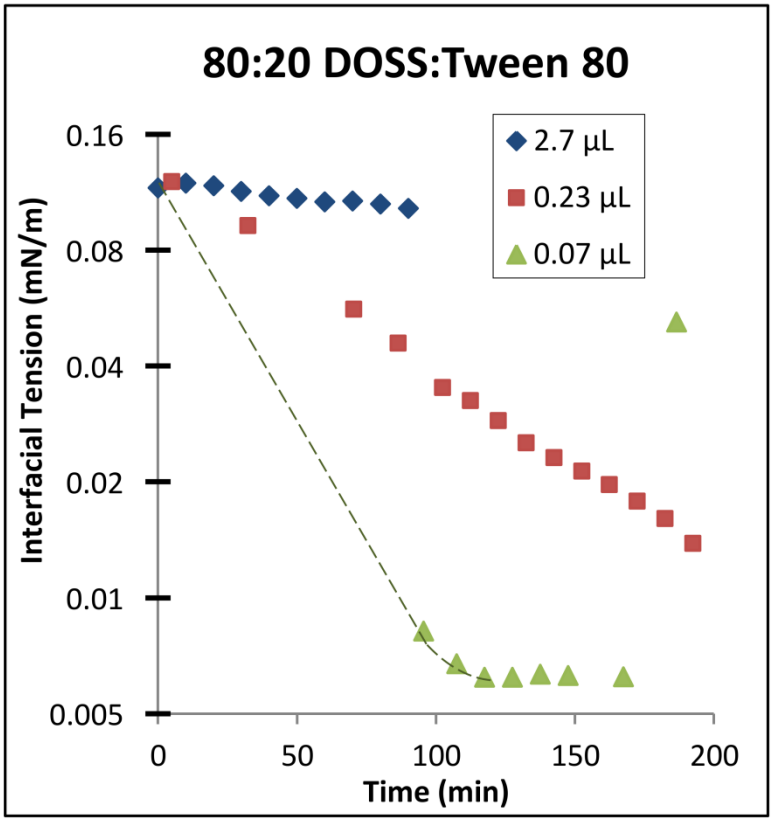

Figure 3.5 Effect of droplet volume on IFT of dispersant-treated crude oil droplets in seawater. Dispersant surfactant blends were 80:20 DOSS:Tween 80 by weight. Dispersant-treated crude oil contains 2.1 wt% total surfactant. All droplets were characterized at 2000 ± 50 RPM. t = 0 coincides with the start of image recording for each droplet, immediately following tensiometer spinup. The dashed green line for the 0.07 µL droplet indicates projected dynamic IFT before the droplet had elongated sufficiently for IFT to be measured.

3.3.2 40 wt% Tween 80, 60 wt% [Span 80 + DOSS]

Observed trends in effectiveness and initial IFT for crude oil treated with mixtures of 40wt% Tween 80 and 60wt% various mixtures of Span 80 & DOSS (Figure 3.6) are also consistent with those reported in prior work. While the peak effectiveness composition reported by Brochu et al. in Figure 3.2, at 0-10 wt% Span 80, differs slightly from the peak effectiveness composition in Figure 3.6 at 40:20 DOSS:Span 80, this may be attributed to the qualitative, visual assessments of effectiveness used by Brochu et al. to construct Figure 3.2. Quantitative effectiveness assessments reported by the same authors using the Mackay-Nadeau-Steelman effectiveness test indicate that 40:40:20 DOSS:Tween 80:Span 80 (by weight) is more effective than 60:40 DOSS:Tween 80, and that both of these mixtures are much more effective than 60:40 Tween 80:Span 80 (compositionally similar to the 40:60 Tween 80:Span 80 mixture tested in this work), which is in agreement with Figure 3.6. Brandvik and Daling[23] conducted a detailed study

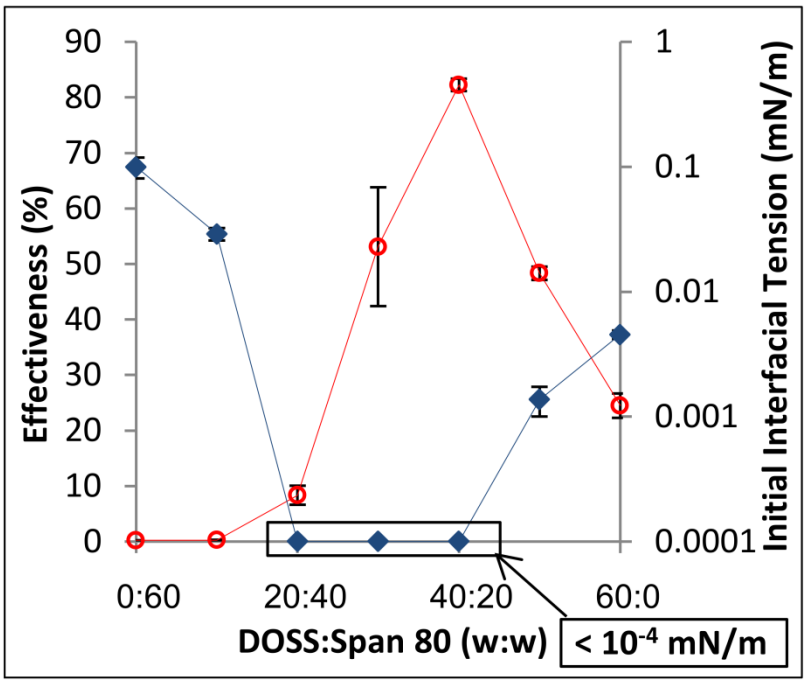

Figure 3.6 Dispersant effectiveness (o) and initial IFT (♦) of dispersant-treated crude oil in seawater as a function of DOSS:Span 80 weight ratio. Dispersant surfactant blends are 40 wt% Tween 80 and 60 wt% [Span 80 + DOSS]. Dispersant-treated crude oil contains 2.0-2.2 wt% total surfactant, depending on DOSS:Span 80 weight ratio. Plotted data points are arithmetic means for effectiveness and geometric means for initial interfacial tension, based on n = 3 repetitions. Error bars extend one standard error above and below each mean. Plotting IFT at 10^{-4} mN/m indicates that IFT fell below this value and could not be measured accurately.

of the effectiveness of various ternary DOSS-Tween 80-Span 80 mixtures, and reported peak effectiveness around 20-30 wt% Span 80, 20-40 wt% Tween 80, and 40-60 wt% DOSS, depending on the dispersant solvent used. They also report that effectiveness falls off steeply, to less than half of its peak value, if any surfactant's weight fraction deviates from the most effective composition by 20 wt% or more, as observed in Figure 3.6. On the whole, then, the results of Brandvik and Daling[23] and of Brochu et al.[3] are in agreement with the data presented here, indicating that conclusions drawn from this data are likely to be broadly applicable and robust.

The dispersion effectiveness of surfactant mixtures containing 40wt% Tween 80 and 60wt% various mixtures of Span 80 & DOSS was strongly influenced by initial oil-water IFT for DOSS:Span 80 ratios ≥40:20. As shown in Figure 3.6, decreases in initial IFT correspond closely with increases in dispersant effectiveness across this compositional region. However, between 40:20 and 20:40 DOSS:Span 80, the effectiveness initially becomes erratic and then drops precipitously, to below 10%, even though initial IFT remains less than 10^{-4} mN/m. It is clear that this cannot be due to rapid increase in IFT over time (e.g., due to DOSS leaching), as the IFT of droplets treated with 20:40 DOSS:Span 80 dispersant remained well below 10^{-3} mN/m for at least 10-15 minutes after the beginning of each tensiometry run.

Qualitative observations of oil breakup dynamics during effectiveness testing suggest instead that replacing DOSS with Span 80 steadily slows and eventually halts the breakup of oil slicks into dispersed droplets in spite of declining IFT. As shown in Figure 3.7, oil slicks treated with 60:0 DOSS:Span 80 dispersant were completely broken up by turbulence within 2-3 min of their addition to the water's surface, while slicks treated with 40:20 DOSS:Span 80 dispersant took 5-15 minutes to fully break up, and slicks treated with 20:40 DOSS:Span 80 dispersant barely broke up at all during the Swirling Flask test's 20 minute long agitation period. Intriguingly, the extent to which oil slicks treated with 30:30 DOSS:Span 80 dispersant broke up was bimodal, with some dispersion tests resulting in 70-80% effectiveness and others resulting in 20-45% effectiveness. The two categories of dispersion effectiveness, each replicated three times, were found to significantly differ ($p=0.007$, 1-tailed Student's t-test, unequal variances). While this bimodality has not been extensively characterized, the effectiveness of 30:30

DOSS:Span 80 dispersant seemed particularly sensitive to minor variations in test setup (e.g., the care with which the slick is initially deposited onto the surface of the water, the precision with which mixing energy is controlled, etc.). Thus, 30:30 DOSS:Span 80 dispersant appears to lie at a critical ratio of Span 80:DOSS, above which mixing energy in the effectiveness test is not sufficient to break up oil slicks even when dynamic IFT is observed to fall well below 10^{-3} mN/m.

Based on the data in Figure 3.8, it is proposed that this inhibition of oil slick breakup by Span 80 is caused by very slow interfacial adsorption from the bulk oil phase to the interface for dispersants with high Span 80:DOSS ratios, resulting in high dynamic IFT during droplet deformation. Dispersants containing <20:40 DOSS:Span 80 do not exhibit a reproducible initial IFT at t = 0 min, as dispersants containing >40:20 DOSS:Span 80 do. Instead, their dynamic IFT declines steadily from a wide range of values (0.14 - 0.45 mN/m) at t = 0 min which vary with droplet volume and rotational speed to a reproducible "endpoint" IFT characteristic of each dispersant, indicated by a red line in Figure 3.8. These reproducible endpoints are interpreted as the initial pseudo-equilibrium between oil treated with Span 80-rich dispersants and the oil-water interface, and are therefore considered comparable to the initial IFT of DOSS-rich dispersants at t =0 min and plotted as the "initial" IFT of Span 80-rich dispersants in Figure 3.6. The

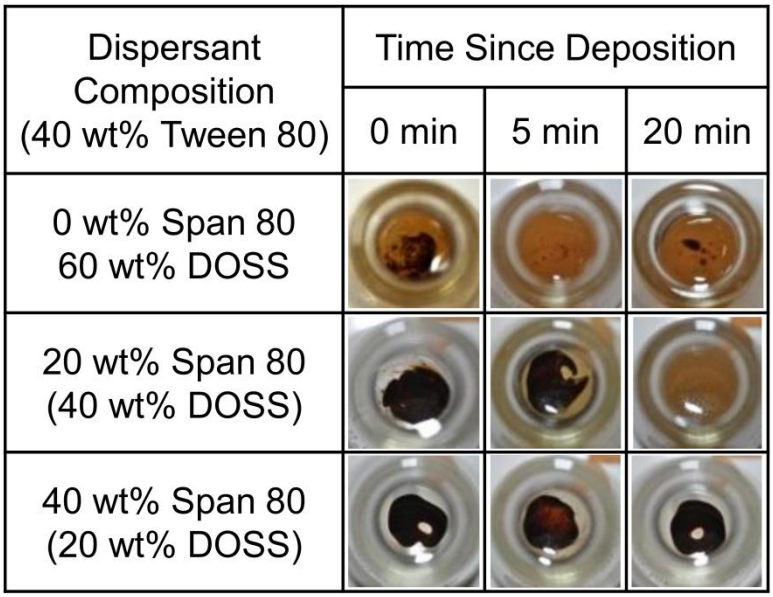

Figure 3.7 Images of dispersant-treated crude oil slicks during the Stirred Flask Test. Dispersant surfactant blends contained 40 wt% Tween 80 and 60 wt% [Span 80 + DOSS]. Images were taken at t = 0, 5, and 20 min after slick deposition.

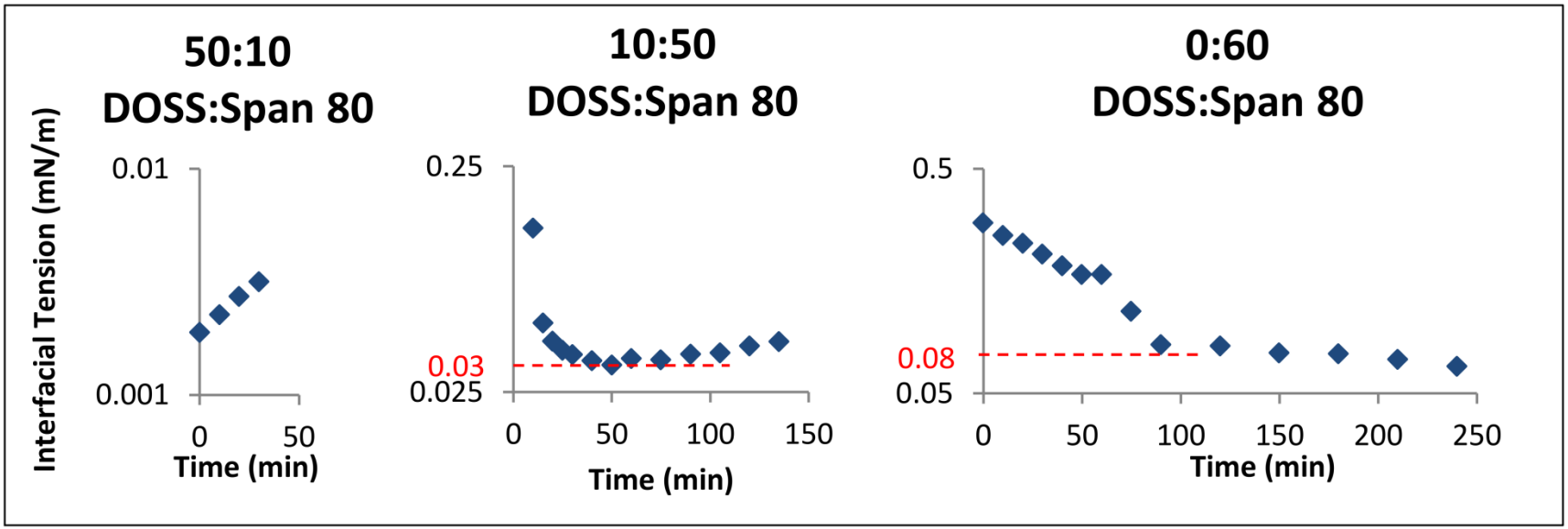

Figure 3.8 IFT of dispersant-treated crude oil droplets in seawater**.** Red lines and labels indicate the end of initial dynamic IFT transients. Dispersant surfactant blends contained 40 wt% Tween 80 and 60 wt% [Span 80 + DOSS]. t = 0 coincides with the start of image recording for each droplet, immediately following tensiometer spinup. Droplet volumes were 0.05 µL (50:10 D:S), 0.22 µL (10:50 D:S), and 0.16 µL (0:60 D:S). 10:50 and 0:60 DOSS:Span 80 data were all collected at 2200 RPM, to facilitate comparison between their initial transient times.

hypothesis that an increase in Span 80 concentration slows dispersant adsorption to the oil-water interface is also supported by the observation that 10:50 DOSS:Span 80 dispersant exhibits a 30-60 min long initial IFT decline at 2200 RPM, while 0:60 DOSS:Span 80 dispersant exhibits an initial IFT decline lasting for > 1 hr at the same rotational speed. 20-40 wt% Span 80 dispersants exhibit dynamic IFT too low to accurately characterize (< 10^{-4} mN/m), but low Span 80 dispersants (>40:20 DOSS:Span 80) presumably produce very rapid initial IFT declines which arrive at their reproducible initial IFT during tensiometer spinup. A range of different droplet volumes will be characterized in future to clarify whether mass transport to the interface is kinetically-limited or diffusion-limited, but high surfactant concentrations in the oil phase (~2 wt%) seem to render diffusion limitation unlikely. It therefore seems clear that a high Span 80:DOSS ratio limits effectiveness by bringing about slow interfacial adsorption kinetics for dispersant from the bulk oil phase, and remains to determine the underlying cause of these slow kinetics.

A straightforward explanation for slow dispersant adsorption kinetics at high Span 80:DOSS ratios would be that Span 80 is very hydrophobic, and thus has a much lower affinity for the bulk aqueous phase than do hydrophilic surfactants like DOSS and Tween 80. Another possible contributing factor is that pure Span 80 is known to facilitate water-in-oil emulsification,[72] which could enable dispersant to adsorb to the oil-water interfaces of water droplets within the oil phase and therefore slow its adsorption to the bulk oil-water interface even further. In this work, however, Span 80 was blended with varying amounts of Tween 80 and/or DOSS to make dispersants which, based on the widely used Hydrophilic-Lipophilic Balance (HLB) system developed by Griffin[73] for classification of nonionic surfactants, were all too hydrophilic to favor water-in-oil emulsification of a clean oil phase. (The HLB system assigns a numerical value between 0 (fully hydrophobic) and 20 (fully hydrophilic) to every nonionic surfactant (based on the functional groups it contains) to denote its overall "hydrophilicity." HLB values are assigned to mixtures by computing the mass-weighted average of the HLB values of surfactants in the mixture.) According to Griffin, surfactants or mixtures of surfactants with HLB values in the range 4-6 are usually water-in-oil emulsifiers, whereas HLB values of 8-18 generally indicate oil-in-water emulsifiers. Given HLB values for Span 80

and Tween 80 of 4.3 and 15.0,[73] respectively, the HLB of the most hydrophobic surfactant mixture characterized in these experiments, 60 wt% Span 80 and 40 wt% Tween 80, is 0.6*4.3 + 0.4*15.0 = 8.6, which makes it an oil-in-water emulsifier. Nevertheless, crude oil is rich in hydrophobic surface-active compounds, such as asphaltenes and resins,[13] which may interact with Span 80-rich dispersants to promote water-in oil emulsification in spite of the presence of more hydrophilic surfactants. Thus, it is possible that high Span 80 concentrations result in slow dispersant adsorption to the bulk oil-water interface in part because dispersant is adsorbing to the surfaces of emulsified water droplets within the oil phase instead.

Another potential cause of the slow interfacial adsorption of Span 80-rich dispersants arises from the fact that DOSS is well known to form thermodynamically stable "reverse micelles" in oil which solubilize water into their highly polar cores, both on its own and when mixed with Tween 80 and/or Span 80. Paul and Mitra[39] found that when Span 80 was added to DOSS/isopropyl myristate/water mixtures, the maximum water-to-surfactant ratio became higher than that of pure DOSS reverse micelles for all mixture compositions tested (0-80 wt% Span 80) and peaked (at 30 wt% Span 80) at more than 2.5 times the pure DOSS reverse micelles' water-to-surfactant ratio. In contrast, Tween 80 was found in a later, similar paper[74] to increase the water-to-surfactant ratio in DOSS/isopropyl myristate/water only when Tween 80-DOSS mixtures contained 0-10 wt% Tween 80, and the peak water-to-surfactant ratio, found at 5 wt% Tween 80, was only ~30% greater than that of pure DOSS reverse micelles. Since the South Louisiana crude oil used in this work is predominantly composed of aliphatic hydrocarbons,[13] then, Span 80 is expected to stabilize dispersant reverse micelles containing DOSS in the oil phase by significantly increasing the amount of water they solubilize, whether or not a macroscopic water-in-oil emulsion is formed in the slick by bulk turbulence. At low concentrations of Span 80, this facilitates dispersant action by preventing all of the surfactants from leaching into the seawater before the oil can be dispersed, while at higher Span 80 concentrations, it slows dispersant adsorption to such an extent that the interface cannot rapidly dilate in response to turbulent shear, and thus dispersion effectiveness becomes very low.

Finally, the data in Figure 3.8 are consistent with the earlier conclusion, based on Figures 3.3-3.5, that relatively rapid loss of DOSS from oil into seawater drives the dynamics of the IFT of DOSS-Tween 80 blends. Oil treated with 0:60 DOSS:Span 80 dispersant contains no DOSS, and therefore even after initial IFT decline has ended, its IFT continues to decline slightly for hours, from 0.08 mN/m at 90 min to 0.065 mN/m at 240 min, despite the fact that the 0.16 µL oil droplet being characterized is surrounded by ~30 mL of saltwater. The absence of an eventual rise in IFT due to surfactant loss from Span 80/Tween 80-treated oil is as expected based on previous findings[62, 64, 65] that loss of Tween 80 from the oil-water interface into saltwater occurs at very low rates. On the other hand, for 10:50 DOSS:Span 80 dispersant, a steady rise in IFT clearly emerges once the initial transient is completed, and for 50:10 DOSS:Span 80, this rise dominates the IFT dynamics just as it does for pure Tween 80/DOSS blends. Thus, the data shown in Figure 3.8 support the proposition that the relatively rapid loss of DOSS from the oil to the aqueous phase drives the dynamics of IFT for dispersants containing mixtures of DOSS, Tween 80, and Span 80.

3.4 Conclusions

Three interfacial phenomena have a significant impact on the effectiveness of dispersants based on Tween 80, Span 80, and DOSS: (1) the initial IFT; (2) the rate and direction of change in IFT as DOSS is lost from the oil to the aqueous phase, and (3) slow adsorption of dispersants with a high Span 80:DOSS ratio to the oil-water interface. These results suggest that employing sufficient DOSS is crucial to the rapid stabilization of new interface formed during the breakup of dispersant-treated oil, while Tween 80 and Span 80 allow low IFT (< 1mN/m) to be maintained for hours, even at oil:water volume ratios of 1:1000 or greater, by increasing the stability of the dispersant mixture in oil. Future work will focus on quantification of interfacial adsorption kinetics of blends of Tween 80, Span 80, and DOSS, direct measurements of surfactant loss from dispersant-treated oil into salt water, and characterization of the reverse micelles and/or other microstructures which are believed to control surfactant transport from the oil phase to the interface.

All of this information will be critical in future efforts to design new, more effective and/or less toxic dispersants, as well as in gaining a better understanding of the environmental impacts of chemical oil dispersants.[75] It should also find a wide range of applications beyond crude oil spill dispersion (e.g., in pharmaceutical and cosmetic emulsions employing Tweens, Spans, and/or DOSS).

Chapter 4: Water-in-oil microstructures formed by marine oil dispersants in a model crude oil*

4.1 Introduction

Oil dispersants are mixtures of surfactants and solvents which are applied to marine oil spills in order to facilitate the emulsification, dilution, and eventual biodegradation of the oil in the ocean.[13, 14] Dispersant-treated oil generally contains about 1-5 wt% surfactant,[11, 14, 40] which raises the question of whether dispersants form water-in-oil (W/O) microstructures with seawater in treated oil slicks and, if so, how such microstructures influence the dispersion of crude oils into seawater.

In a prior work,[54] we explored the relationship between dispersant effectiveness (the fraction of a dispersant-treated slick dispersed into seawater by an agitation protocol) and interfacial tension (IFT) for dispersants composed of blends of DOSS (dioctyl sodium sulfosuccinate), Tween 80 (PEO_{20}-sorbitan monooleate), and Span 80 (sorbitan monooleate). DOSS, Tween 80, and Span 80 are of interest because they have been used as primary surfactants in oil dispersants around the world for decades.[11, 13] The most effective of these DOSS/Tween 80/Span 80 surfactant blends exhibited two characteristics: (1) they produced very low oil-water IFTs ($<10^{-4}$ mN/m), and (2) they were relatively DOSS-rich. The crucial role of DOSS in effective crude oil dispersion is highlighted most strikingly by the fact that, although surfactant blends with DOSS:Tween 80:Span 80 ratios of both 40:40:20 and 20:40:40 produced IFTs $<10^{-4}$ mN/m, the 40:40:20, DOSS-rich surfactant blend exhibited 80-85% dispersion effectiveness, whereas the 20:40:40, Span 80-rich surfactant blend exhibited <10% dispersion effectiveness.

The low effectiveness of dispersants with low DOSS:Span 80 ratios was attributed in part to their slow rate of adsorption to the oil-water interface. Upon crude

* This chapter was adapted from the publication: Riehm, D. A.; Rokke, D. J.; McCormick, A. V. Water-in-Oil Microstructures Formed by Marine Oil Dispersants in a Model Crude Oil. *Langmuir* **2016**, *32*, 3954-62. DOI: 10.1021/acs.langmuir.6b00643.

The underlying raw data is publicly available through GRIIDC (DOI: 10.7266/N7VT1Q2D).

oil-seawater contact, crude oil treated with these dispersants exhibited an initial decline in IFT lasting tens of minutes, compared with tens of seconds or less for crude oil treated with high DOSS:Span 80 ratio dispersants. In order to understand why decreasing the DOSS:Span 80 ratio in a DOSS/Tween 80/Span 80 dispersant slows interfacial adsorption so dramatically, it is important to know whether or not these surfactants form W/O microstructures in the crude oil, and what the size and shape of any such microstructures are.

DOSS,[76] like a number of other surfactants,[77, 78] is well-known to form monodisperse spherical W/O microstructures in nonpolar solvents above its critical micelle concentration of ~1 mM[38] (~0.05 wt%), which is well below typical surfactant concentrations (1-5 wt%) in dispersant-treated oil spills. In contrast, Tween 80 is insoluble in most nonpolar solvents[79] and Span 80 is generally observed to form polydisperse microstructures in oils,[80] as are mixtures of Tween 80 and Span 80.[81, 82] Mixed DOSS/Tween 80/Span 80 W/O microstructures have not previously been studied, but Paul and Mitra[39] report that blends of Span 80 and DOSS in paraffinic solvents, and blends of Tween 80 and DOSS in aromatic solvents, exhibit strong water solubilization maxima at high DOSS:nonionic surfactant molar ratios (70:30 and 90:10, respectively), suggesting that these two sets of surfactants form DOSS-rich mixed W/O microstructures. W/O microstructures formed by blends of DOSS with other nonionic surfactants[83-86] are spherical and generally larger than pure DOSS W/O microstructures at the same water:surfactant molar ratio (ω), as nonionic surfactants typically have larger hydrophilic groups and/or smaller hydrophobic groups than DOSS which favor reduced interfacial curvature.

Most of these studies of mixed DOSS/nonionic W/O microstructures, however, measure "mean droplet size" using dynamic light scattering (DLS) without also reporting polydispersity index (PDI), which is a DLS metric for variance in particle size (vide infra), or otherwise characterizing microstructure dispersity (e.g., using cryogenic electron microscopy). Kundu and Paul[85] do report both mean diameter and PDI for DOSS/Tween 85 W/O microstructures in a paraffinic solvent (isopropyl myristate) as measured via dynamic light scattering (DLS). They report that as the DOSS:Tween 85 ratio is decreased, microstructure size and PDI increase, and that increasing ω also

increases microstructure size but decreases PDI. However, most of the surfactant-oil-seawater mixtures they characterize contain microstructures with PDI > 0.1, generally considered[59, 87, 88] to be the threshold between a relatively monomodal particle size distribution and a polydisperse one, and almost half of their systems exhibit PDI > 0.2. This is problematic because a scattering-derived "mean diameter" is a relatively limited description of a polydisperse system of particles, and raises the question of whether other DOSS/nonionic W/O microstructures characterized via scattering in prior work are similarly polydisperse.

In this work, direct imaging studies using cryogenic transmission electron microscopy (cryo-TEM) have been conducted to complement characterization of DOSS/Tween 80/Span 80 microstructures' size, shape, and dispersity via DLS. Additionally, changes in microstructures' size and PDI have been observed for 7 days following the initial preparation of the samples, in order to study the potentially slow equilibration of such a complex W/O microstructure system which, to the best of our knowledge, has not been investigated in any prior work. Unfortunately, characterizing these dispersant microstructures in crude oil would be very challenging, as crude oils are typically opaque and contain naturally surface-active and aggregate-forming compounds,[89] making it difficult to identify any microstructures formed in crude oil by dispersants. In this work, therefore, blends of DOSS, Tween 80, and Span 80, along with synthetic seawater, are dissolved in a model oil in which the surfactant blends produce dynamic oil-seawater IFTs similar to those which they produce in crude oil, enabling characterization of any W/O microstructures' size, shape, and PDI/dispersity using DLS and cryo-TEM. As alluded to earlier, these techniques complement each other well, as cryo-TEM enables direct, model-free observation of a few dispersant aggregates' shapes and sizes, while DLS measures the intensity-weighted average diameter and dispersity of all of the aggregates in a macroscopic volume of dispersant-treated oil.

4.2 Experimental

4.2.1 Materials

The model oil standing in for crude oil in this work is a blend of 83.5 wt% Isopar M (a mixture of branched isoparaffins in the C_{11}-C_{16} range)[90], 10 wt% toluene, and 6.5 wt% naphthalene. Its transparency enables characterization of dispersant microstructures using dynamic light scattering, and its viscosity (3.1 cSt @ 20 C) is low enough to make cryo-TEM feasible. The high concentrations of branched isoparaffins found in Isopar M are also important to ensure that the oil can be vitrified in liquid nitrogen during cryo-TEM sample preparation.[91] The incorporation of aromatics into the model oil is necessitated by the insolubility of Tween 80 in paraffinic solvents. A paraffin:aromatic ratio of 5:1, similar to the paraffin:aromatic ratios found in South Louisiana crude oil,[92, 93] has been selected so that our results will better inform the design of dispersants for use in future Gulf of Mexico spills—a primary aim of this work. Isopar M (Seacole Chemical), toluene (Fisher Scientific), and naphthalene (Acros Organics) were used as received.

Synthetic seawater (SSW) was prepared by adding 427 mM NaCl, 55 mM $MgCl_2$, and 27 mM Na_2SO_4 to distilled water—a simplified version of the SSW formulation reported by Kester et al.[66] For seawater added to cryo-TEM samples, 427 mM CsCl was substituted for 427 mM NaCl to improve electron mass contrast between oil and water phases. Magnesium chloride (Fisher) was used as received. Sodium chloride (Sigma-Aldrich) or cesium chloride (Sigma) and sodium sulfate (Macron Chemicals) were baked for 5 hrs at 500 °C to remove contaminants before being added to the synthetic seawater. Tween 80 (Sigma-Aldrich) and Span 80 (Sigma) were filtered using 0.1 μm Whatman PTFE syringe filters before use. As described by Zulauf and Eicke,[76] DOSS (Sigma) was dissolved in methanol (Sigma-Aldrich) with active charcoal (Sigma-Aldrich) (one part DOSS, one part active charcoal, and three parts methanol by weight), stirred for two hours, centrifuged to remove the charcoal and filtered to remove insoluble salts, and then dried at 60-70 °C under vacuum until no further mass loss was observed.

All surfactant blend compositional ratios in this work (e.g., 50:50:0 DOSS:Tween 80:Span 80) are given as weight ratios; seawater:surfactant ratios (ω) are given as molar ratios, in accordance with convention.[76, 85] Calculations of the molar mass of synthetic

seawater may be found in the Supporting Information; for SSW made using NaCl, a molar mass of 18.28 g/mol was calculated, while for SSW made using CsCl, a molar mass of 19.13 g/mol was calculated.

4.2.2 Spinning Drop Tensiometry

Dynamic IFT was measured between synthetic seawater and various surfactant-oil-seawater mixtures, using a spinning drop tensiometer originally built by D. Joseph,[68] in order to compare dynamic IFT exhibited by DOSS/Tween 80/Span 80 blends at a model oil/seawater interface with dynamic IFT previously observed[54] for DOSS/Tween 80/Span 80 blends at the crude oil/seawater interface. The surfactant-oil-seawater mixtures were solutions of DOSS, Tween 80, Span 80, and seawater in the model crude oil, containing a total of 2 wt% surfactant and 0.5 wt% seawater, corresponding to a seawater:surfactant molar ratio $\omega \approx 10$. (Tween 80 was found to be insoluble in surfactant-model oil blends without the addition of at least 0.25-0.5 wt% seawater, depending on the surfactant blend.) In a typical experiment, a 1-5 uL droplet of surfactant-oil-seawater mixture was injected using s syringe into a tensiometer tube containing ~20-30 mL of synthetic seawater. The tube was then spun about its longitudinal axis at a speed between 300 RPM and 1500 RPM, depending on the oil-water IFT exhibited by that surfactant-oil-seawater mixture, so that the droplet was pulled to the center of the tube and elongated by centripetal forces (sometimes unavoidably breaking up into several smaller droplets due to extremely low IFTs). Once the surfactant-oil-seawater mixture reached gyrostatic equilibrium (typically 1-2 minutes after it was first injected into the sample tube), its oil-water IFT was determined from images of the droplet's profile, according to the method of Princen et al.[5]

4.2.3 Dynamic Light Scattering

The size and polydispersity index (PDI) of W/O microstructures formed by blends of DOSS, Tween 80, Span 80, and seawater in model oil has been measured via dynamic light scattering (DLS) in a NanoBrook ZetaPALS Particle Size Analyzer (Brookhaven Instruments Corporation). Samples were characterized at 20 ± 1 °C in a 1 x 1 x 4 cm glass fluorescence cuvette, using a laser wavelength of 659 nm and a scattering angle of 90°. Total surfactant concentration in surfactant-oil-seawater mixtures was 2 wt%, as in

the IFT measurements, and seawater concentration was varied from a minimum soluble ω ($\omega_{min} \approx$ 5-10) up to the maximum soluble ω in each surfactant-oil mixture, which ranged from ω = 15 to ω = 40. 1 mL of each surfactant-oil-seawater mixture of interest was blended together with a stirbar at 150 RPM for 24 hrs (or until a clear solution formed) in a water bath at 20 ± 0.5 °C. Samples were then stored in the same water bath at 20 ± 0.5 °C, and DLS measurements were conducted at intervals of 1, 2, 4, and 7 days after the start of mixture preparation.

Particle sizes and polydispersity index were calculated from the scattered intensity autocorrelation function using the "cumulant analysis" method, described by Brown et al,[59] which yields the moments of the distribution of normalized autocorrelation function decay rates. The first moment of this distribution is the z-average autocorrelation function decay rate, from which it is possible to calculate the z-average diffusion coefficient for the scattering particles and thus (assuming the particles are spherical, dilute, and non-interacting) their z-average hydrodynamic diameter. The second moment of this distribution is its variance, often termed the "polydispersity index" (PDI), which can serve as a metric of the variance in the particles' sizes.

4.2.4 Cryogenic Transmission Electron Microscopy

Cryogenic transmission electron microscopy (cryo-TEM) was used to verify that the W/O microstructures observed in dispersant-oil-seawater mixtures via DLS (a) were spherical; (b) had diameters consistent with those calculated from the DLS correlation function; and (c) had a dispersity consistent with the PDI calculated from the DLS correlation function. Surfactant-oil-seawater mixtures were prepared in the same manner as for DLS, except that cesium chloride was substituted for sodium chloride in the synthetic seawater to improve contrast between the oil and aqueous phases during imaging. The acceptability of this substitution was validated by dynamic light scattering data (see Supplementary Information), which showed no discernible difference between the measured diameters of microstructures in samples prepared using NaCl seawater and using CsCl seawater which were otherwise identical in composition. 2-3 µL of sample was deposited on a lacey carbon film supported by a 300 mesh Cu grid (Electron Microscopy Sciences) which was mounted on tweezers in an FEI Mark III Vitrobot

controlled environment vitrification system. The sample chamber in the Vitrobot was maintained at 20 °C and relative humidity was kept to a minimum. Once the sample had been deposited, the solution was blotted down to a film thin enough to be transparent to the TEM electron beam, and then plunged into liquid nitrogen. (Liquid nitrogen is a poor cryogen, but can vitrify highly branched hydrocarbons,[91] which is one reason why Isopar M, composed of branched isoparaffins, was chosen as the main constituent of the model oil, as discussed earlier.) After vitrification, samples were transferred into a Gatan 626 cryo-holder and imaged using an Eagle 2k CCD camera (FEI) at 120 kV in an FEI Tecnai G2 Spirit BioTWIN transmission electron microscope. Images were processed using TEM Imaging and Analysis software (FEI), and microstructures' diameter and dispersity were measured by hand. Dispersity (Đ), another metric of variance in particle size, is defined by $Đ = M_w/M_n$ in which M_w and M_n are, respectively, the weight-average and number-average masses of the microstructures and d is microstructure diameter.[94]

4.3 Results and Discussion

4.3.1 Dispersant-oil mixture IFT: Crude oil vs. Model oil

Figure 4.1 shows that IFT between seawater and crude oil treated with DOSS/Tween 80/Span 80 surfactant blends resembles IFT at model oil-seawater interfaces treated with similar surfactant blends. Most notably, surfactant mixtures containing 50 wt% Tween 80, and a DOSS:Span 80 ratio near 1:1 produce very low IFTs ($<10^{-4}$ mN/m) between seawater and model oil. As depicted in Figure 4.1a, these surfactant mixtures are compositionally similar to the surfactant blends containing 40 wt% Tween 80 and a DOSS:Span 80 ratio near 1:1 which we have previously shown[54] to produce very low IFTs ($<10^{-4}$ mN/m) between seawater and crude oil. In Figure 4.1b, the oil/seawater IFT of model oil treated with surfactant blends containing 50:50 Tween 80:[DOSS + Span 80] (left side) is compared with data from a prior work of ours[54] on the oil/seawater IFT of crude oil treated with surfactant blends containing 60:40 Tween 80:[DOSS + Span 80] (right side). In general, surfactant blends containing similar DOSS:Span 80 ratios exhibit IFTs of a similar order of magnitude in crude oil and in model oil.

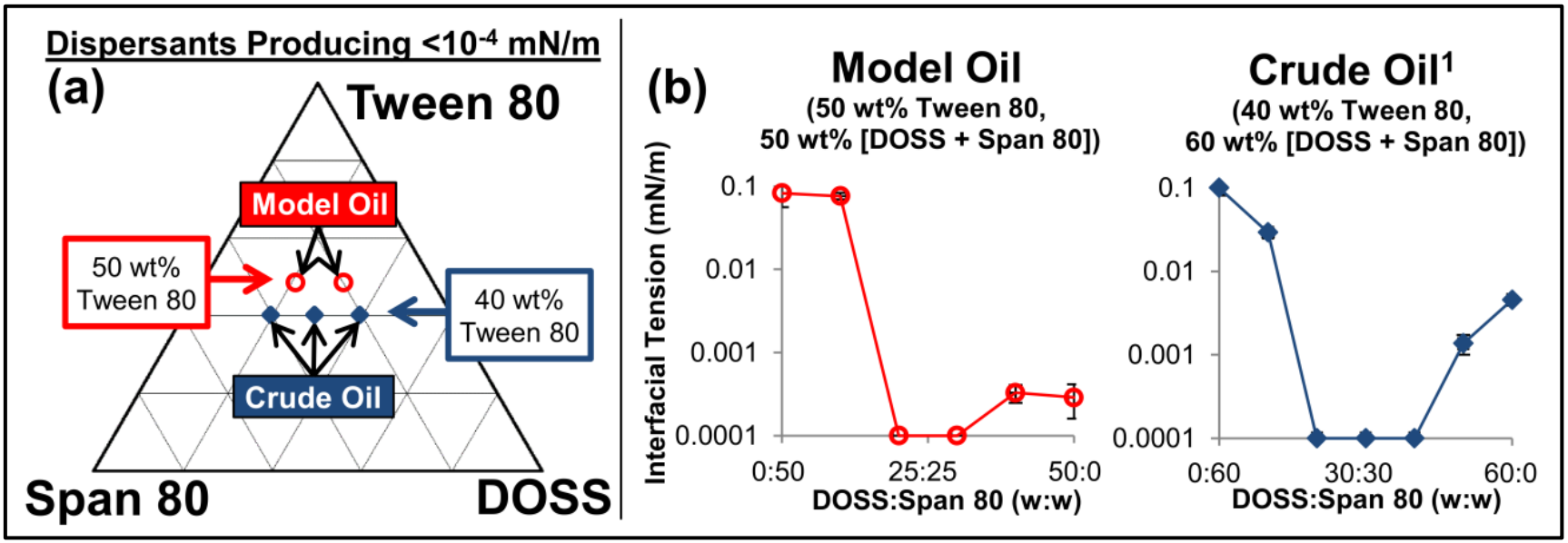

Figure 4.1 (a) Tween 80:Span 80:DOSS dispersant compositional diagram marked at compositions which produce IFT $<10^{-4}$ mN/m in crude oil (blue) and in model oil (red).
(b) Initial IFTs between seawater and Tween 80/Span 80/DOSS blends dissolved in model oil (left, red) and in crude oil (right, blue). Surfactant blends in model oil were 50 wt% Tween 80; surfactant blends in crude oil were 40 wt% Tween 80. Crude oil IFT data is from Figure 3.5. IFT was measured in triplicate at each composition; error bars extend one standard error above and below each mean. Data plotted at 10^{-4} mN/m indicate IFT $<10^{-4}$ mN/m, and correspond to the points in Figure 4.1a.

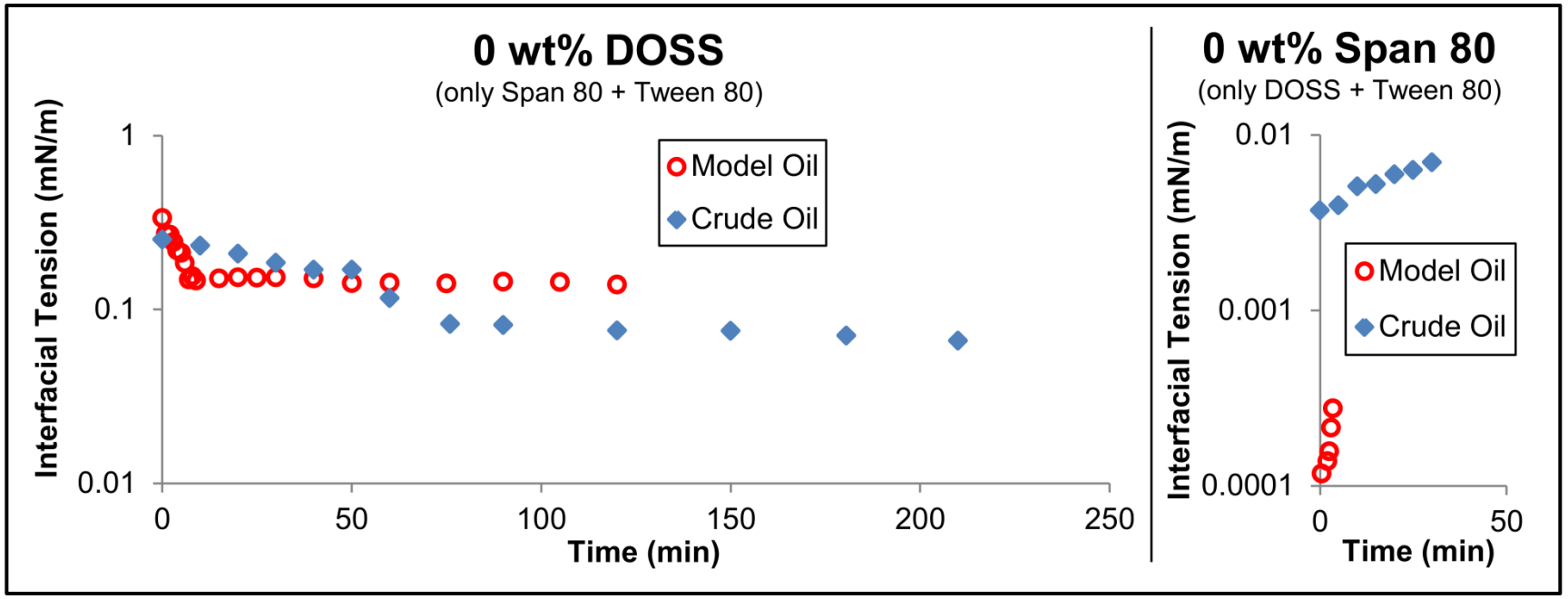

Figure 4.2 Dynamic IFT between seawater and Tween 80/Span 80/DOSS blends dissolved in model crude oil (o) and in crude oil (♦). Surfactant blends in model oil were 50 wt% Tween 80 and either 50 wt% DOSS (left) or 50 wt% Span 80 (right). Surfactant blends in crude oil were 40 wt% Tween 80 and either 60 wt% DOSS (left) or 60 wt% Span 80 (right). t = 0 coincides with the start of image recording for each droplet once tensiometer spinup is complete (1-2 minutes after droplets' initial contact with seawater). Crude oil IFT data is from Figure 3.7.

Figure 4.2 shows that dynamic IFT at crude oil-seawater interfaces treated with various surfactant blends also strongly resembles that produced at model oil-seawater interfaces treated with similar surfactant blends. On the left side of Figure 4.2, dynamic IFT produced by crude oil treated with a 60:40 DOSS:Tween 80 surfactant blend isplotted alongside dynamic IFT produced by model oil treated with a 50:50 DOSS:Tween 80 surfactant blend. For both of these systems, the initial decline in IFT as surfactants adsorb to the oil-water interface is so fast that it is completed within the 1-2 minutes required to initially load and spin up the tensiometer. Thus, only a steady rise in IFT with time is observed, until droplets become too spherical for IFT measurement. This behavior contrasts sharply with that observed on the right side of Figure 4.2, in which dynamic IFT produced by treating crude oil with 60:40 Span 80:T80 dispersant is plotted alongside dynamic IFT produced by treating model oil with 50:50 Span 80:T80 dispersant. These systems exhibit a much slower initial decline in IFT down to a reproducible minimum, followed by a plateau in IFT at that minimum for hours.

Thus, DOSS-rich dispersants exhibit much faster IFT dynamics than Span 80-rich dispersants, both during the initial adsorption of surfactants to a clean oil-water interface and during the long-term desorption and loss of surfactants from the oil-water interface into bulk seawater. The fact that DOSS-rich dispersants' IFT rises faster than that of Span 80-rich dispersants in the long term has been attributed in our prior work[54] to the fact that DOSS desorbs from an oil-water interface into seawater much more readily than Tween 80 (as shown by Kirby et al.[65]) or hydrophobic Span 80, depleting surfactant from dispersant-treated oil droplets over time. The dynamics of dispersants' initial IFT transients as they first adsorb to a clean oil-water interface, on the other hand, are presumably controlled by rates of surfactants' adsorption from bulk oil to the interface, which in turn depend in part on the characteristics of dispersant W/O microstructures which this work aims to elucidate.

The qualitative similarities between oil-seawater IFT exhibited by crude oil and by model oil when treated with similar DOSS/Tween 80/Span 80 blends also suggest that, while the surface-active components of crude oil certainly have a non-negligible effect on dispersant-treated oil-seawater IFT, our model oil is ultimately an acceptable surrogate for crude oil in the study of these surfactants' microstructures. This lends

further credence to the idea that studies of surfactant blends in model oil systems can be of use in improving the design of crude oil dispersants.

4.3.2 Solubility of Dispersant and Seawater in Model Oil

Seawater was soluble in each surfactant-oil mixture of interest at seawater:surfactant molar ratios (ω) ranging from a minimum ω, $\omega_{min} \approx$ 5-10, up to a maximum ω, ω_{max}, which varied considerably with the composition of the surfactant blend in the mixture (Figure 4.3). For $\omega < \omega_{min}$, Tween 80 was insoluble in the surfactant-oil-seawater mixtures. For $\omega_{min} < \omega < \omega_{max}$, surfactant-oil-seawater mixtures formed clear solutions exhibiting Rayleigh scattering, which are characterized in detail in this work. For $\omega > \omega_{max}$, mixtures remained turbid, and separated into two phases once mixing stopped. Study of these systems was beyond the scope of this work, due in part to the complexity of so many compounds partitioning between the two phases. However, it was evident that a significant fraction of the volume of lower, water-rich phases was comprised of oil, since they often occupied 10% or more of a mixture's volume despite the fact that surfactants and seawater never collectively constituted more than 5% of any mixture's volume. It therefore seems likely that these water-rich phases also contain W/O microstructures which, if this phase were emulsified into an oil slick, might influence oil

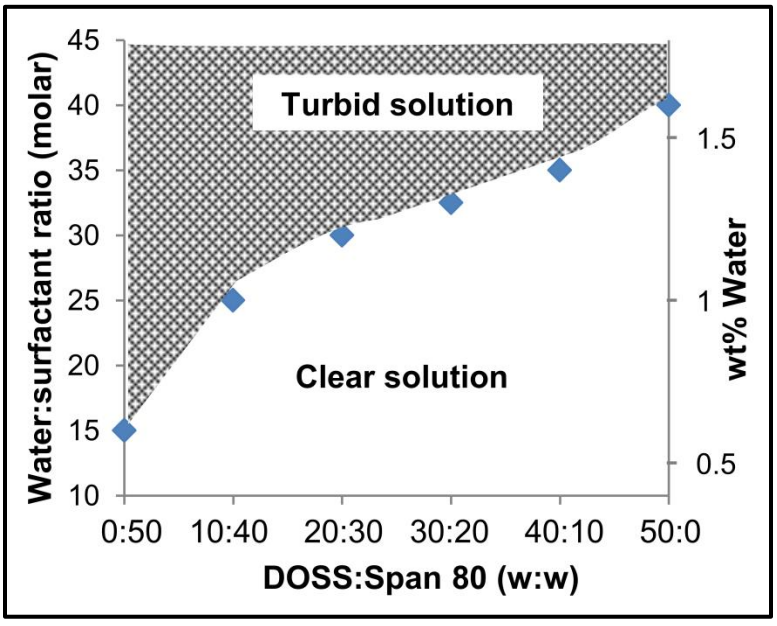

Figure 4.3 Maximum seawater:surfactant molar ratio (ω_{max}) at which seawater forms a clear solution in 2 wt% solutions of DOSS:Tween 80:Span 80 surfactant blends in the model oil. The surfactant blends were 50 wt% Tween 80, 50 wt% [Span 80 + DOSS].

dispersion and the dynamics of oil spill aging processes (such as "mousse"[95] formation). Thus, the composition and structure of such water-rich phases merit further study in future work.

ω_{max} was found to be much higher for DOSS-rich surfactant blends than for Span 80-rich surfactant blends (Figure 4.3). This is expected, since Span 80 is a hydrophobic nonionic surfactant and DOSS is an anionic surfactant known to form inverse micelles which solubilize water in certain nonpolar solvents up to water:surfactant molar ratios of 60 (at 20 °C).[76] Thus, these data simultaneously highlight Span 80's hydrophobicity as a possible reason for the slower interfacial adsorption of Span 80-rich surfactant blends and hint at the differences between DOSS-rich and Span 80-rich W/O microstructures, suggesting that it is necessary to characterize these microstructures in order to fully understand dispersant adsorption dynamics.

4.3.3 Dispersant Microstructures: Cryo-TEM Imaging

Figure 4.4 shows images of surfactant-oil-seawater mixtures (2 wt% surfactant) which have been vitrified in liquid nitrogen and observed via cryogenic transmission electron microscopy (cryo-TEM). Figure 4.4a shows a Span 80-rich mixture (0:50:50 DOSS:Tween 80:Span 80 surfactant blend with $\omega = 12.5$); Figure 4.4b shows two images of a mixture containing both DOSS and Span 80 (30:50:20 DOSS:Tween 80:Span 80 surfactant blend with $\omega = 25$); and Figure 4.4c shows a DOSS-rich mixture (50:50:0 DOSS:Tween 80:Span 80 surfactant blend with $\omega = 25$). The dark network bounding the lighter areas is the lacey carbon backing on the TEM grid; the clear areas are vitrified model oil; and the dark spots are W/O microstructures formed by the surfactant blend and seawater. The sodium chloride in the seawater was replaced with cesium chloride in the imaged sample(s) to improve mass contrast between the microstructures and the model oil; dynamic light scattering data in the Supporting Information shows that this substitution does not significantly change the microstructures' size.

It is evident from Figure 4.4 (and similar images in the Supporting Information) that all of these surfactant-oil-seawater mixtures contain spherical W/O microstructures.

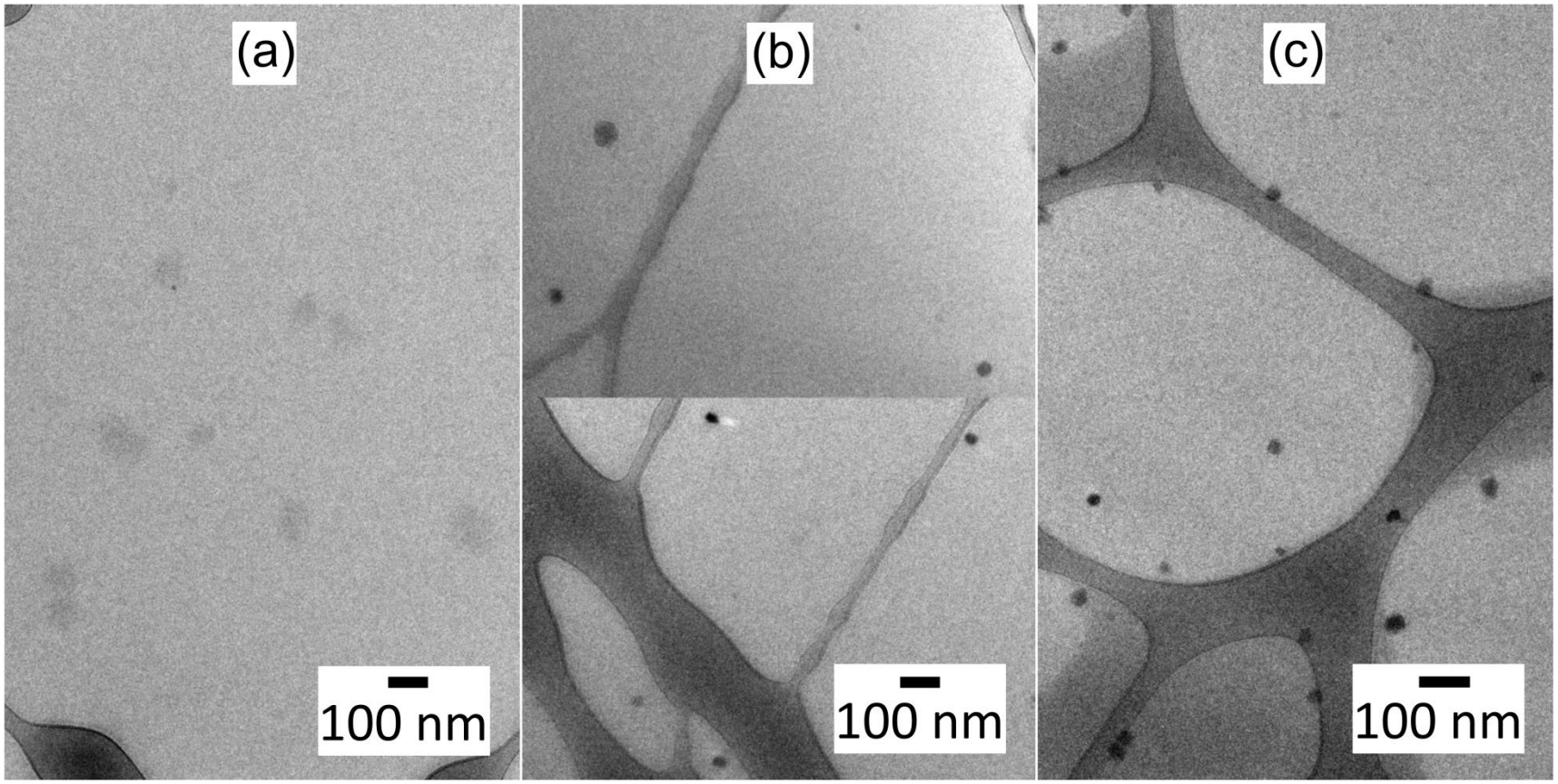

Figure 4.4 Cryo-TEM images of W/O microstructures formed in vitrified surfactant-oil-seawater mixtures, containing, from left to right: (a) 0:50:50 DOSS:Tween 80:Span 80, ω = 12.5; (b) 30:50:20 DOSS:Tween 80:Span 80, ω = 25 [two images]; and (c) 50:50:0 DOSS:Tween 80:Span 80, ω = 25. Additional images of these and other surfactant-oil-seawater mixtures are available in Appendix B.

The DOSS-rich microstructures in Figure 4.4c exhibit a monomodal distribution with a number-weighted mean diameter of 31 ± 5 nm and a low dispersity, Đ = 1.22, corresponding to a narrow particle size distribution[59, 96, 97] (Đ = M_w/M_n in which M_w and M_n are, respectively, the weight-average and number-average masses of the particles[94]). These DOSS/Tween 80 microstructures are significantly larger than the 10-15 nm diameter W/O microstructures reported by Zulauf and Eicke[76] for DOSS in isooctane at ω = 25, consistent with prior studies of other DOSS/nonionic W/O microstructures[83-85] and with the expected effect of Tween 80 molecules' large hydrophilic head groups on interfacial packing. The 30:20 DOSS:Span 80 microstructures in Figure 4.4b, thoughmore sparsely distributed, exhibit a similar morphology. The Span 80-rich microstructures in Figure 4.4a are larger (102 ± 23 nm) and more polydisperse (Đ = 1.34) than the DOSS-rich microstructures in Figures 4.4b and 4.4c. The lower contrast they exhibit is likely due to their lack of DOSS, as each DOSS molecule contributes a sulfur atom and a sodium cation to the mass contrast of its microstructure, whereas Span 80 and Tween 80, containing only carbon, hydrogen, and oxygen, produce little mass contrast with the surrounding hydrocarbon solvent.

Thus, as DOSS is replaced with Span 80 in the surfactant blend, the microstructures' size and dispersity increase, but their shape remains spherical. The size increase is expected based on the larger hydrophilic group and more linear shape of Span 80 compared with DOSS, as both of these characteristics favor less curvature at the interface and, thus, larger microstructures. The dispersity increase is also expected given the monodispersity of DOSS W/O microstructures,[76] in contrast with the polydispersity of Tween 80/Span 80 microstructures,[81, 82] and the wide range of isomers present in Tween 80 and Span 80.[98, 99] Finally, the spherical shape, expected because both DOSS and Tween 80/Span 80 blends are known to form spherical microstructures[76, 81, 82], validates complementary characterization of the lower dispersity, DOSS-rich microstructures via dynamic light scattering, which is ideally employed to study monodisperse spherical particles.

An important caveat to these results is that in actual crude oil, the morphology of these microstructures would be influenced by native surface-active components such as asphaltenes, resins, and waxes. One natural follow-up to this work might therefore be to

add such compounds to the model oil, at low enough concentrations that cryo-TEM and perhaps even DLS could still be performed on the sample, and observe any changes in dispersant microstructures. It might also be possible to image dispersant microstructures in one or more crude oils using cryo-SEM or freeze fracture TEM instead of cryo-TEM, since the former two techniques do not require a low-viscosity sample and have previously been employed to image microstructures in crude oil.[100, 101]

4.3.4 Dispersant Microstructures: Dynamic Light Scattering

4.3.4.1 Low-polydispersity-index microstructures

Since cryo-TEM confirms that W/O microstructures in our surfactant-oil-seawater mixtures are spherical, dynamic light scattering (DLS) has been used to study microstructure size and polydispersity index (PDI) in macroscopic volumes of these mixtures, complementing model-free observation of only a handful of microstructures via cryo-TEM. DLS data were collected at DOSS:Span 80 ratios ranging from 50:0 to 0:50 and at ω values which, depending on the surfactant blend, ranged as low as 10 and as high as 40. However, PDI < 0.1, indicating low particle dispersity[59, 87, 88] and a good single-exponential fit to the DLS autocorrelation function, was only observed for DOSS:Span 80 ratios of 30:20 or higher and $\omega \geq 20$. Thus, only microstructure diameters and PDIs from this compositional region are plotted in Figures 4.5-4.7. Figure 4.5 shows the measured diameters and PDIs of W/O microstructures formed by 2 wt% solutions of 50:50:0 DOSS:Tween 80:Span 80 blends in model oil with values of ω ranging from 20 to 40, at intervals of 1, 2, 4, and 7 days after their initial preparation. Figures 4.6 and 4.7 show similar data, but for a range of DOSS:Tween 80:Span 80 ratios at, respectively, ω = 25 (Fig. 6) and a range of ω values which follow maximum seawater solubility (shown in Fig. 3) as a function of surfactant blend composition (Fig. 7). Similar DLS data for other surfactant-oil-seawater mixtures exhibiting PDI < 0.1 may be found in the Supporting Information.

Analysis of these microstructures' diameters as a function of surfactant blend composition and ω is complicated by the fact that microstructure diameters plotted in Figures 4.5-4.7 shrink continuously over the 7-day period for which samples were studied. Ending DLS characterization of microstructure after 7 days was deemed

reasonable because dispersant-treated oil slicks are generally dispersed within a few days of dispersant application,[53] and thus any further changes which the microstructures' morphology might undergo over weeks or months are presumably irrelevant to the functionality of oil spill dispersants. However, the stability of all DLS samples against eventual phase separation was validated by keeping the samples for 6-12 months after characterization and observing visually that phase separation did not occur. Thus, surfactant-oil-seawater mixtures which initially form clear solutions are also stable against phase separation in the long term.

There are two overarching trends for the microstructure diameters plotted in Figures 4.5-4.7: Diameters reach 20-40 nm by day 7; and microstructure shrinkage is slower for surfactant-oil-seawater mixtures that are closer to their seawater solubility limit. That is, microstructure diameter shrinks more slowly for higher ω at a given dispersant blend composition (Figure 4.5) and for lower DOSS:Span 80 ratios at a given ω (Figure 4.6), whereas there is no clear trend in the rate of microstructure shrinkage as DOSS:Span 80 ratio is varied and ω is held close to the maximum soluble ω for each surfactant blend (Figure 4.7). Kundu and Paul[85] analogously report that DOSS/Tween 85 W/O microstructures have 15-40 nm diameters, and that these diameters are larger at higher ω and lower DOSS:Tween 85 ratio, though they do not explore whether the microstructures' diameters change over time. One factor which may drive the microstructures' slow equilibration is the compositional complexity of the characterized systems, which contain 2-3 surfactants, three model oil components, and seawater. Another possible factor is the insolubility of Tween 80 and seawater in model oil, which may inhibit their compositional equilibration between microstructures via molecular diffusion and force them to equilibrate through the relatively slow process of micellar fission and fusion instead.

As alluded to earlier, the most notable trend in PDIs is that, for $\omega \geq 20$, DOSS:Span 80 ratios $\geq$ 30:20, and particle diameters above 20 nm, PDIs remain below 0.1 (Figures 4.5-4.7), indicating[59, 87, 88] a narrow, monomodal distribution of microstructure sizes consistent with the low dispersities observed via cryo-TEM (Figure 4.4) for surfactant-oil-seawater mixtures of similar compositions. This is a significant finding, given that commercially-available Span 80 and Tween 80 are mixtures of a

number of sorbitan-fatty acid esters (also polyoxyethylenated in a variety of ways, in the case of Tween 80) rather than pure compounds.[98, 99]

4.3.4.2 High-polydispersity-index microstructures

On the other hand, for $\omega < 20$; for DOSS:Span 80 ratios lower than 30:20; and for initially monodisperse samples in which particle sizes fall below 20 nm, PDI generally ranges from 0.2 to 0.5, indicating a broad, polydisperse distribution of microstructure sizes. These observations are consistent with trends in PDI reported by Kundu and Paul[85] for DOSS/Tween 85 W/O microstructures: higher PDI at lower DOSS:Tween 85 ratios and at lower ω. Although it is not clear to what extent average particle diameters obtained via DLS are meaningful for such polydisperse microstructures, samples with $\omega < 20$ exhibit apparent mean diameters of < 20 nm, consistent with the observation that monodisperse microstructures which shrink below a 20 nm mean diameter also become polydisperse. Samples with $\omega \geq 20$ and DOSS:Span 80 ratios below 30:20 have apparent diameters ranging from 100-250 nm, consistent with the ~100 nm microstructures in the image of a 0:50:50 DOSS:Tween 80:Span 80 surfactant-oil-seawater mixture in Figure 4.4a.

The rationale for high PDI at low ω and low DOSS:Span 80 ratio is straightforward. Since Tween 80 is insoluble in oil for $\omega < 10$, it seems reasonable to posit that high PDI for $\omega < 20$ is driven by Tween 80 continuing to be water-starved. At low DOSS:Span 80 ratios, the microstructures' high PDI is consistent with prior work[81, 82] and likely derives from the wide range of isomers[98, 99] in Tween 80 and Span 80. It is less obvious why the nearly monodisperse microstructures initially formed in some surfactant-oil-seawater mixtures become more polydisperse once their sizes fall below ~20 nm. Whether this phenomenon is driven by partitioning of the various isomers of Tween 80 and Span 80 into different microstructures over time, by the various isomers of Tween 80 being crowded out of increasingly curved interfaces and forced into microstructures' aqueous cores to different extents, or by some other factor should be investigated in future work.

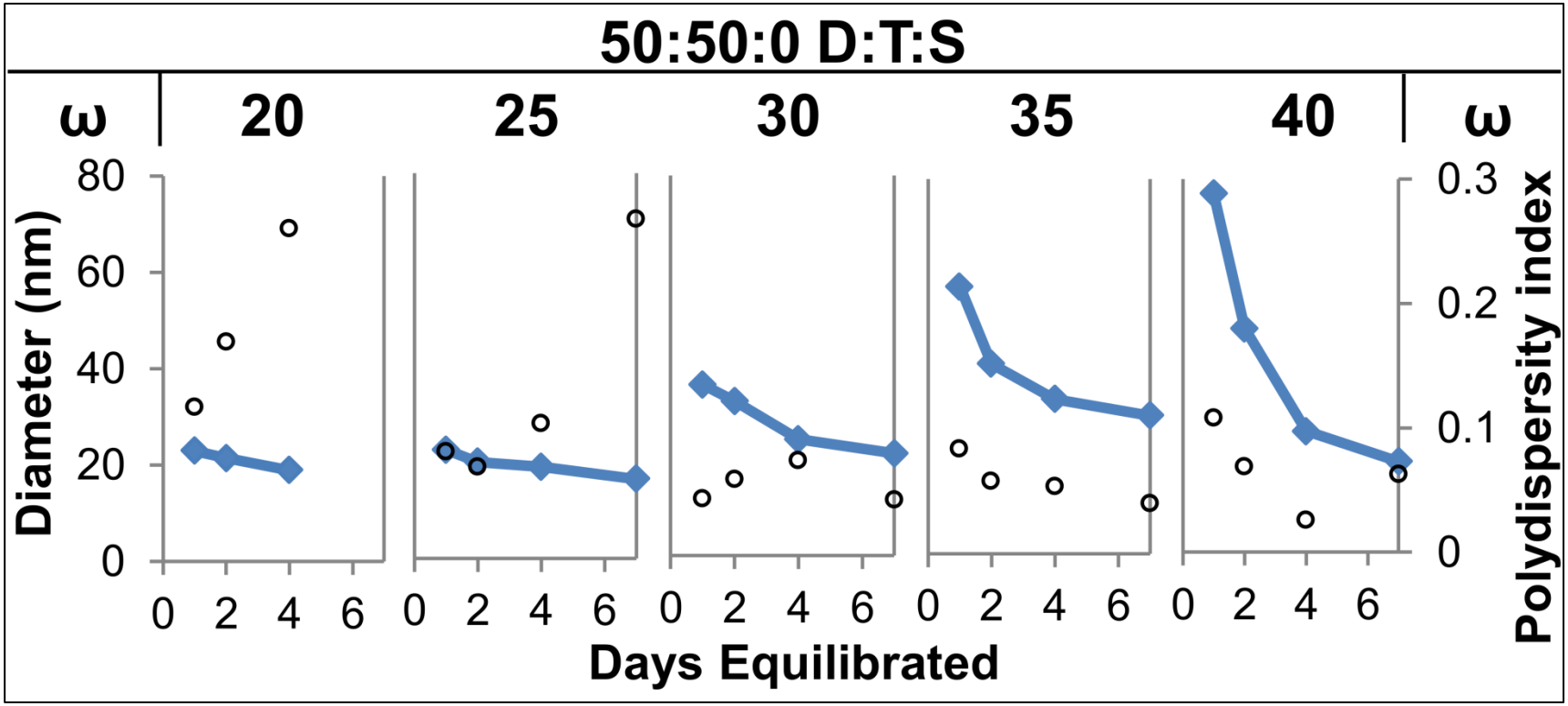

Figure 4.5 Diameter (♦) and polydispersity index (o) of W/O microstructures formed by a 50:50:0 DOSS:Tween 80:Span 80 blend in model oil at ω = 20-40, measured via DLS.

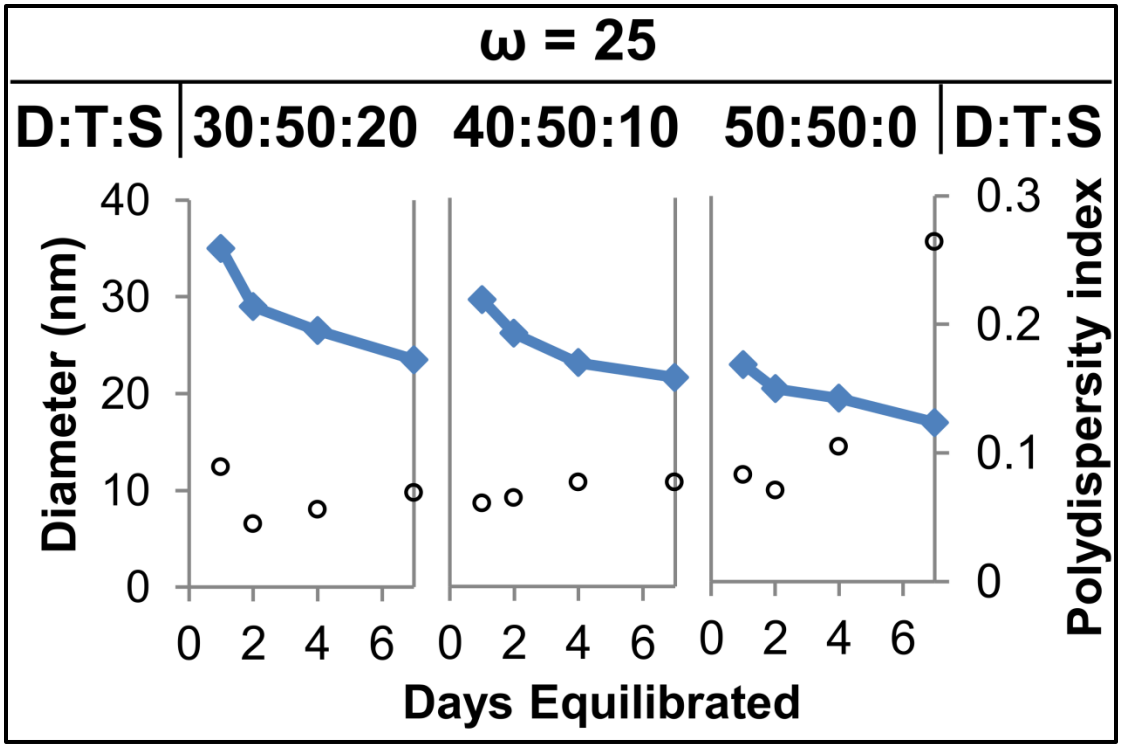

Figure 4.6 Diameter (♦) and polydispersity index (o) of W/O microstructures formed by various DOSS:Tween 80:Span 80 blends in model oil at ω = 25, measured via DLS.

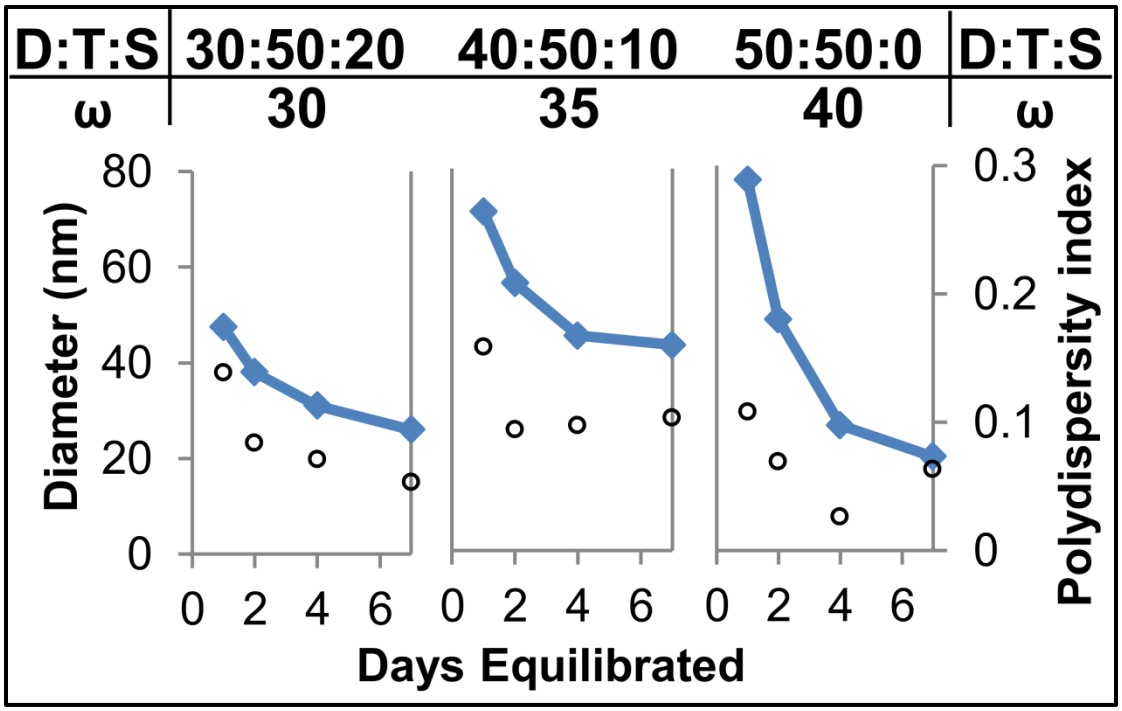

Figure 4.7 Diameter (♦) and polydispersity index (o) of W/O microstructures formed by various DOSS:Tween 80:Span 80 blends in model oil at values of ω near the maximum seawater solubility ω_{max} for each surfactant blend, measured via DLS.

4.3.5 Implications and Future Work

In light of the data presented above on W/O microstructures formed by DOSS/Tween 80/Span 80 blends, it is now possible to consider why DOSS-poor blends of these surfactants exhibit slow initial adsorption to an oil-water interface (Figure 4.2), which has been linked in our prior work[54] to diminished dispersant effectiveness even for DOSS-poor blends which eventually reach very low IFT ($< 10^{-4}$ mN/m). DLS and cryo-TEM indicate that dispersant W/O microstructures' diameters are generally 20-40 nm for DOSS-rich surfactant blends and ≥100 nm for Span 80-rich blends, suggesting one possible explanation: DOSS-poor dispersants form larger W/O microstructures, which take longer to diffuse to the interface. This suggests that effective marine oil dispersants should contain surfactants which, like DOSS, have small hydrophilic heads and wide hydrophobic tails, and therefore favor the formation of small W/O microstructures with high interfacial curvature towards the oil phase.

Another possible explanation stems from the differing solubilities of DOSS, Tween 80, and Span 80, in seawater and in nonpolar solvents. Tween 80 is so hydrophilic that (as shown in Figure 4.3) it can only be solubilized into the oil phase within W/O microstructures, and thus can only diffuse and adsorb to the interface as quickly as these relatively large microstructures can. Span 80 is oil-soluble, but insoluble in water, whereas DOSS is both highly soluble in oil[76] and sparingly soluble in water.[102] Thus, it is not surprising that, of these three surfactants, DOSS is associated with the most rapid dispersant adsorption from bulk oil to the oil-water interface. This suggests that an effective marine oil spill dispersant will contain surfactants which, like DOSS, readily form W/O microstructures, as such surfactants must be both hydrophobic enough to be soluble in oil and hydrophilic enough to solubilize water into the oil with them.

Recent work indicating that lecithin-Tween 80 blends are effective oil dispersants supports this hypothesis, as lecithin is also well-known to readily form W/O microstructures.[40, 41] The suitability of other W/O microstructure-forming surfactants for oil spill dispersion should be evaluated in future work. More generally, dynamic IFT studies of the adsorption of W/O microstructures to the oil-water interface should be conducted to validate the mechanisms of dispersant action proposed above. For example,

the effects of microstructure size on DOSS' interfacial adsorption rate could be studied by using pendant drop tensiometry or capillary drop tensiometry[56] to measure the timescales over which DOSS W/O microstructures of various sizes (a parameter controlled by varying the water:surfactant molar ratio in DOSS-oil-water mixtures) adsorb to an oil-water interface. Eventually, this effort should be extended to encompass mixed DOSS/nonionic W/O microstructures, at which point characterization of microstructures' dispersity and equilibration dynamics will also become important, as demonstrated in this chapter.

4.4 Conclusions

In conclusion, DOSS/Tween 80/Span 80 blends which are compositionally similar to widely used marine oil dispersants were mixed at 2 wt% total surfactant into a model oil, together with 0.5-1.5 wt% seawater, to better understand these surfactants' self-assembly in nonpolar solvents and relate it to their IFT dynamics and previously reported dispersion effectiveness.[54] Trends in these mixtures' dynamic oil-seawater IFT as a function of surfactant blend composition were similar to those observed in prior work for crude oil treated with blends of DOSS, Tween 80, and Span 80. Specifically, surfactant blends containing 50 wt% Tween 80 and a DOSS:Span 80 ratio near 1:1 produce ultralow IFT in the model oil ($< 10^{-4}$ mN/m) just as similar surfactant blends do in crude oil, and in both model oil and crude oil Span 80-rich surfactant blends exhibit much slower initial declines in dynamic IFT than DOSS-rich surfactant blends. At all DOSS:Span 80 ratios, surfactant blends containing 50 wt% Tween 80 form clear solutions with seawater in the model oil. Cryo-transmission electron microscopy (cryo-TEM) and dynamic light scattering (DLS) show that these solutions contain spherical W/O microstructures, the size and dispersity of which vary with surfactant blend composition and surfactant:seawater molar ratio. Span 80-rich microstructures exhibit high polydispersity index (PDI > 0.2) and diameters of ≥100 nm, whereas DOSS-rich microstructures exhibit diameters of 20-40 nm and low polydispersity index (PDI < 0.1), indicating a narrow microstructure size distribution. The increase in size and dispersity/PDI as DOSS is replaced with Span 80 in the surfactant blends is expected based on the more linear shape of Span 80 and the wide range of isomers it contains, as well as on prior work.

These results, and the fact that Tween 80 can only be solubilized into the oil within these microstructures, suggest a few possible reasons why DOSS-rich DOSS/Tween 80/Span 80 marine oil dispersants produce a faster initial decline in dynamic IFT than Span 80-rich blends do. First, DOSS makes microstructures smaller, as its shape favors high interfacial curvature towards the oil phase; this should allow microstructures to diffuse to the oil-water interface from bulk oil faster. Second, oil-soluble DOSS monomers should be able to diffuse to the interface faster than even the smallest (20-40 nm diam.) W/O microstructures characterized in this work. Future work should focus on validating these mechanisms for oil dispersant action via dynamic IFT studies of the interfacial adsorption of DOSS W/O microstructures; on the extent to which asphaltenes, resins, and waxes interact with dispersant W/O microstructures in crude oil; and on the study of alternative dispersants containing W/O microstructure-forming surfactants other than DOSS.

Chapter 5. Efficient Dispersion of Crude Oil by Blends of Food-Grade Surfactants: Toward Greener Oil-Spill Treatments*

5.1 Introduction

Oil dispersants are an important tool for the remediation of marine oil spills[13], but their deployment in the marine environment continues to be a subject of controversy. While modern oil dispersants are considerably less toxic than dispersed crude oil[14-18] and are applied to spills at relatively low dispersant:oil ratios (typically 1:20 to 1:100)[11], they are also not entirely nontoxic.[15, 16, 19] In order to secure broader acceptance of dispersant use, therefore, it is important to investigate alternative dispersant formulations made of unequivocally nontoxic compounds. Recently, Athas et al.[40] reported qualitatively that crude oil treated with mixtures of lecithin (L) and Tween 80 (T) in ethanol readily

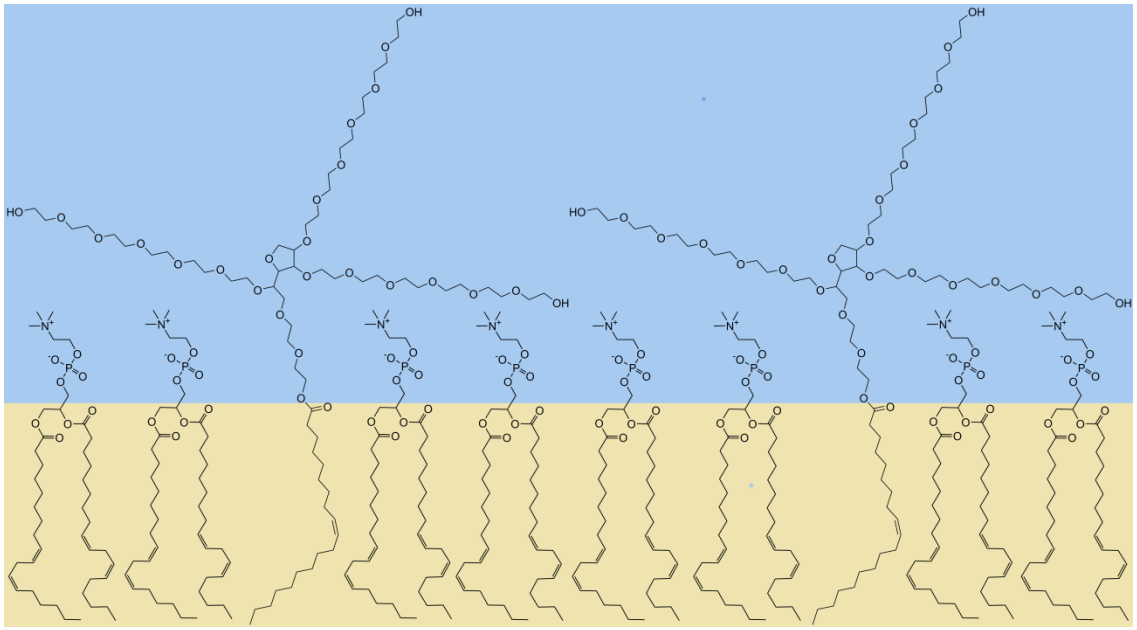

Figure 5.1 Schematic of Tween 80 and lecithin in a monolayer at the oil-water interface (oil = lower, brown phase; water = upper, blue phase).

* This chapter was adapted from the publication: Riehm, D.; Neilsen, J.; Bothun, G.; John, V.; Raghavan, S.; McCormick, A. Efficient Dispersion of Crude Oil by Blends of Food-Grade Surfactants: Toward Greener Oil-Spill Treatments. *Mar Poll Bull* **2015**, 101, 92-97. DOI: 10.1016/j.marpolbul.2015.11.012

The underlying raw data is publicly available through GRIIDC (DOI: 10.7266/N7833Q0R).

emulsifies into seawater. They attribute the effectiveness of these L-T blends as oil-in-water emulsifiers both to the complementary shapes of Tween 80 (hydrophilic) and lecithin (hydrophobic), which enable a densely-packed surfactant monolayer to form at the oil-water interface (see Figure 5.1), and to the steric hindrance of oil droplet coalescence by Tween 80's large polyoxyethylene chains. Since lecithin and Tween 80 are nontoxic surfactants,[33, 103] the prospect of an oil dispersant based on lecithin-Tween 80 blends warrants further study.[42]

In this chapter, the Baffled Flask dispersant effectiveness test (developed by Venosa et al.[50]) has been used to measure the effectiveness of L-T oil dispersants as a function of L:T ratio and dispersant:oil dosage ratio (DOR), and compare it to the effectiveness of DOSS-Tween 80-Span 80 dispersants as a function of D:T:S ratio and DOR. These dispersion effectiveness data improve upon the observations of emulsification reported in Athas et al. in several respects. First and foremost, the BFT is a widely used protocol which quantitatively measures the fraction of an oil slick dispersed into seawater, so BFT effectiveness data may be used to directly compare the performance of lecithin:Tween 80 dispersants to that of other, more established dispersants.[50] Additionally, oil-water dispersions generated by the BFT are more realistic approximations to real dispersant-treated spills on the ocean, as the BFT imparts a known mixing energy to the oil-water mixture which produces turbulence similar to that observed within breaking waves at sea,[104] and employs a much higher seawater:oil ratio (1200:1) than Athas et al. used (10:1) so that oil droplets are dilute in the dispersion, as they would be at sea. Finally, Athas et al. only reported dispersant performance at a single, unusually high[11] DOR (1:10) and three different dispersant L:T ratios (100:0, 0:100, and 60:40), which does not permit identification of the optimum L:T ratio and DOR. In this work, the effects of each of these variables on dispersant performance are explored thoroughly. The results of these tests not only confirm the prediction by Athas et al. that L-T blends are effective marine oil dispersants, but shed further light on the fundamental mechanisms of L-T dispersant action and indicate promising directions for future investigations.

5.2 Experimental

5.2.1 Materials

Tween 80 (Sigma-Aldrich), ethanol (AAPER), and lecithin (95% L-α-phosphatidylcholine, soy) were used as received. Synthetic seawater (SSW) was prepared by adding 427 mM NaCl, 55 mM $MgCl_2$, and 27 mM Na_2SO_4 to distilled water—a simplified version of the SSW formulation reported by Kester et al[66]. South Louisiana Macondo surrogate crude, a light sweet crude with a viscosity of 12 cSt @ 20 C provided courtesy of BP through the Gulf of Mexico Research Initiative, was received on ice, stored at -5 °C, and used as received.

5.2.2 Baffled Flask Test (BFT)

Tests exploring the effects of dispersant composition (i.e., lecithin:Tween 80 or DOSS:Tween 80:Span 80 ratio) and dispersant:oil ratio on dispersant effectiveness employed a slightly modified version of the high-mixing-energy Baffled Flask Test procedure developed by Venosa et al.[105, 106] DOSS-Tween 80-Span 80 dispersants were prepared as described in Section 3.2.3. L-T dispersants were composed of 80 wt% total surfactant (i.e., various mixtures of lecithin and Tween 80) and 20 wt% ethanol as solvent.

A 120 mL baffled Wheaton trypsinizing flask with a stopcock added at its base was filled with 120 mL of synthetic seawater, taking care to introduce an air bubble into the stopcock so oil would not accumulate there during the test. A wire containment ring 1.5 cm in diameter was suspended 1-2 mm above the surface of the water so that it pulled up a meniscus of seawater, and 100 µL of oil was deposited within that meniscus using a Rainin positive displacement pipette, forming a confined slick. 1-4 µL of dispersant (depending on the desired volumetric dispersant:oil ratio) was deposited onto the slick using a 25 µL fixed-needle syringe, and then the containment ring was removed and the flask agitated for 10 min at 200 RPM on an orbital shaker with an orbital diameter of ~2 cm. After the agitation period, the oil-water dispersion was allowed to settle for 10 min, and then the stopcock at the base of the flask was purged by releasing 2-3 mL of dispersion into the waste. A 30 mL sample of the dispersion was taken through the stopcock, and the crude oil was extracted from that sample in a separatory flask using 3 x

3.5 mL aliquots of dichloromethane (DCM). Finally, DCM was added to the extract to bring it up to a final volume of 10.5 mL (some DCM would evaporate during the extraction).

The absorbance of this crude oil-DCM extract was measured between 200 and 600 nm at 0.2 nm intervals using a Thermo Scientific Evolution 60S UV-Vis spectrophotometer. A 100%-dispersion-standard oil-DCM mixture, containing 10 µL of oil-dispersant mixture in 2.8 mL of DCM, was also prepared after every extraction, and its absorbance was measured at the same wavelengths. (30 mL/120 mL = 25% of the oil-water dispersion was sampled, so 100% dispersion would have put 25% of the original slick, or (100 µL x 0.25 x (2.8/10.5)) = 10 µL, into a 2.8 mL oil-DCM extract.) Prior work by Riehm and McCormick[54] demonstrated that the absorbance of these crude oil-DCM mixtures within the wavelength range 360-400 nm varies linearly with crude oil concentration. Thus, the ratios of the absorbance of each sample's extract to the absorbance of the 100% oil-DCM standard at corresponding wavelengths were averaged between 360-400 nm to yield each sample's effectiveness. If the range of all measured effectiveness values between 360 and 400 nm spanned more than one percentage point of measured effectiveness, typically due to scattering from emulsified seawater or another contaminant in the oil-DCM extract, the data from that sample were discarded.

5.2.3 Oil-Water Dispersion Imaging

Oil-water dispersions from the post-settling dispersion sample generated by this test procedure were imaged in a 1 x 0.2 cm glass cuvette using a Hirox KH-7700 Digital Microscope System. Images were converted to greyscale using ImageJ and particle sizes were measured manually.

5.3 Results

5.3.1 DOSS-Tween 80-Span 80 Effectiveness: Baffled Flask Test vs. Swirling Flask Test

Before employing the Baffled Flask Test to characterize the new L-T dispersants, the performance of DOSS-Tween 80-Span 80 dispersants in the Baffled Flask Test was compared with their performance in the Stirred Flask test (see Section 3.2.4). Figure 5.2 shows measured effectiveness in both the Stirred Flask Test and the Baffled Flask Test for DOSS-Tween 80-Span 80 dispersants containing 40 wt% DOSS and 60 wt% [Tween 80 + Span 80]. The tests in Figure 5.2 were conducted at a dispersant:oil ratio (DOR) of 1:25, slightly lower than the 1:20 DOR employed in Chapter 3. Nevertheless, the much higher mixing energy of the Baffled Flask Test resulted in higher dispersant effectiveness than the Swirling Flask Test at almost all compositions, which unfortunately reduced the magnitude of compositional trends in effectiveness and made it more difficult to clearly identify them.

Figure 5.3 shows measured effectiveness in both the Stirred Flask Test and the Baffled Flask Test for DOSS-Tween 80-Span 80 dispersants containing 40 wt% Tween 80 and 60 wt% [DOSS + Span 80], like those characterized in Section 3.3.2 (Figures 3.6-3.8). A DOR of 1:50 was employed to ensure that the high mixing energy of the Baffled Flask test would not obscure trends in dispersant effectiveness. In Figures 5.2 and 5.3, the most effective dispersant compositions generated by both the Stirred Flask test and the Baffled Flask test are 30:40:30 and 40:30:30 DOSS:Tween 80:Span 80, which is consistent with the peak effectiveness at 40:30:30 DOSS:Tween 80:Span 80 in Figure 3.6. Compositional trends in dispersant effectiveness are also generally consistent between the two tests, as well as with the compositional effectiveness trends in Figure 3.6, though the rate at which effectiveness changes as a function of composition does vary somewhat between the Stirred Flask test and the Baffled Flask Test.

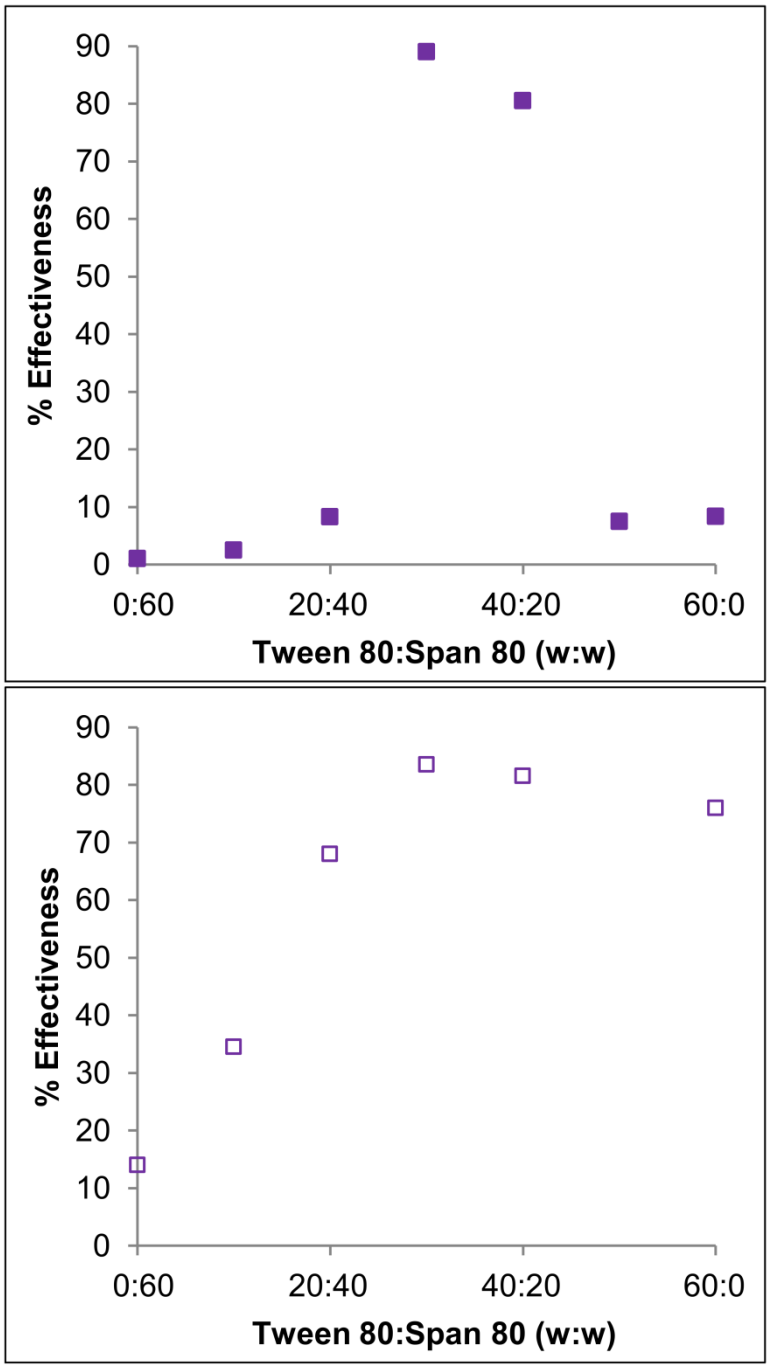

Figure 5.2 Effectiveness of DOSS-Tween 80-Span 80 dispersants as a function of DOSS:Span 80 ratio, evaluated using the Stirred Flask test (■, top) and the Baffled Flask test (□, bottom). Dispersant surfactant blends are 40 wt% DOSS, 60 wt% [Tween 80 + Span 80]. A dispersant:oil ratio of 1:25 resulted in 1.6-1.8 wt% total surfactant in the dispersant-treated oil. Plotted data points each represent a single experiment.

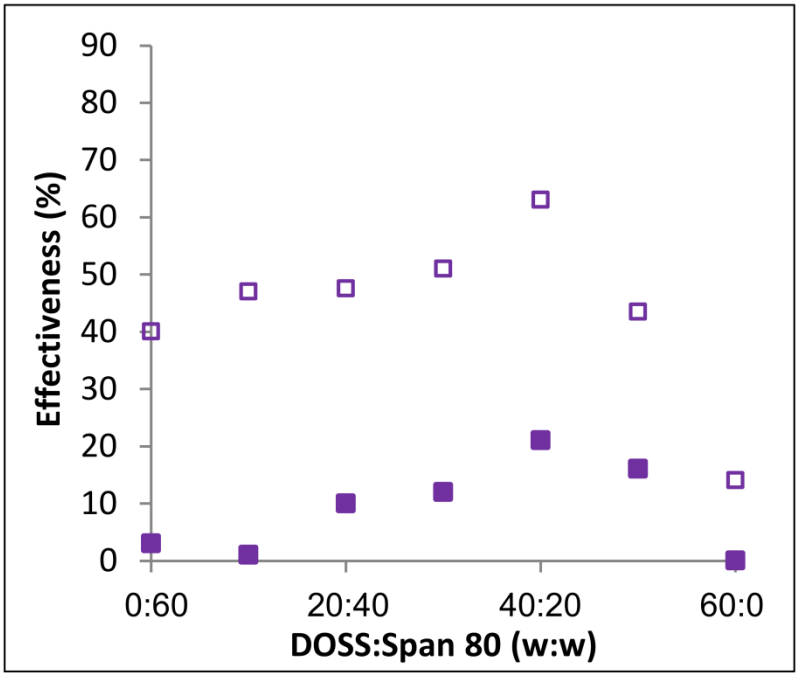

Figure 5.3 Effectiveness of DOSS-Tween 80-Span 80 dispersants as a function of DOSS:Span 80 weight ratio, evaluated using the Stirred Flask test (■) and the Baffled Flask test (□). Dispersant surfactant blends are 40 wt% Tween 80 and 60 wt% [DOSS + Span 80]. A dispersant:oil ratio of 1:50 resulted in 0.8-0.9 wt% total surfactant in the dispersant-treated oil. Plotted data points each represent a single experiment.

5.3.2 Lecithin-Tween 80 Effectiveness

5.3.2.1 L:T Ratio

Figure 5.4 shows dispersant effectiveness and IFT as a function of dispersant composition for, on the top, the DOSS-Tween 80-Span 80 system characterized in Section 3.3.2 (Figure 3.6), and on the bottom, lecithin-Tween 80 (L-T) dispersants. The most effective L-T dispersants have a L:T ratio between 60:40 and 80:20; there is not a statistically significant difference in measured effectiveness for dispersants in this compositional range. This result is consistent with the excellent emulsification reported by Athas et al.[40] for 60:40 L:T blends. The high mixing energy[104] employed in the Baffled Flask Test pushes maximum observed dispersion effectiveness above 80%, making it difficult to optimize dispersant composition more precisely than this. Other, commercial dispersants exhibit similarly high values (80-90% effectiveness) under this test protocol when a comparable DOR, temperature, and crude oil is employed.[50, 107, 108]

At L:T ratios higher than 80:20 (i.e., when Tween 80 is eliminated from the formulation), dispersant effectiveness is likely constrained by high interfacial tension (IFT). Measurements of IFT between seawater and dispersant-treated crude oil (DOR 1:50) reveal that, while the IFT at an L:T ratio of 60:40 is 0.08 mN/m, the IFT produced by a L:T ratio of 100:0 is considerably higher, at 0.65 mN/m. Athas et al.[40] also conducted measurements of IFTs between seawater and a similar crude oil treated with L-T dispersants in an ethanol solvent (though at a DOR of 1:10 rather than 1:50), and observed a dramatic increase in IFT over this same range of dispersant compositions. This sharp rise in IFT when Tween 80 is eliminated from the dispersant explains the corresponding sharp dropoff in effectiveness.

For L:T ratios below 60:40, however, something beyond IFT must account for the decline in dispersant effectiveness. IFT between seawater and dispersant-treated crude oil (DOR 1:50) for L:T ratios of 40:60 and 20:80 remains low (0.02 mN/m and 0.16 mN/m, respectively) despite the fact that the effectiveness of these dispersant compositions is considerably lower than that of 60:40 to 80:20 L:T dispersants. Athas et al.[40], too, found that IFT at the dispersant-treated crude oil/seawater interface (1:10 DOR) remains consistently low (~0.05 mN/m) for dispersant L:T ratios as low as 10:90. Riehm and McCormick[54] observed low effectivenesses at low IFT ($<10^{-4}$ mN/m) for certain oil dispersant blends of Tween 80, Span 80, and DOSS, and attributed this to much longer dynamic IFT transients (and, thus, slower interfacial adsorption of surfactants) at low-effectiveness dispersant compositions than were observed for high-effectiveness dispersant compositions. For L-T blends, however, we do not observe such a compositional trend in the length of dynamic IFT transients, so another mechanism must be operative here. One other possible explanation for lower effectiveness at lower L:T ratios despite low IFT is that the geometries of the surfactants as they pack at the oil-water interface (see Figure 5.1) are less able to form a dense monolayer, or perhaps even a multilayered lamellar structure, at a L:T ratio of 20:80 than at a L:T ratio of 80:20. A careful investigation of this hypothesis, via cryogenic electron microscopy, dilatational interfacial viscoelasticity measurements, etc., is conducted using a model crude oil (in order to prevent interfacially-active components of crude oil from confounding study of the dispersant's interfacial assembly) in Chapter 6.

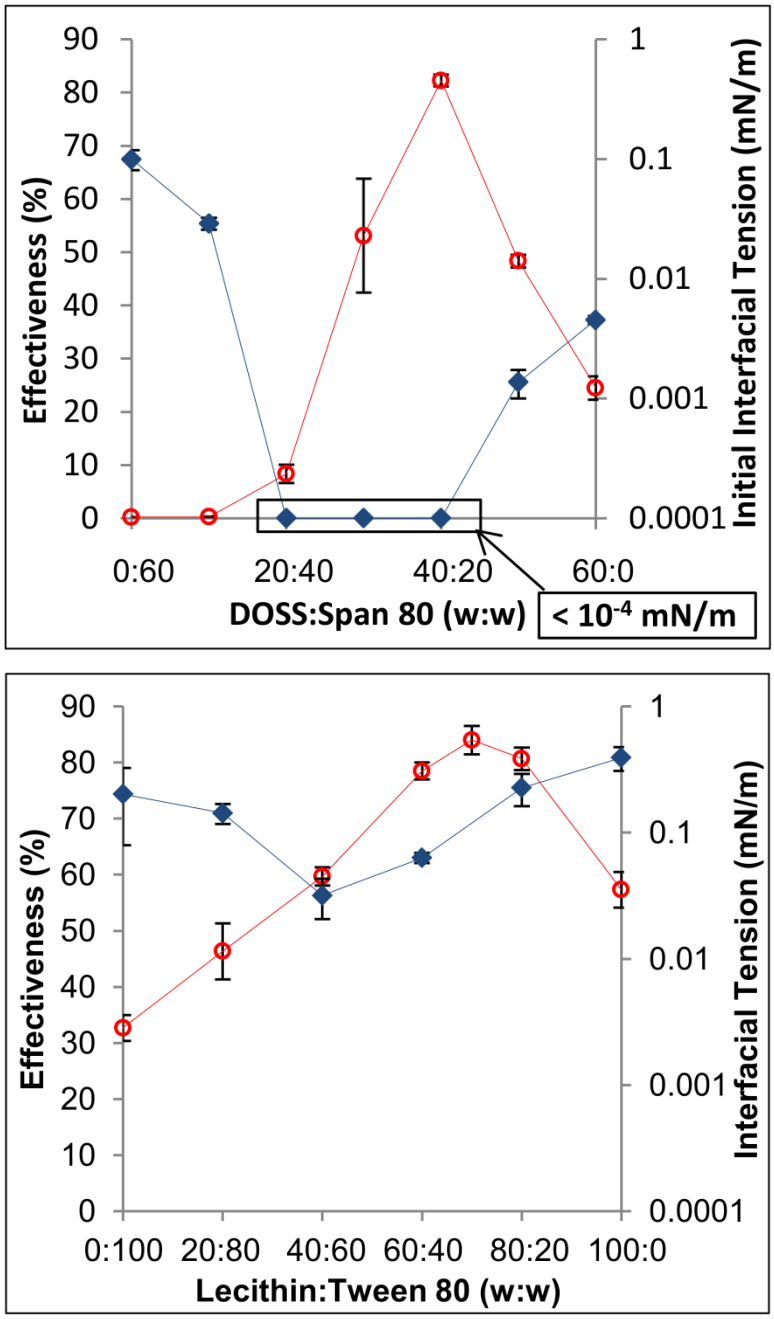

Figure 5.4 Dispersant effectiveness (o) and IFT (♦) for dispersant-treated crude oil in seawater. Plotted data points are arithmetic means for effectiveness and geometric means for IFT, based on n = 3 repetitions. Error bars span one standard error above and below each mean.

Top: Stirred Flask test, DOSS-Tween 80-Span 80 blend, 2.0-2.2 wt% total surfactant in dispersant-oil mixture (reproduction of Figure 3.6).

Bottom: Baffled Flask test, lecithin-Tween 80 blend, 2.3 wt% total surfactant in dispersant-oil mixture.

5.3.2.2 Dispersant:Oil Ratio

In Figure 5.5, the effectiveness of dispersant containing 80:20 L:T, one of the most effective L:T ratios, is shown over a range of DORs. Remarkably, decreasing the DOR from 1:25 to 1:100 only reduces effectiveness a small amount, from 89% to 77%. This dispersant is therefore not only highly effective, but also highly efficient,[108] since it nearly reaches its maximum effectiveness at such a low DOR. The sharp dropoff in dispersant effectiveness between DORs of 1:100 and 1:200 is consistent with abrupt declines in effectiveness observed for other dispersants below a particular dispersant:oil ratio,[108, 109] and it has been proposed that this critical DOR may correspond to a critical micelle concentration for the dispersant in the crude oil. The critical micelle concentrations for lecithin in various nonpolar solvents have been found by others to range from 0.05-0.5 mM[44], which is 1-2 orders of magnitude lower than the ~5 mM lecithin concentration in the crude oil treated with 80:20 L:T dispersant at a DOR of 1:200 which is characterized in Figure 5.5. However, solutions of lecithin in oil which are

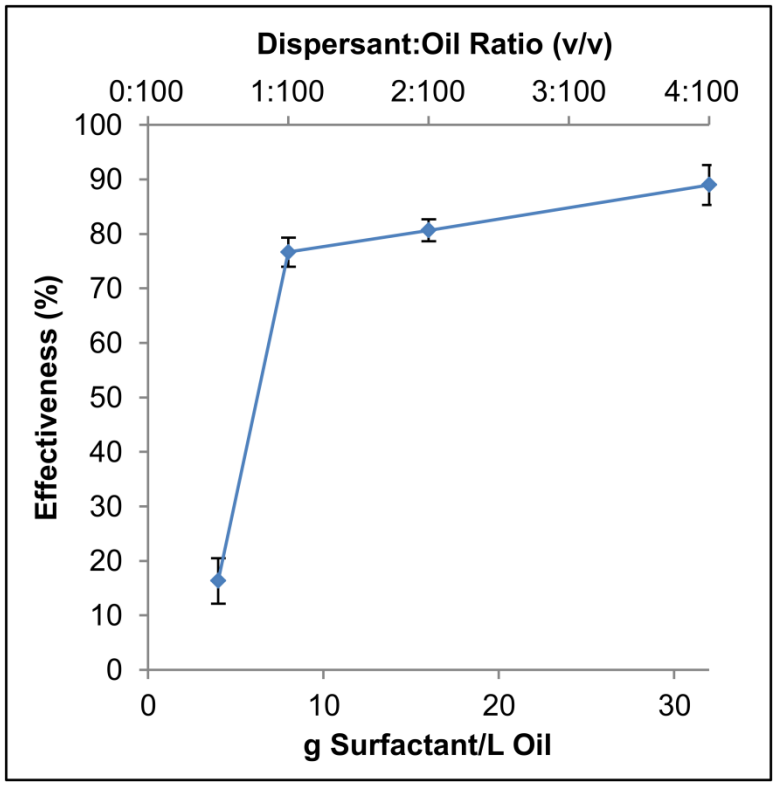

Figure 5.5. Effectiveness of dispersant containing an 80:20 L:T surfactant blend at various dispersant:oil ratios, measured using the Baffled Flask Test. Error bars span one standard error above and below each plotted mean of n = 3 repetitions.

exposed to water have been reported to form an "organogel" phase, consisting of entangled rod-like water-in-oil micelles, at minimum lecithin concentrations of 5-10 mM,[110, 111] which is the approximate concentration of lecithin at which we have observed the abrupt dropoff in effectiveness. (Tween 80 is insoluble in oil on its own, but is readily incorporated into water-in-oil microstructures formed by a variety of hydrophobic surfactants.[39, 112]) Thus, further investigation of the role (if any) of this "organogel" in effective oil dispersion by L-T mixtures is warranted, via studies of IFT, dilatational viscoelasticity, and any water-in-oil microstructures which are formed by L-T mixtures within (model) crude oil or at the oil-water interface.

5.3.3 Oil-Water Dispersion Imaging

Images were taken of dispersions of crude oil treated with 80:20 L:T dispersant at DORs of 1:25, 1:50 and 1:100 and with 100:0 L:T dispersant at a DOR of 1:50 (Figure 5.6). The median particle diameters in these dispersions were all 3-4.5 μm, smaller than the 6-7 μm median particle diameters of the oil-in-water emulsions made by Athas et al. at similar dispersant compositions and a higher DOR (1:10). This is likely due to the fact that the emulsions made by Athas et al. had a much higher oil:water volume ratio (1:10) than the dispersions generated using the high-energy Baffled Flask Test (1:1200), so that droplets collided and coalesced much more readily in the emulsions than they did in the high-energy BFT dispersions.

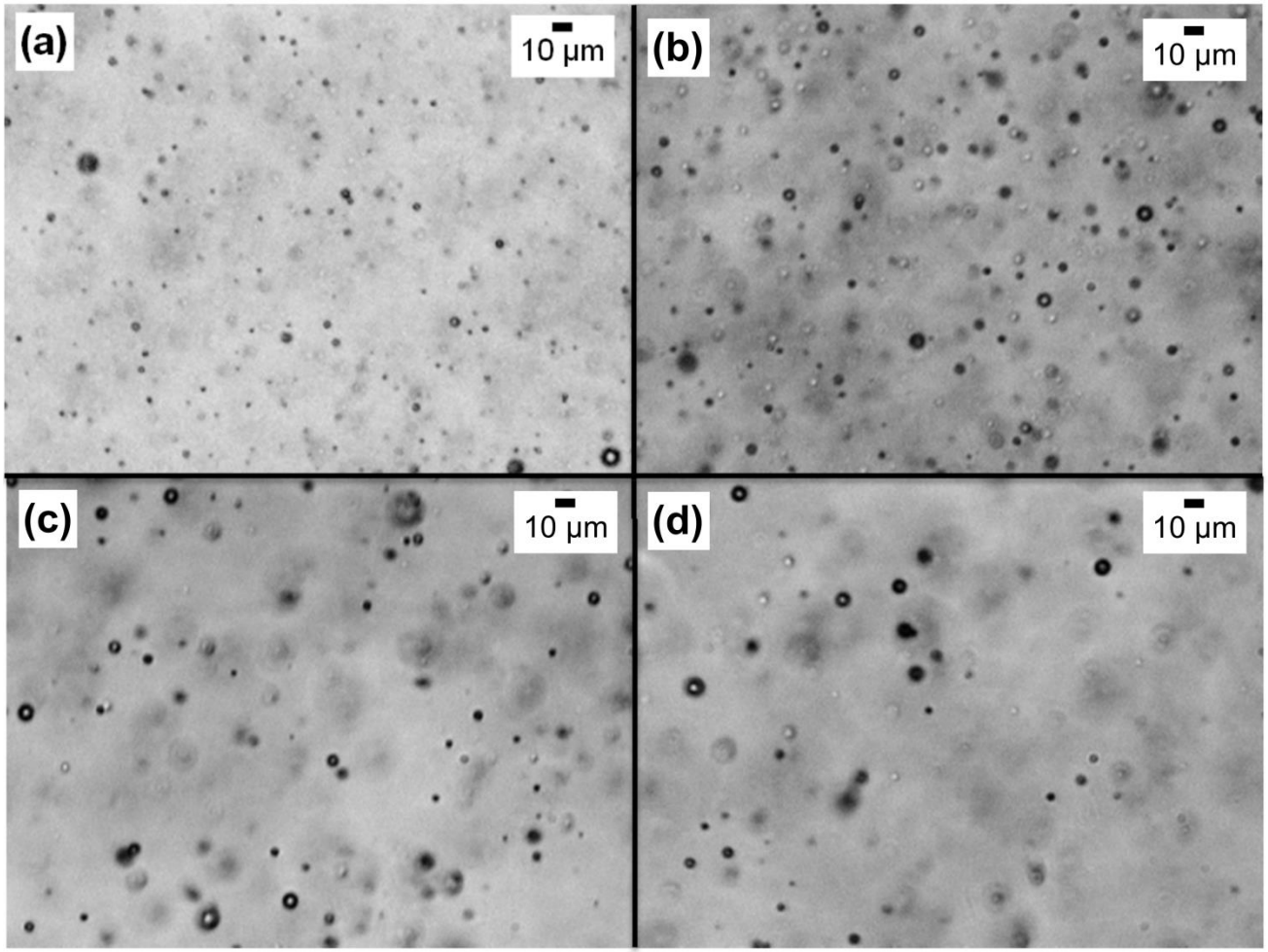

Figure 5.6. Optical micrographs of dispersions of crude oil in seawater produced using the high-energy Baffled Flask Test (the dispersions were imaged immediately following the 10 min settling period). The dispersions were produced using the following DORs and dispersant L:T ratios: (a) 1:25 DOR, 80:20 L:T; (b) 1:50 DOR, 80:20 L:T; (c) 1:100 DOR, 80:20 L:T; (d) 1:50 DOR, 100:0 L:T.

5.4 Conclusions

The predicted[40] effectiveness of lecithin-Tween 80-ethanol blends as marine oil dispersants has been confirmed using Baffled Flask effectiveness testing. The most effective L:T ratios are 60:40 to 80:20. At L:T ratios higher than this, effectiveness is limited by high IFT, while at L:T ratios lower than this, insufficient lecithin is present to pack into a dense interfacial monolayer with the Tween 80. Dispersant containing an 80:20 L:T ratio and an 80:20 surfactant:ethanol ratio is also highly efficient, since decline in effectiveness as DOR is reduced from 1:25 to 1:100 is minimal. It is proposed that the sharp dropoff in effectiveness observed as DOR is reduced from 1:100 to 1:200 occurs because dispersant surfactant concentration falls below a critical concentration for self-assembly of L:T blends into microstructures in the crude oil and/or at the crude oil/seawater interface. Future work will explore the importance of dispersant microstructures both within bulk crude oil and at the oil-water interface in effective crude oil dispersion, likely using a model crude oil, as well as further exploring more oil-miscible solvent formulations for lecithin:Tween 80 dispersants.

Chapter 6. Dispersion of oil into water using lecithin-Tween 80 blends: The role of spontaneous emulsification*

6.1 Introduction

Lecithin and Tween 80 are nontoxic surfactants widely used in foods and pharmaceuticals.[113, 114] Blends of lecithin and Tween 80 have also recently been found to be effective dispersants for marine crude oil spills, performing comparably to established dispersants in standard dispersant effectiveness tests.[3, 40, 41, 54] At standard testing conditions and dispersant dosages, however, these lecithin-Tween 80 (L-T) dispersants produce crude oil-seawater interfacial tension (IFT) of 0.03-0.4 mN/m[40, 41], whereas other effective dispersants produce IFT $<10^{-4}$ mN/m.[3, 54] Moreover, in prior work by Riehm et al.[41] (Figure 6.1), lecithin-rich dispersants were found to be significantly more effective than Tween 80-rich dispersants with lower or comparable IFT, suggesting that other interfacial phenomena, beyond IFT, underlie the effectiveness of L-T dispersants. In particular, lecithin and Tween 80 have each been found to cause spontaneous emulsification and to form gels at oil-water interfaces, so one or both of these phenomena may influence L-T dispersants' effectiveness.

Interfacial gels formed by lecithin are documented extensively[110, 115-117], and gels based on mixtures of Tween 80 and Span 80 are also well-known.[118, 119] A L-T interfacial gel could help disperse oil into water by making surfactant available to rapidly cover newly-formed interface as oil droplets are sheared apart. It could also prevent dispersed oil droplets from recoalescing, although this is expected to be less important at the high water:oil ratios used in marine oil dispersant tests (>1000:1 by volume)[41, 48] than it is in more concentrated emulsions.

Both lecithin and Tween 80 have also been observed to cause spontaneous emulsification at oil-water interfaces.[117, 120, 121] Davies and Rideal[122] promulgated classic

* This chapter was adapted from the publication: Riehm, D; Rokke, D.; Paul, P.; Vizanko, B.; Lee, H; McCormick, A. Dispersion of oil into water using lecithin-Tween 80 blends: The role of spontaneous emulsification. *J Colloid Interface Sci* **2017**, 487, 52-59. DOI: 10.1016/j.jcis.2016.10.010.

The underlying raw data is publicly available through GRIIDC (DOI: 10.7266/N7KW5D2D).

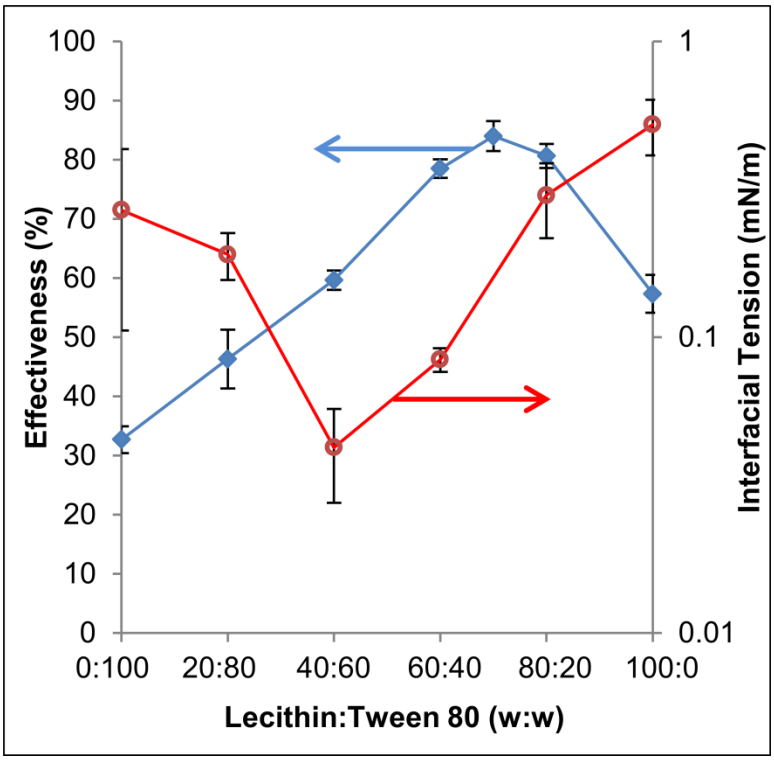

Figure 6.1: Dispersant effectiveness (♦) and IFT (o) of dispersant-treated crude oil in seawater. Dispersants were mixtures of Tween 80 and lecithin in ethanol, and were added to the oil at a volumetric dispersant:oil ratio of 1:50, corresponding to 2.3 wt% dispersant in the dispersant-oil mixtures. Plotted data points denote the arithmetic mean of observed effectiveness and geometric mean of observed IFT, and error bars span ± one standard error, based on n = 3 repetitions. Arrows indicate the axis on which each dataset is plotted.

interfacial mechanisms for spontaneous emulsification in 1961 involving (i) interfacial turbulence from Marangoni flow, (ii) vigorous diffusion of surfactants across the interface ("diffusion and stranding"), or (iii) dilatational surface pressures high enough to cause interfacial buckling ("negative interfacial tension"). More recent work[123, 124] has shown that one phase may diffuse into the other and form self-assembled structures (e.g., vesicles, myelinic figures, bicontinuous microemulsions) near the interface, which swell with the diffusing phase and eventually burst or undergo phase inversion, causing spontaneous emulsification. Other recent work[125, 126] reports spontaneous nucleation of water droplets into surfactant-laden oil near the oil-water interface.

If spontaneous emulsification occurs at crude oil-seawater interfaces treated with L-T dispersants, its impact on dispersants' effectiveness may depend on which interfacial phenomena are driving it. If it is caused by surfactant buildup and interfacial self-

assembly, this could aid dispersion of oil into water by making surfactant immediately available at the interface as oil is broken up and by impeding droplet coalescence. On the other hand, if spontaneous emulsification is primarily driven by interfacial turbulence or by surfactants rapidly moving through the interface into the seawater, this could deplete the oil of surfactants, making it more difficult to disperse the oil into the seawater.

In this work, oil-water interfaces are imaged using light microscopy and cryogenic scanning electron microscopy (cryo-SEM), and coalescence times are measured for dispersant-treated crude oil droplets in seawater, in order to determine whether interfacial gel or spontaneous emulsification play a role in L-T dispersants' effectiveness. Light microscopy allows the oil-water interface and any emulsified droplets in the surrounding bulk phases to be imaged down to a resolution of ~0.2 μm. Cryo-SEM complements light microscopy by allowing emulsified droplets and other nanoscale features to be imaged and sized using secondary electrons, and then chemically identified as oil or water using energy-dispersive x-ray spectroscopy (EDS). Finally, it has been suggested in prior work[40-42] that dispersant-oil mixture droplets' resistance to coalescence may limit dispersant effectiveness, so it is important to investigate this possibility, as well as to determine the extent to which any interfacial gel or spontaneous emulsification impacts droplets' resistance to coalescence.

6.2 Experimental

6.2.1 Materials

Tween 80 (PEO_{20} sorbitan monooleate, Sigma-Aldrich), Tween 85 (PEO_{20} sorbitan triooleate, Sigma-Aldrich), lecithin (95% L-α-phosphatidylcholine, Avanti Polar Lipids), isooctane (2,2,4-trimethylpentane, Sigma-Aldrich) and ethanol (Fisher Scientific, Pharmco-AAPER) were used as received. South Louisiana Macondo surrogate crude, a light sweet crude with a viscosity of 12 cSt @ 20 °C provided courtesy of BP through the Gulf of Mexico Research Initiative, was received on ice, stored at -5 °C, and used as received. Synthetic seawater was prepared by adding 427mM NaCl, 55mM $MgCl_2 \bullet 6H_2O$, and 27mM Na_2SO_4 to distilled water, a simplified version of the synthetic seawater formulation described by Kester et al.[66] Magnesium chloride hexahydrate (Fisher) was used as received; sodium chloride (Sigma-Aldrich) and sodium sulfate (Macron

Chemicals) were baked for at least 5 hrs at 500 °C to remove contaminants before being added to the synthetic seawater.

6.2.2 Sample Preparation

Oil-dispersant mixtures were prepared by first dissolving lecithin and/or Tween 80 in ethanol, at the same overall surfactant:ethanol weight ratio of 80:20 employed in Riehm et al.,[41] to make L-T dispersants like those studied in prior work.[40, 41] Lecithin:Tween 80 (L:T) ratios in these dispersants, reported by weight, were the primary compositional variable of interest in this work. Dispersants were then added to either crude oil or isooctane and vigorously stirred with a magnetic stir bar to make dispersant-oil mixtures containing 1.25-10 wt% dispersant (1-8 wt% surfactant), the typical range of dispersant concentrations in dispersant-treated marine oil spills. Dispersant-oil mixtures were stirred for 15 minutes at 1.25-5 wt% dispersant and for 24 hours at 10 wt% dispersant, to ensure dispersant had sufficient time to blend with the oil.

6.2.3 Light Microscopy

Droplets of various dispersant-oil mixtures were sandwiched together with seawater between pairs of glass slides and the resulting oil-water interfaces imaged via light microscopy. Each pair of slides was separated by a single layer of Parafilm M (127 μm thick[14]) with a 12.1mm x 44.5mm rectangle cut out of its center. This Parafilm spacer was melted onto one of the slides and covered with a layer of vacuum grease in order to seal the cavity which it enclosed. A 5 μL droplet of dispersant-oil mixture was then deposited into the cavity, followed by 70 μL of seawater in several droplets surrounding the dispersant-oil mixture. When the second glass slide was pressed down onto this assembly, the liquids were sealed into the cavity and the dispersant-oil mixture and seawater were pushed into contact, forming an oil-water interface. The thickness of this cavity was 150-175 μm, yielding an overall cavity volume of 80-95 μL. Digital images and video of this interface were captured using a Nikon Optiphot-Pol light microscope enhanced with a Canon SL1 digital camera, at magnifications ranging from 50-200x.

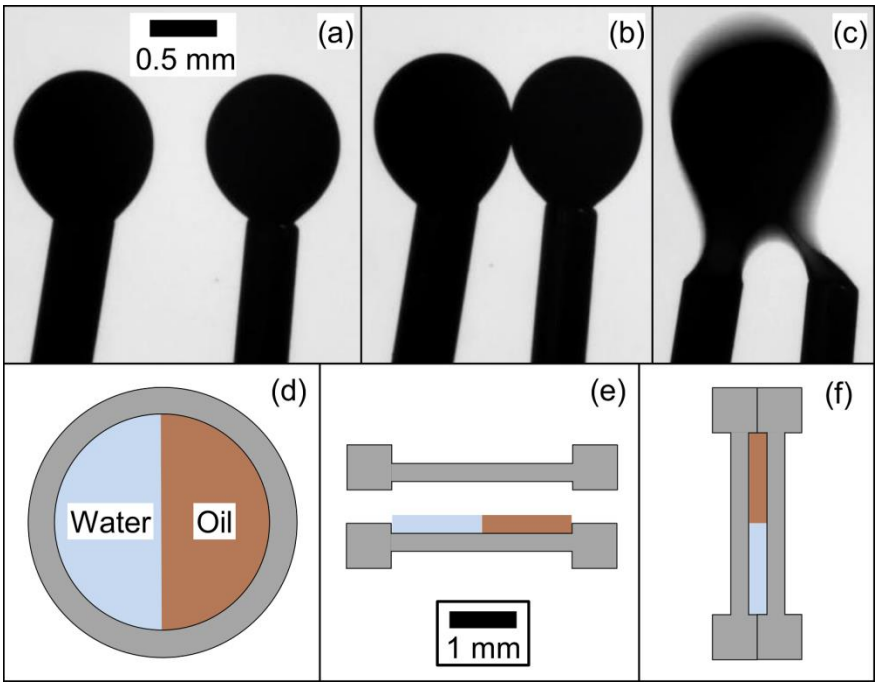

Figure 6.2: (a-c) Progression of droplet coalescence test. a) Droplets are dispensed into seawater and initially held separate. b) After 1 minute, the droplets are contacted. c), Droplets eventually either merge (shown above) or detach separately (not shown). (d-f) Cryo-SEM sample preparation. d) 0.5 µL each of dispersant-oil mixture and seawater are deposited into planchet (top view). e) A second planchet is pressed onto the filled planchet (side view). f) The planchet sandwich is held vertically for 5 minutes, allowing oil to rise to the top of the cavity and form an oil-water interface perpendicular to the sample fracture plane (side view).

6.2.4 Pendant Drop Coalescence Tests

The time required for two droplets of a dispersant-crude oil mixture to coalesce in synthetic seawater was measured using a Kruss DSA30 pendant drop tensiometer. Two J-shaped stainless steel needles, of which one was 26-gauge and the other 27-gauge, were plasma cleaned (Basic Plasma Cleaner, Harrick Plasma) on "high" for 2-3 minutes and then attached to 50 µL glass-barrel syringes (SGE Analytical Science). After each syringe was filled with dispersant-crude oil mixture, one syringe was mounted on the pendant drop tensiometer and the other was mounted on a ringstand adjacent to the tensiometer. The J-shaped needles were positioned in front of the tensiometer's camera and their tips were immersed in a 3 cm x 3 cm x 3 cm glass cuvette filled with 25 mL of synthetic seawater. Before tests began, 1 µL of dispersant-crude oil mixture was dispensed from each syringe to purge any water which might have entered the needles upon their

immersion in the cuvette. In a typical coalescence test (Figure 6.2a-c), small (0.25-0.5 μL) oil droplets of approximately equal size were dispensed from the needles and held separate in the seawater for one minute, at a distance of 0.25-1 mm. The droplets were then carefully moved towards each other, at a speed of <0.1 mm/s, until they just contacted each other, without either droplet being deformed or deflected by the contact. Contacted droplets were subsequently observed until they either coalesced or (eventually) detached from the needles separately. To facilitate the accurate measurement of coalescence/detachment times, as well as to capture any unusual behavior (e.g., spontaneous emulsification of oil from the droplet into the seawater), every test was recorded as a video using the tensiometer's camera, from initial dispensing of the droplets to coalescence or detachment.

6.2.5 Cryogenic Scanning Electron Microscopy

The interface between various dispersant-oil mixtures and seawater was also studied using cryogenic scanning electron microscopy (cryo-SEM), using a methodology similar to that employed by Lee et al.[127] 0.5 μL of oil-dispersant mixture and 0.5 μL of seawater were deposited into a 2 mm diameter, 100 μm deep cylindrical cavity in a brass planchet (Type A, Ted Pella Inc., Redding, CA). The cavity's floor was pre-scored to increase sample adhesion after cryogenic fixation. Once filled, the planchet was covered with an identical, inverted planchet to make a sandwich; picked up and oriented so that the plane of the sandwiched disks was perpendicular to the floor; and held in this orientation for five minutes (Figure 6.2d-f). This allowed time (a) for the oil-dispersant mixture to rise to the top of the cavity and form a bulk oil-water interface, and (b) for surfactants to adsorb and self-assemble at the oil-water interface. The sample was then cryogenically fixed by manual plunging into liquid ethane before being transferred to a liquid nitrogen bath.

To prepare samples for imaging in the electron microscope, two planchet sandwiches at a time were loaded into a cryo-sample holder in a Leica EM ACE600 high-vacuum sputter coater. Within the coater, the sandwiches were cleaved with a chilled scalpel at -110 °C and $<10^{-5}$ mbar. One half of each sandwich was then discarded, leaving the other half exposed and mounted in the cryo-sample holder. These exposed samples

were sublimed at -100 °C for 15 min and then coated with 2 nm of platinum at -110 °C under argon at $8*10^{-3}$ mbar, before being cooled to -130 °C and transferred to a Hitachi SU8230 field emission gun scanning electron microscope using the Leica VCT100 cryo-transfer system. Samples were imaged using an Everhart-Thornley secondary electron detector at -130 °C and 5 kV. A Thermo Noran System 7 Spectral Imaging System with UltraDry Si Drift Detector was using for elemental mapping of samples via energy-dispersive X-ray spectroscopy (EDS) so that oil and water could be clearly distinguished.

6.3 Results and Discussion

6.3.1 Microscopy & Imaging

6.3.1.1 Low L:T dispersants: Oil-into-water spontaneous emulsification

The interface between synthetic seawater and dispersant-crude oil mixtures containing low L:T ratio dispersants was imaged using light microscopy and cryo-SEM, in order to determine whether spontaneous emulsification and/or interfacial gel play a role in the low effectiveness of low L:T dispersants (see Figure 6.1).[41] Figure 6.3 shows spontaneous emulsification of dispersant-crude oil mixtures into seawater between two glass slides spaced 150-175 μm apart. Dispersant-oil mixtures shown contain either 20:80 L:T, 40:60 L:T, or 60:40 L:T and either 5 wt% or 2.5 wt% dispersant. Figure 6.4 also shows spontaneous emulsification, at 2.5 wt% dispersant and the same L:T ratios shown in Figure 6.3, but from ~0.25 μL pendant drops of dispersant-oil mixture into 25 mL of seawater, imaged 30 seconds after droplet formation. Thus, Figure 6.4 shows that the oil-into-water spontaneous emulsification observed between sandwiched slides also occurs at the high water:oil ratios and droplet surface area:volume ratios typical of dispersant-treated marine oil spills. L:T ratios not depicted in Figures 6.3 and 6.4 (0:100 L:T, 80:20 L:T, and 100:0 L:T) caused little or no oil-into-water spontaneous emulsification (i.e., less than that shown for 60:40 L:T dispersant in Figures 6.3c and 6.3f) (Appendix C, Figure C.6).

For the dispersant-oil mixtures depicted in Figures 6.3 and 6.4, more oil-into-water spontaneous emulsification was observed at higher wt% dispersant in oil and at lower L:T ratios, presumably because dispersant causes spontaneous emulsification and because Tween 80 is more hydrophilic than lecithin, respectively. Remarkably, though,

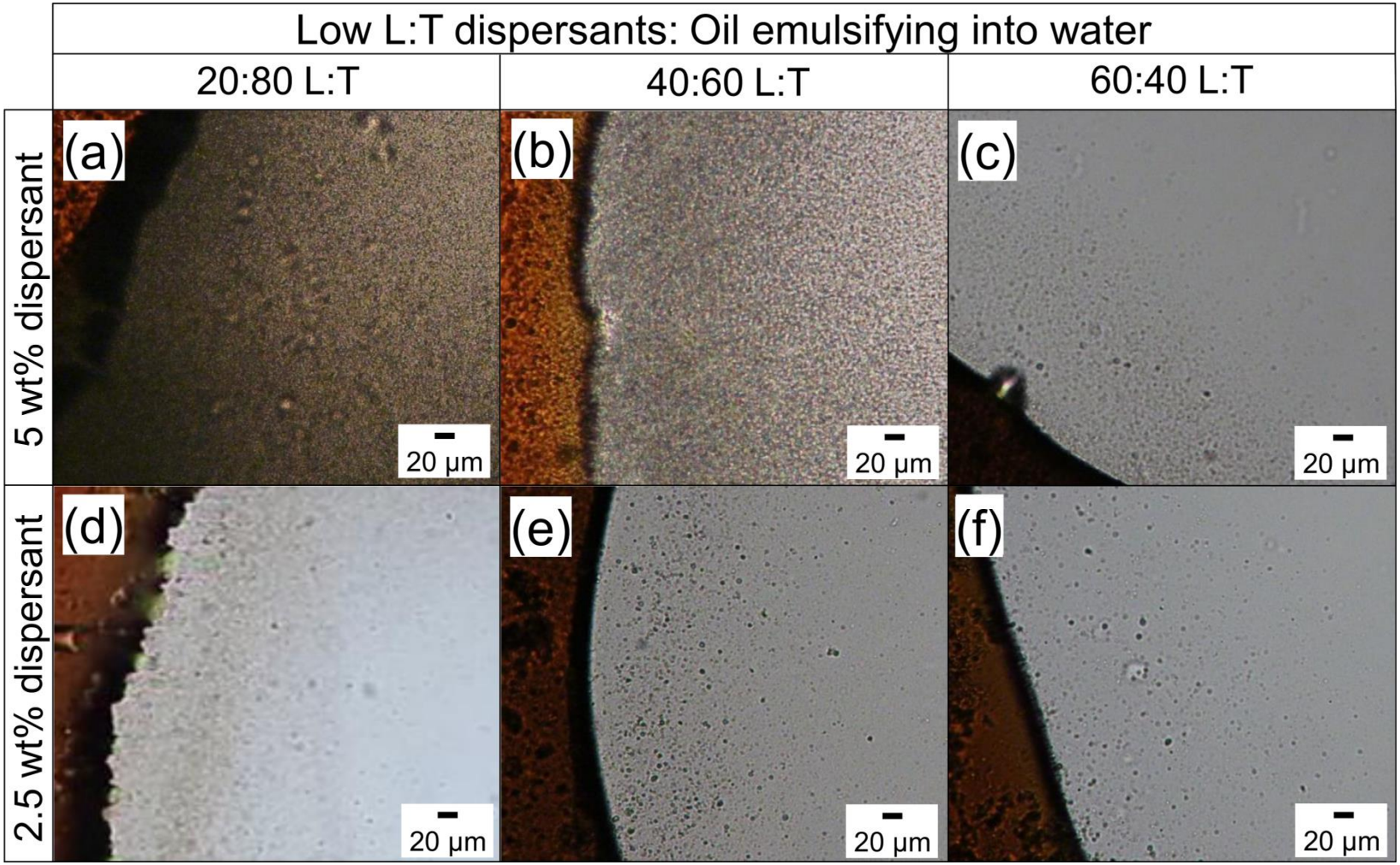

Figure 6.3: Light microscopy images of dispersant-crude oil mixtures spontaneously emulsifying into seawater. Dispersant-oil mixtures contain: (a) 5 wt% 20:80 L:T dispersant; (b) 5 wt% 40:60 L:T dispersant; (c) 5 wt% 60:40 L:T dispersant (d) 2.5 wt% 20:80 L:T dispersant; (e) 2.5 wt% 40:60 L:T dispersant; and (f) 2.5 wt% 60:40 L:T dispersant. Images were taken 15-20 minutes after oil-water contact.

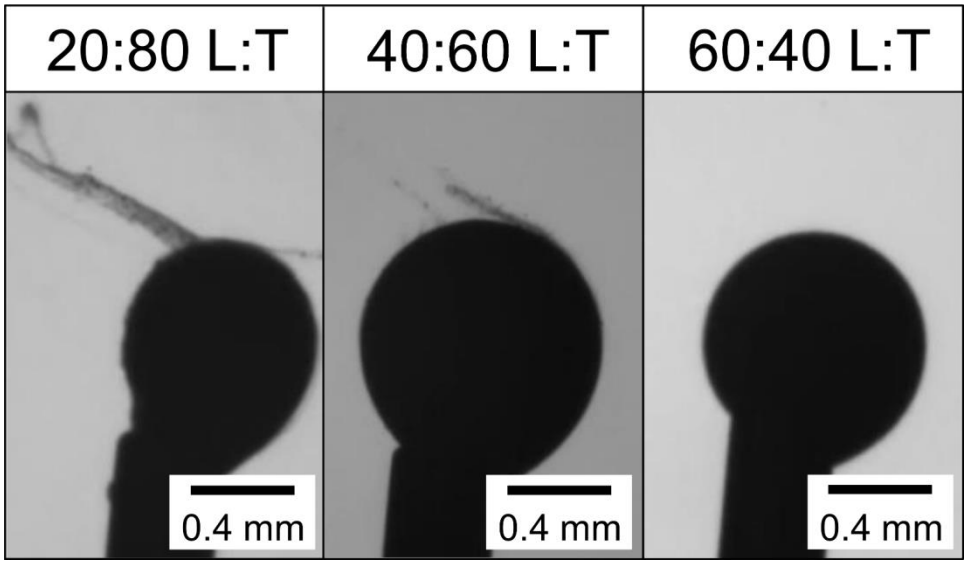

Figure 6.4: Light microscopy images of ~0.25 μL pendant droplets of dispersant-crude oil mixture spontaneously emulsifying into ~25 mL seawater. Dispersant-oil mixtures contain 2.5 wt% dispersant with the following L:T ratios: (a) 20:80; (b) 40:60; and (c) 60:40. All images were taken 30 sec after initial droplet formation.

the extent of oil-into-water spontaneous emulsification produced by 20:80 L:T dispersant is greater than or comparable to that produced by 40:60 L:T dispersant, even though in Riehm et al.,[41] 20:80 L:T dispersant was found to produce an oil-water IFT five times higher than that produced by 40:60 L:T dispersant (at 2.5 wt% dispersant). This fact, as well as the fact that IFTs reported for 20:80 and 40:60 L:T dispersants in prior work[41] (Figure 6.1) are significantly greater than 0 mN/m ($p < 0.05$, confidence interval for Student's t-distribution), suggests that the observed spontaneous emulsification is not driven by the "negative IFT" mechanism proposed by Davies and Rideal.[122] Interfacial turbulence, another mechanism proposed by Davies and Rideal, was only observed for 5 wt%20:80 L:T dispersant in crude oil (Figure 6.3a), and even then only in isolated pockets along the interface, so at most it plays a minor role in the trends in spontaneous emulsification depicted in Figures 6.3 and 6.4. This leaves "diffusion and stranding" and complex microstructure formation as possible mechanisms for the observed oil-into-water spontaneous emulsification.

Figure 6.5 shows cryo-SEM images of spontaneous oil-into-water emulsification at 5 wt% dispersant. Oil and water have been identified using EDS mapping of the imaged areas (Appendix C, Figures C.1 & C.2). Spontaneous emulsification was most

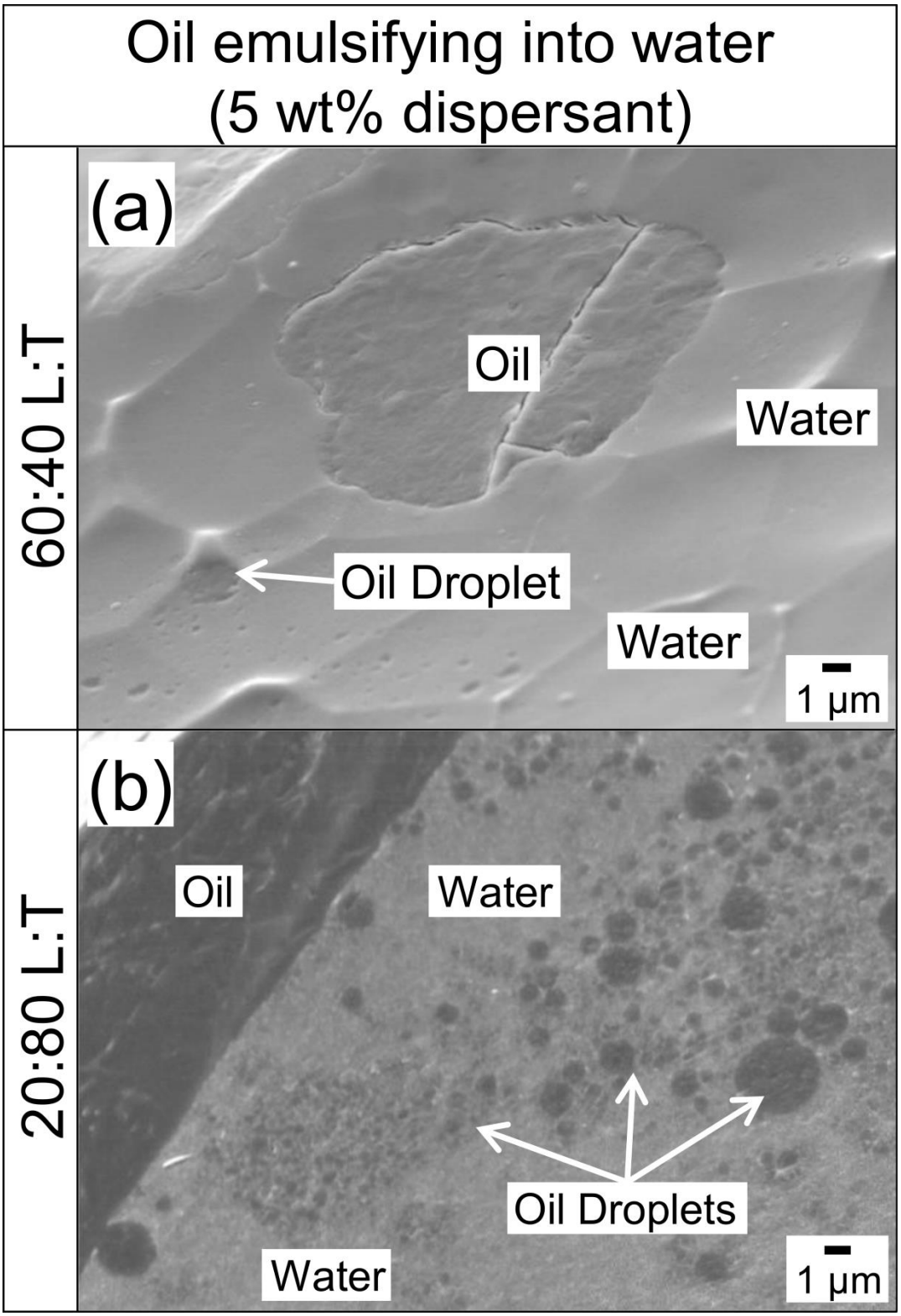

Figure 6.5: Cryo-SEM images of oil-into-water spontaneous emulsification. Dispersant-oil mixtures contain 5wt% dispersant; L:T ratio is 60:40 in image (a) and 20:80 in image (b). Oil and water are identified via EDS (Appendix C, Figures C.1 and C.2).

clearly observed at 20:80 L:T (Figure 6.5a), producing hundreds of oil droplets with a median diameter of 0.7 μm (Appendix C, Figure C.5). The 2 μm droplet in the lower left corner of Figure 6.5a is even frozen in the process of pinching off from an oil-water interface, indicating that this interface was still actively emulsifying crude oil droplets into seawater at the moment of cryogenic fixation, 5 min after oil-water contact.

It is therefore notable that no complex microstructure is evident in Figure 6.5a, either at the bulk oil-water interface or within the oil droplets, even though droplets with diameters < 0.5 μm are readily resolved. The spontaneously emulsified oil in Figure 6.5b, with its more lecithin- rich 60:40 L:T dispersant that might be expected to form a gel,[110, 115-117] also shows no evidence of complex microstructures at the oil-water interface. It is possible that there is a self-assembled interfacial layer of surfactants which is too thin to resolve, or which does not have a chemical composition sufficiently different from oil to be detected via EDS. Even if this is the case, however, the lack of any infiltration or swelling of the crude oil by seawater rules out bursting or phase inversion of water-in-oil microstructures as the cause of oil-into-water spontaneous emulsification. Thus, of the mechanisms for spontaneous emulsification identified in prior work, the most plausible one for this system seems to be "diffusion and stranding", in which surfactants vigorously diffusing across an interface eject droplets of the phase they leave into the phase they enter. An important implication of this hypothesis is that spontaneous emulsification at low L:T ratios is a symptom of rapid surfactant loss from oil into seawater, which may explain why Riehm et al.[41] found that Tween 80-rich dispersants exhibit lower dispersion effectiveness than lecithin-rich dispersants which produce comparable oil-water IFTs (see Figure 6.1).

6.3.1.2 High L:T dispersants: Water-into-oil spontaneous emulsification

The role of spontaneous emulsification and/or interfacial gel in the high effectiveness of high L:T ratio dispersants (see Figure 6.1)[41] was also investigated via light microscopy and cryo-SEM imaging. Figure 6.6 shows water-into-oil spontaneous emulsification at 5 wt% dispersant in crude oil for lecithin:Tween 80 weight ratios of 80:20 and 60:40 L:T. Oil and water have been identified using EDS mapping of the imaged areas (Appendix C, Figures C.3 and C.4). Oil-into-water spontaneous

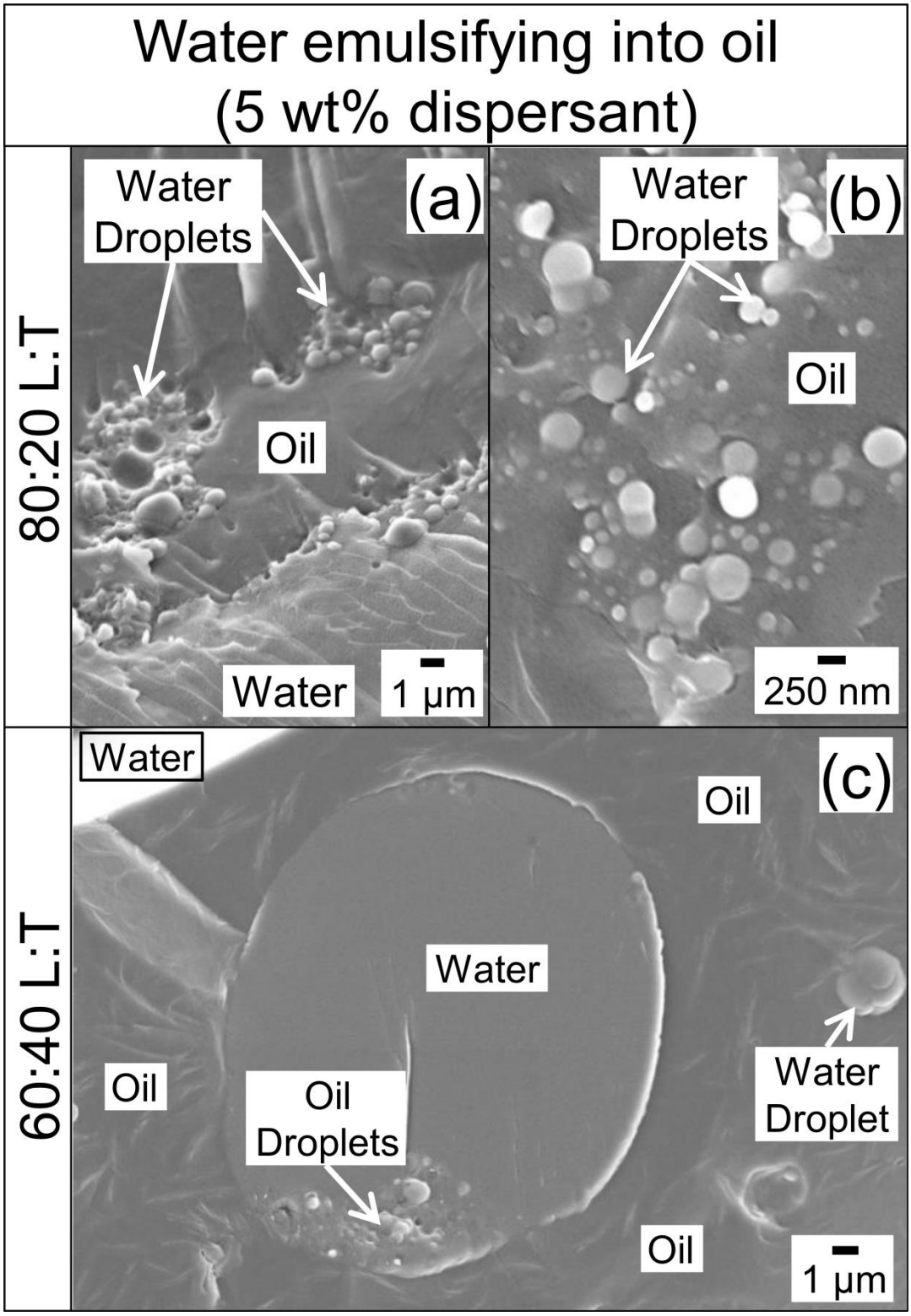

Figure 6.6: Cryo-SEM images of spontaneous emulsification of oil into water. Dispersant-oil mixtures contained 5 wt% dispersant; L:T ratio is 80:20 in images (a) and (b), and 60:40 in image (c). Oil and water are identified via EDS (Appendix C, Figures C.3 and C.4).

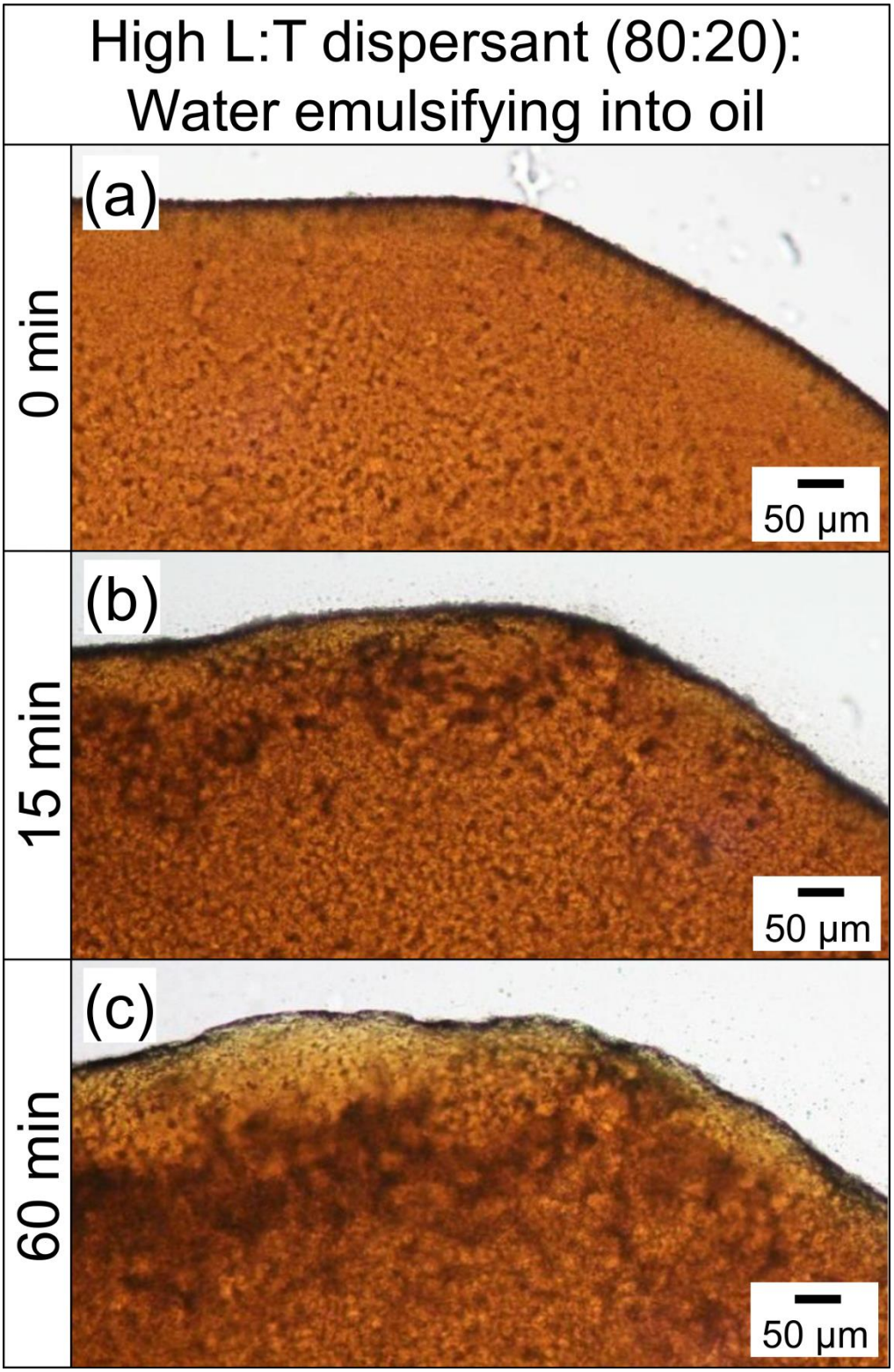

Figure 6.7: Light microscopy images of seawater spontaneously emulsifying into dispersant-crude oil mixture which contains 10 wt% 80:20 L:T dispersant. Both oil and water are confined between two glass slides spaced ~150 μm apart. Images (a), (b), and (c) were taken 0, 15, and 60 minutes after oil-water contact, respectively.

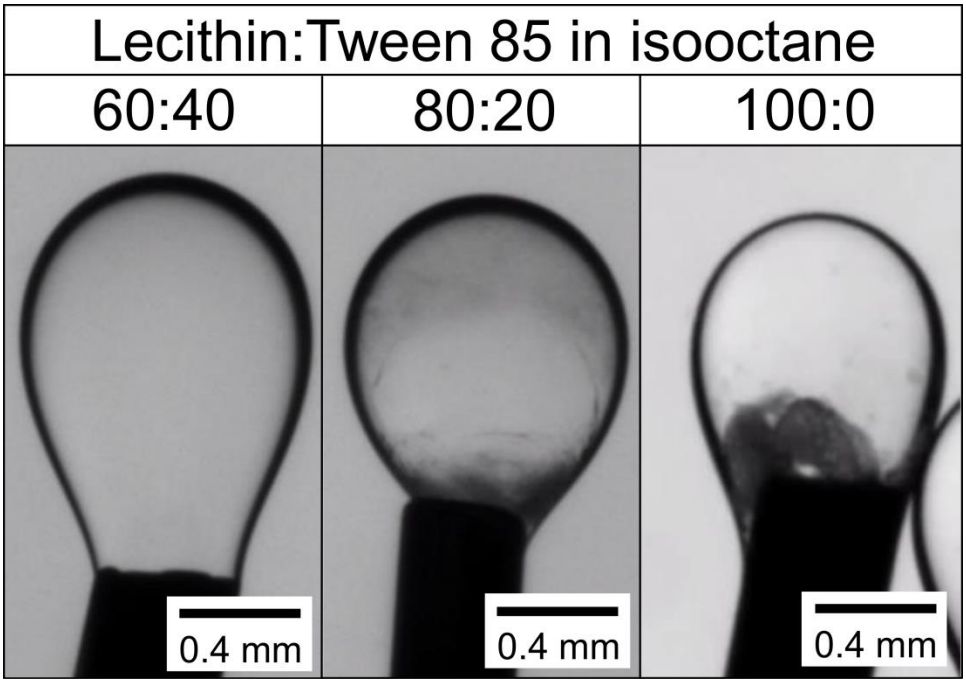

Figure 6.8: Light microscopy images of ~0.25 μL pendant droplets of dispersant-isooctane mixture in ~25 mL seawater. Dispersant-oil mixtures contain 2.5 wt% of the following dispersants: (a) 100:0 lecithin:Tween 85; (b) 80:20 lecithin:Tween 85; and (c) 60:40 lecithin:Tween 85. All images were taken 60 sec after droplet formation.

emulsification was also observed for both of these dispersant-oil mixtures, and was the dominant mode of spontaneous emulsification for 60:40 L:T dispersant, but water-into-oil spontaneous emulsification predominated for 80:20 L:T dispersant. Due to the opacity of crude oil, it was not possible to clearly image water-into-oil emulsification within it using light microscopy at 5 wt% dispersant, but at 10 wt% dispersant it was readily visible. Figure 6.7 therefore shows the progression, over the course of an hour, of water-into-oil emulsification into dispersant-oil mixture containing 10 wt% 80:20 L:T dispersant. Similar images taken of dispersant-oil mixtures containing 10 wt% dispersant with other L:T ratios and exposed to seawater for an hour show less water-into-oil emulsification as L:T ratio decreases (Appendix C, Figure C.7). It was also possible to observe water-into-oil emulsification in transparent dispersant-isooctane mixtures at 2.5 wt% dispersant, although Tween 85 (PEO_{20} sorbitan triooleate) had to be substituted for Tween 80 (PEO_{20} sorbitan monooleate), as the latter is insoluble in pure alkanes. As shown in Figure 6.8, spontaneous emulsification of seawater into isooctane occurred at lecithin:Tween 85 ratios of 100:0 and 80:20, but not at lower lecithin:Tween 85 ratios. It

is not clear whether the lack of water-into-oil spontaneous emulsification into isooctane at 60:40 lecithin:Tween 85, in contrast to observed water-into-oil spontaneous emulsification for 60:40 lecithin:Tween 80 in crude oil, is due to the substitution of Tween 85 for Tween 80 or to the low (2.5 wt%) dispersant concentration employed in isooctane.

As with the low L:T-ratio dispersant-oil mixtures, it is notable that no gel is visible in cryo-SEM images of the actively emulsifying crude oil-water interfaces in Figure 6, as might have been expected based on prior work.[110, 115-117] It is possible that, had the cryo-SEM samples been allowed to equilibrate for longer than 5 minutes before being cryogenically fixed, a macroscopic amount of gel like that observed in isooctane (Figure 6.8) would have formed. Evidently, however, the initial water-into-oil emulsification observed in Figure 6 does not require or involve such a gel. The explanations proposed by Davies and Rideal[122] for spontaneous emulsification also do not apply. No interfacial turbulence was observed for high L:T ratio dispersants (Figures 6.6-6.8), even at 10 wt% dispersant; "diffusion and stranding" is impossible, since surfactants are not leaving the crude oil; and the IFT reported for 80:20 and 60:40 L:T dispersants in prior work[41] (Figure 6.1) is significantly greater than 0 mN/m ($p < 0.05$, confidence interval for Student's t- distribution). Thus, based on prior work,[125, 126]spontaneous nucleation of water droplets into the oil seems the most plausible mechanism for the observed water-into-oil spontaneous emulsification, though additional light microscopy would be needed to confirm this.

The fact that lecithin-rich L-T dispersants exhibit water-into-oil spontaneous emulsification, rather than Tween 80-rich dispersants' vigorous oil-into-water spontaneous emulsification, may explain why they are so much more effective than Tween 80-rich dispersants which produce lower or comparable IFT,[41] and are comparable in effectiveness to other dispersants which produce much lower IFT.[3, 54] Prior work[128] indicates that the high effectiveness of widely-used dispersants containing the surfactants dioctyl sodium sulfosuccinate (DOSS), Tween 80, and Span 80 (sorbitan monooleate) is due in part to the water-in-oil microstructures formed by DOSS and Span 80, which solubilize the hydrophilic Tween 80 into the oil. Water-into-oil emulsification may serve a similar purpose for lecithin-rich L-T dispersants, solubilizing Tween 80 into the crude

oil so that it does not escape into bulk seawater. This suggests that L-T dispersants could be improved by increasing the solubility of Tween 80 in crude oil, perhaps by replacing ethanol with a more hydrophobic solvent like vegetable oil to facilitate the dissolution of Tween 80 in crude oil, or by adding a cosurfactant similar to DOSS which could incorporate Tween 80 into water-in-oil microstructures, even at L:T ratios which do not produce water-into-oil spontaneous emulsification.

6.3.2 Droplet Coalescence Testing

Droplet coalescence tests (see Figure 2a-c) were conducted to investigate the influence of dispersant-treated crude oil droplets' resistance to coalescence in seawater on the compositional trends in dispersant effectiveness shown in Figure 6.1[41]. Table 6.1 shows mean coalescence time ± 1 standard error for ~0.25 μL pendant droplets of various dispersant-crude oil mixtures. Both 1.25 wt% dispersant and 2.5 wt% dispersant exhibited three tiers of coalescence times. Dispersant-oil mixtures which contained>0

Droplet Coalescence Times (s)		
L:T Ratio	2.5 wt% dispersant	1.25 wt% dispersant
100:0	15 ± 2	5 ± 1
80:20	100 ± 17	21 ± 5
60:40	126 ± 41	19 ± 4
40:60	NC	NC
20:80	NC	22 ± 4
0:100	110 ± 19	19 ± 5

Table 6.1: Mean coalescence time ± one standard error (based on n ≥ 5 repetitions) for pendant droplets of dispersant-treated crude oil in seawater. Droplets were simultaneously dispensed from separate J-shaped needles, allowed to equilibrate for 1 min, and then brought into contact. "NC" indicates that pendant droplets never coalesced, even after remaining in contact for 300-500 seconds before one of the droplets detached from the needle.

wt% Tween 80 and produced readily visible oil-into-water spontaneous emulsification (e.g., 20:80 and 40:60 L:T) failed to coalesce, even when droplets remained in contact for > 5 min before one or both of them detached from the needle(s). Dispersant-oil mixtures which contained >0 wt% Tween 80 but did not produce readily visible oil-into-water spontaneous emulsification coalesced in 90-150 seconds for 2.5 wt% dispersant and in 15-25 seconds for 1.25 wt% dispersant. Dispersant-oil mixtures which contained 0 wt% Tween 80 (i.e., 100:0 L:T) exhibited coalescence times significantly lower than those of other dispersant-oil mixtures ($p<0.05$, one-tailed Student's t-test).

In prior work on L-T dispersants,[40-42] we and others posited that the formation of an interfacial monolayer of surfactants contributes to the effectiveness of L-T dispersants by preventing dispersed oil droplets' coalescence. This hypothesis is supported to some extent by the fact that 100:0 L:T dispersant, which contains 0 wt% Tween 80, produces both significantly lower droplet coalescence time and significantly lower dispersion effectiveness than 80:20 L:T dispersant. However, for dispersants containing > 0 wt% Tween 80, there is no clear relationship between L:T ratio and droplet coalescence time, as droplet coalescence times are similar for L:T ratios as varied as 80:20, 60:40, and 0:100 L:T. The L:T ratios which exhibit the highest effectiveness, 60:40 and 80:20 L:T (see Figure 6.1), are also not the same L:T ratios which are most resistant to droplet coalescence, 20:80 and 40:60 L:T. It is certainly possible that the strong resistance to droplet coalescence exhibited by dispersants containing 20:80 and 40:60 L:T increases their effectiveness and mitigates the effects of surfactant loss via oil-into-water spontaneous emulsification to some extent. Nevertheless, these data indicate that resistance to droplet coalescence does not, as we and others had proposed in prior work, play a primary role in determining dispersant effectiveness.

The fact that 80:20 L:T dispersant produces both significantly longer droplet coalescence times and a significantly higher dispersion effectiveness than dispersant containing 0 wt% Tween 80 (i.e., 100:0 L:T dispersant) is consistent with prior work showing that Tween 80 greatly inhibits coalescence of oil droplets in an aqueous phase. Reichert and Walker[64] studied a Tween 80 monolayer at the interface between a 100 μm diameter droplet of squalane and 3 mL of 0.5 M aqueous NaCl, and measured coalescence times for such Tween 80-coated squalane droplets in a follow-up work.[129]

Squalane droplets equilibrated for 5 minutes in a 1 μM aqueous solution of Tween 80 (which also contained 0.5 M NaCl) developed monolayers with a surface pressure of 30 mN/m and droplet coalescence times of 5-10 seconds. The concentration of Tween 80 in crude oil treated with even 1.25 wt% 80:20 L:T dispersant is ~10,000 μM, albeit confined to the oil droplet rather than filling the bulk aqueous phase. Thus, the comparable droplet coalescence times for dispersants containing 80:20, 60:40, and 0:100 L:T may be due to complete saturation of the interface with Tween 80 at all of these L:T ratios.

Finally, it is worthwhile to note that pendant drop experiments yielded no more evidence of an interfacial gel than the cryo-SEM images of dispersant-laden oil-water interfaces in Figures 6.5 & 6.6. It was not possible to use oscillating drop tensiometry to compare the interfacial rheology of different dispersant-oil mixtures, as the very small needles (0.21-0.26 mm inner diameter) necessitated by the dispersant-oil mixtures' low IFT greatly restricted flowrates in and out of the droplets, making oscillation faster than 0.01 Hz impractical. However, withdrawing oil from surfactant-covered droplets did not cause interfacial wrinkles or an insoluble rigid shell to form at any L:T ratio. This is not surprising given the high solubility of lecithin in oil and Tween 80 in seawater (another obstacle to detecting a lecithin-Tween 80 interfacial gel using oscillating drop tensiometry). Prodding dispersant-laden pendant oil droplets with beveled needles also did not reveal any interfacial gel or "skin" resisting the needles (Appendix C, Figure C.8).

6.4 Conclusion

In conclusion, Tween 80-rich lecithin-Tween 80 dispersants cause vigorous oil-into water spontaneous emulsification, while lecithin-rich dispersants primarily cause water-into-oil spontaneous emulsification. Cryogenic scanning electron microscopy reveals no complex microstructures or interfacial gel at the oil-water interface; light microscopy shows negligible interfacial turbulence, and all lecithin-Tween 80 dispersants produced non-negative IFT in prior work.[40, 41] Thus, based on prior literature,[122-126] the most plausible mechanism for oil-into-water spontaneous emulsification is "diffusion and stranding", or Tween 80 diffusion across the interface vigorous enough to emulsify the oil. For water-into-oil spontaneous emulsification, the most plausible mechanism is

spontaneous nucleation of water droplets into the oil, as this does not require surfactants to cross the interface.

Spontaneous emulsification may explain why lecithin-rich dispersants exhibit higher effectiveness than Tween 80-rich dispersants with lower or comparable oil-water IFT, as reported in prior work.[41] Oil-into-water emulsification indicates rapid leaching of surfactants from oil into water, depleting oil droplets of surfactant and lowering dispersant effectiveness. On the other hand, water-into-oil emulsification indicates stabilization of surfactants in the oil, maintaining high surfactant concentration in the oil and thus raising dispersant effectiveness. The deleterious effects of oil-into-water emulsification on dispersant effectiveness may be partially mitigated by the fact that the Tween 80-rich dispersant-oil mixtures which produce the most oil-into-water spontaneous emulsification also exhibit the greatest resistance to coalescence in droplet coalescence testing. Nevertheless, droplets' resistance to coalescence largely does not appear to have an impact on dispersant effectiveness, contrary to what we and others had posited in prior work.[40-42]

Future work should seek to reformulate lecithin-Tween 80 dispersants (e.g., by changing the solvent or adding a new surfactant/cosurfactant), in order to improve Tween 80's solubility in crude oil and minimize the effects of surfactant leaching on dispersant effectiveness. The possibility that lecithin-Tween 80 dispersants form a multilayer or gel which was not detected by cryogenic scanning electron microscopy or pendant drop experiments should also be investigated, perhaps by studying dispersants' interfacial rheology, or by visualizing surfactant accumulation at the oil-water interface using fluorescent light microscopy. Finally, the environmental impact of the crude oil nanoparticles generated by lecithin-Tween 80 dispersants in this work merits further study.

Chapter 7: Outlook and Recommendations

7.1 Dispersant Components

7.1.1 Formulation

Current formulations of Corexit 9500 also contain a fourth surfactant, Tween 85 (polyoxyethylenated sorbitan trioleate).[24] Since this surfactant is chemically similar to Tween 80 and was absent from Canevari's original 1971 patent, we have omitted it from our experiments in order to simplify our analysis of the relationships between dispersant composition, effectiveness, dynamic IFT, etc. It may be desirable in future, however, to evaluate the impact which adding Tween 85 to Tween 80/Span 80/DOSS blends has on their effectiveness and other interfacial properties.

More generally, lowering the IFT of lecithin-Tween 80 dispersants by adding another surfactant (or two) could significantly improve dispersant effectiveness. As the IFT data in Figure 5.4 show, the most effective DOSS-Tween 80-Span 80 dispersants produce IFT over 100x lower than that produced by the most effective lecithin-Tween 80 dispersants. Supplementary cryo-SEM (Figure A.4) of a crude-oil-seawater interface treated with a high-effectiveness DOSS-Tween 80-Span 80 dispersant (42:38:20 D:T:S by weight) suggests the formation of a microemulsion at the oil-water interface, which is consistent with the $<10^{-4}$ mN/m IFT observed for this dispersant. Thus, developing a crude oil-seawater microemulsion using Tween 80, lecithin, and one or two additional surfactants would likely improve the performance of lecithin-Tween 80 dispersants.

It is also important to investigate an alternative to ethanol as the solvent for lecithin-Tween 80 dispersants. Ethanol excels at dissolving high concentrations (80-90 wt%) of lecithin and Tween 80 into homogeneous mixtures, but it is also relatively volatile. It is therefore necessary to find a blend of nonvolatile, low-toxicity solvents, such as propylene glycol or dearomatized petroleum distillates, which is capable of solubilizing similarly high concentrations of these surfactants into a dispersant. Ultimately, lecithin-Tween 80 dispersants will also have to be tested on a wider variety of oils, and in large wave tanks which better approximate dispersion at sea (as described in Section 2.2), before they can be deployed on real-world oil spills.

7.1.2 Environmental Impact

The primary environmental impact of replacing DOSS with lecithin in oil dispersants which we have considered up to this point is the two compounds' individual toxicity to marine animals. In fact, overall dispersant toxicity is potentially far more complex than this, both because mixtures of dispersant components may have synergistic toxic effects and because dispersing crude oil into seawater speeds the aqueous dissolution of water-soluble components of crude oil, such as toxic polyaromatic hydrocarbons. Additional effects of dispersant use may include the formation of oil-associated marine snow and its sedimentation and uptake into the benthic ecosystem,[130] the effects of dispersant and oil metabolism on the genetic makeup and diversity of marine bacterial populations, and the influence of interfacial dispersant monolayers on the rate of oil metabolism by bacteria.[7]

This last phenomenon is especially important, because if dispersants form persistent interfacial monolayers which impede the ability of bacteria to metabolize dispersed crude oil droplets, this defeats the ultimate purpose of dispersants—to promote the biodegradation and removal of crude oil from the environment. Understanding this phenomenon is complicated by the diversity of bacteria, as they have a variety of strategies for metabolizing the crude oil and may be impacted differently by various dispersant components—one bacterium's toxin may be another bacterium's nutrient. Such a line of inquiry goes beyond the surfactant science which is the main focus of this thesis, but is crucial for the ultimate success of any future marine oil dispersant.

7.2 Interfacial Characterization of Dispersants

7.2.1 Dynamic Interfacial Tensiometry

The kinetics of dispersant water-in-oil microstructures' adsorption to the oil-water interface, and the impact of this process on dynamic IFT, remain poorly understood. This is partly because mixtures of dispersant, crude oil, and seawater are so complex, but even the dynamic IFT of water-in-oil microstructures containing only DOSS, distilled water, and an n-alkane such as dodecane is poorly characterized in the surfactant literature. Future work should explore, for example, the effect of increasing the diameter of DOSS water-in-oil microstructures by increasing their water:surfactant molar ratio on the rate of DOSS adsorption to the interface (the initial concentration of DOSS in the aqueous phase will also be an important variable to control and study in this work). A follow-up paper could explore the effect of adding an aromatic compound (e.g. toluene) to the oil, and perhaps even introduce a simple cosurfactant such as an alcohol or ethoxylated alcohol.

The biggest challenge in such work would be the high surfactant concentrations involved The author has conducted preliminary studies of the interfacial adsorption of 0.01-0.1 mM DOSS in squalane to a squalane-seawater interface in a capillary drop tensiometer[56], well below the ~1 mM critical micelle concentration of DOSS in most nonpolar solvents. IFT declined from a "clean" initial value of ~52 mN/m to a final pseudo-equilibrium value of 10-15 mN/m, near the lower limit of the instrument's measuring capability, within 5-10 seconds. Presumably, increasing surfactant concentration in the oil by another order of magnitude or more would lead to an even faster and greater decline in IFT.

The main requirements for an experimental method to characterize such a large and rapid decline in IFT are (1) the ability to form a clean, physically stable interface in much less time than it takes for the surfactant to adsorb to the interface (i.e., less than a second), and (2) the ability to keep the oil-water interface physically stable as its IFT declines by 1-2 orders of magnitude within a few seconds. Spinning drop tensiometry might be able to accomplish (2), but involves droplet injection and tensiometer spinup lasting tens of seconds, so (1) is out of the question. Conversely, it might be possible to

precisely dispense a pendant drop in under a second, but the fact that accurately measuring droplet IFT requires that the droplet be close to falling off of the needle (i.e. "pendant") would make it difficult to keep the interface physically stable as IFT declined from, say, 50 to 5 mN/m.

An improved capillary drop tensiometer is more promising: A droplet could potentially be dispensed in under a second and maintained in a stable spherical cap shape, as IFT is calculated using the pressure behind the droplet and its radius of curvature. A semi-automated capillary drop tensiometer could monitor a rapid, expected decline in IFT by dispensing a droplet and then rapidly decreasing the pressure behind it, keeping its radius of curvature constant as IFT falls. Another, more "exotic" approach to the problem is oscillating jet tensiometry, in which a jet of surfactant-treated oil is steadily released into a volume of seawater and the development of Rayleigh instabilities is imaged along the length of the jet in order to determine its IFT. Advantages of this method are the ability to access very short timescales after oil-water contact and to observe a steady-state IFT gradient along the length of the jet. Disadvantages include the large volumes of sample involved in each experiment and the difficulty of setting up such a system. Whichever method is chosen, its development and successful use could itself make for a high-impact paper, if the system were sufficiently practical to use and could readily characterize an IFT decline of an order of magnitude or more within a few seconds.

7.2.2 Interfacial Rheology

One method of characterizing an interfacial monolayer or gel not attempted in Chapter 6 is interfacial shear rheometry with a biconical bob rheometer.[131] This could characterize surfactant self-assembly at spontaneously emulsifying oil-water interfaces, like those treated with lecithin-Tween 80 dispersants,[132] while avoiding issues with surfactant adsorption/desorption inherent in any dilatational interfacial rheology on interfaces laden with soluble surfactants. Another possible way to investigate the formation of interfacial gels is doping dispersants with fluorescent surfactants, such as the fluorescent lecithin analogue BODIPY-PC,[133] and then visualizing surfactant aggregation using fluorescent light microscopy.

7.3 Microstructure Characterization in Crude Oil

In Chapter 4, dispersant water-in-oil microstructures were characterized in an alkane-aromatic blend instead of actual crude oil. In part, this is because crude oil is opaque, which prevents dispersant microstructures from being characterized via light scattering. If this were the only obstacle to studying dispersant microstructures in crude oil, however, it could perhaps be overcome by performing X-ray scattering on the microstructures instead.

The larger issue is that crude oils contain thousands of different compounds which could interact with dispersant microstructures, the identities and relative abundances of which vary greatly from oil field to oil field.[92] It is therefore effectively impossible to determine the exact composition of a crude oil and the influence of each molecule on the morphology of dispersant microstructures. Instead, the goal should be to identify representative compounds from the various operationally-defined classes of compounds in crude oil[134], such as asphaltenes, resins, and waxes, which can be added to a model oil to study their effects.

Additionally, cryo-SEM should be more widely used in understanding how dispersants act at the oil-water interface. The cryo-SEM in Chapter 6 showed that organogel was not forming at the oil-water interface; on the other hand, the image in Appendix A.4 suggests that DOSS-Tween 80-Span 80 dispersants may well form interfacial microemulsions, or at least something more complex than a monolayer. Future lecithin-Tween 80 dispersant formulations which produce $<10^{-4}$ mN/m, comparable to the IFT of the most effective DOSS-Tween 80-Span 80 dispersants, may also produce complex oil-water interfacial microstructure which could be imaged using cryo-SEM. Finally, cryo-SEM could be used to study the interface between untreated crude oil and various dispersants, in order to better understand the dispersant-oil mixing process.

References

1. Lee, H. S. Cryogenic Electron Microscopy Studies: Structure and Formation of Self-assembled Nanostructures in Solution. University of Minnesota, Minneapolis, MN, 2014.

2. Bellare, J. R. Cryo-electron and optical microscopy of surfactant microstructures. PhD Thesis, University of Minnesota, Minneapolis, MN, 1988.

3. Brochu, C.; Pelletier, E.; Caron, G.; Desnoyers, J. E. Dispersion of crude oil in seawater: The role of synthetic surfactants. *Oil Chem. Pollut.* **1986**, *3*, 257-279, DOI 10.1016/S0269-8579(86)80030-2.

4. Steen, A.; Findlay, A. Frequency of Dispersant Use Worldwide. *International Oil Spill Conference Proceedings* **2008**, *2008*, 645-649, DOI 10.7901/2169-3358-2008-1-645.

5. Princen, H. M.; Zia, I. Y. Z.; Mason, S. G. Measurement of interfacial tension from the shape of a rotating drop. *J. Coll. Interface Sci.* **1967**, *23*, 99-107, DOI 10.1016/0021-9797(67)90090-2.

6. Kim, H. A.; Seo, J. K.; Kim, T.; Lee, B. T. Nanometrology and its perspectives in environmental research. *Environ Health Toxicol* **2014**, *29*, e2014016, DOI 10.5620/eht.e2014016.

7. Kleindienst, S.; Paul, J. H.; Joye, S. B. Using dispersants after oil spills: impacts on the composition and activity of microbial communities. *Nat Rev Microbiol* **2015**, *13*, 388-96, DOI 10.1038/nrmicro3452.

8. Martin, J. D.; Velankar, S. S. Unusual behavior of PEG/PPG/Pluronic interfaces studied by a spinning drop tensiometer. *J Colloid Interface Sci* **2008**, *322*, 669-74, DOI 10.1016/j.jcis.2008.03.050.

9. The Federal Interagency Solutions Group (Oil Budget Calculator Science and Engineering Team). *Oil Budget Calculator, Deepwater Horizon*; 2010. http://www.restorethegulf.gov/sites/default/files/documents/pdf/OilBudgetCalc_Full_HQ-Print_111110.pdf

10. Limb, R. M. *Improvements in Intervention and Response Since Macondo*; Petroleum Association of Japan: February 6-7, 2014. http://www.pcs.gr.jp/doc/esymposium/2014/1_Mr_Robert_M_Limb_word_E.pdf

11. European Maritime Safety Agency. *Manual on the Applicability of Oil Dispersants*; Version 2; 2009. http://emsa.europa.eu/opr-documents/opr-manual-a-guidelines/download/1166/719/23.html

12. Buist, I.; Nedwed, T.; Mullin, J. Herding agents thicken oil spills in drift ice to facilitate in-situ burning: a new trick for an old dog. In *International Oil Spill Conference Proceedings*, Savannah, Georgia, 2008; Vol. 2008, pp 673-679.

13. Committee on Effectiveness of Oil Spill Dispersants (National Research Council Marine Board). Using Oil Spill Dispersants on the Sea. National Academy Press: Washington, D.C., 1989. http://www.nap.edu/openbook.php?record_id=736 (accessed Oct. 31, 2015).

14. Committee on Understanding Oil Spill Dispersants: Efficacy and Effects (National Research Council). Oil Spill Dispersants: Efficacy and Effects. The National Academies Press: Washington, D.C., 2005. http://www.nap.edu/openbook.php?record_id=11283 (accessed Oct. 31, 2015).

15. Almeda, R.; Hyatt, C.; Buskey, E. J. Toxicity of dispersant Corexit 9500A and crude oil to marine microzooplankton. *Ecotoxicol. Environ. Saf.* **2014**, *106*, 76-85, DOI 10.1016/j.ecoenv.2014.04.028.

16. Rico-Martinez, R.; Snell, T. W.; Shearer, T. L. Synergistic toxicity of Macondo crude oil and dispersant Corexit 9500A((R)) to the Brachionus plicatilis species complex (Rotifera). *Environ. Pollut.* **2013**, *173*, 5-10, DOI 10.1016/j.envpol.2012.09.024.

17. Hemmer, M. J.; Barron, M. G.; Greene, R. M. Comparative toxicity of eight oil dispersants, Louisiana sweet crude oil (LSC), and chemically dispersed LSC to two aquatic test species. *Environ. Toxicol. Chem.* **2011**, *30*, 2244-52, DOI 10.1002/etc.619.

18. Wetzel, D. L.; Van Fleet, E. S. Cooperative studies on the toxicity of dispersants and dispersed oil to marine organisms: A 3-year Florida study. In *International Oil Spill Conference Proceedings*, 2001; Vol. 2001, pp 1237-1241.

19. Wise, C. F.; Wise, J. T.; Wise, S. S.; Thompson, W. D.; Wise, J. P., Jr.; Wise, J. P., Sr. Chemical dispersants used in the Gulf of Mexico oil crisis are cytotoxic and genotoxic to sperm whale skin cells. *Aquat. Toxicol.* **2014**, *152*, 335-340, DOI 10.1016/j.aquatox.2014.04.020.

20. Resby, J.; Brandvik, P. J.; Daling, P. S.; Guyomarch, J.; Eide, I. In *Effects of Time on the Effectiveness of Dispersants*, 2007; p 116.

21. Proceedings of the European Oil Spill Conference (Interspill). London, England, 2012. http://www.interspill.org/previous-events/2012/ (accessed March 11, 2015).

22. Proceedings of the International Oil Spill Conference. London, England, 2014. http://ioscproceedings.org/toc/iosc/2014 (accessed March 11, 2015).

23. Brandvik, P. J.; Daling, P. S. Optimising oil spill dispersants as a function of oil type and weathering degree: a multivariate approach using partial least squares (PLS). *Chemom. Intell. Lab. Syst.* **1998**, *42*, 73-91, DOI 10.1016/S0169-7439(98)00006-9.

24. NALCO Environmental Solutions LLC. COREXIT Ingredients. https://web.archive.org/web/20130921055543/http://www.nalcoesllc.com/nes/1602.htm (accessed Oct 16, 2016).

25. Venkataraman, P.; Tang, J.; Frenkel, E.; McPherson, G. L.; He, J.; Raghavan, S. R.; Kolesnichenko, V.; Bose, A.; John, V. T. Attachment of a hydrophobically modified biopolymer at the oil-water interface in the treatment of oil spills. *ACS Appl Mater Interfaces* **2013**, *5*, 3572-80, DOI 10.1021/am303000v.

26. Alcantar, N. A. F., Dawn I.; Thomas, Sylvia; Toomey, Ryan G. Use of cactus mucilage as a dispersant and absorbant for oil in oil-water mixtures. US 9,163,374, Nov 28, 2012.

27. Saha, A.; Nikova, A.; Venkataraman, P.; John, V. T.; Bose, A. Oil emulsification using surface-tunable carbon black particles. *ACS Appl Mater Interfaces* **2013**, *5*, 3094-100, DOI 10.1021/am3032844.

28. Rodd, A. L.; Creighton, M. A.; Vaslet, C. A.; Rangel-Mendez, J. R.; Hurt, R. H.; Kane, A. B. Effects of surface-engineered nanoparticle-based dispersants for marine oil spills on the model organism Artemia franciscana. *Environmental science & technology* **2014**, *48*, 6419-27, DOI 10.1021/es500892m.

29. Dong, J.; Worthen, A. J.; Foster, L. M.; Chen, Y.; Cornell, K. A.; Bryant, S. L.; Truskett, T. M.; Bielawski, C. W.; Johnston, K. P. Modified montmorillonite clay microparticles for stable oil-in-seawater emulsions. *ACS Appl Mater Interfaces* **2014**, *6*, 11502-13, DOI 10.1021/am502187t.

30. Wan, W.-M.; Pickett, P. D.; Savin, D. A.; McCormick, C. L. Structurally controlled "polysoaps" via RAFT copolymerization of AMPS and n-dodecyl acrylamide for environmental remediation. *Polym. Chem.* **2014**, *5*, 819-827, DOI 10.1039/c3py01073b.

31. Canevari, G. P. Oil Slick Dispersant and Method. U.S. Patent 3,793,218, 1974.

32. Ross, S. T., K. *Assessment of the Use of Dispersants on Marine Oil Spills in California*; OSRR-413; S.L. Ross Environmental Research: 2004. https://www.bsee.gov/sites/bsee.gov/files/osrr-oil-spill-response-research//413aa.pdf

33. Carlsson, C.; Johansson, A. K.; Alvan, G.; Bergman, K.; Kuhler, T. Are pharmaceuticals potent environmental pollutants? Part II: environmental risk assessments of selected pharmaceutical excipients. *Sci. Total. Environ.* **2006**, *364*, 88-95, DOI 10.1016/j.scitotenv.2005.06.036.

34. Aliphatic Esters Panel (American Chemistry Council). Final Submission Document for the Sorbitan Esters Category of the Aliphatic Esters Chemicals *High Production Volume (HPV) Chemical Challenge Program Technical Reports* [Online], 2013. http://www.epa.gov/hpv/pubs/summaries/alipestr/c13466rr10.pdf.

35. Maggi, P. C., D. . Relative harmfulness of five anionic detergents in the sea. l-Acute toxicity with regard to fifteen organisms. *Rev. Trav. Inst. Peches Marit.* **1973**, *37*, 4114-4117, DOI.

36. Peri, J. B. The state of solution of aerosol OT in nonaqueous solvents ☆. *Journal of Colloid and Interface Science* **1969**, *29*, 6–15, DOI 10.1016/0021-9797(69)90340-3.

37. Mukherjee, K.; Moulik, S. P.; Mukherjee, D. C. Thermodynamics of micellization of Aerosol OT in polar and nonpolar solvents. A calorimetric study. *Langmuir* **1993**, *9*, 1727-1730, DOI 10.1021/la00031a020.

38. Smith, G. N.; Brown, P.; Rogers, S. E.; Eastoe, J. Evidence for a critical micelle concentration of surfactants in hydrocarbon solvents. *Langmuir* **2013**, *29*, 3252-3258, DOI 10.1021/la400117s.

39. Paul, B. K.; Mitra, R. K. Water solubilization capacity of mixed reverse micelles: effect of surfactant component, the nature of the oil, and electrolyte concentration. *J. Colloid Interface Sci.* **2005**, *288*, 261-279, DOI 10.1016/j.jcis.2005.02.088.

40. Athas, J. C.; Jun, K.; McCafferty, C.; Owoseni, O.; John, V. T.; Raghavan, S. R. An effective dispersant for oil spills based on food-grade amphiphiles. *Langmuir* **2014**, *30*, 9285-9294, DOI 10.1021/la502312n.

41. Riehm, D. A.; Neilsen, J. E.; Bothun, G. D.; John, V. T.; Raghavan, S. R.; McCormick, A. V. Efficient dispersion of crude oil by blends of food-grade surfactants: Toward greener oil-spill treatments. *Mar. Poll. Bull.* **2015**, *101*, 92-7, DOI 10.1016/j.marpolbul.2015.11.012.

42. Nyankson, E.; DeCuir, M. J.; Gupta, R. B. Soybean Lecithin as a Dispersant for Crude Oil Spills. *ACS Sustain. Chem. Eng.* **2015**, *3*, 920-931, DOI 10.1021/acssuschemeng.5b00027.

43. Palacios, L. E.; Wang, T. Egg-yolk lipid fractionation and lecithin characterization. *Journal of the American Oil Chemists' Society* **2005**, *82*, 571-578, DOI 10.1007/s11746-005-1111-4.

44. Walde, P.; Giuliani, A. M.; Boicelli, C. A.; Luisi, P. L. Phospholipid-based reverse micelles. *Chem. Phys. Lipids* **1990**, *53*, 265-288, DOI 10.1016/0009-3084(90)90026-n.

45. Shinoda, K.; Araki, M.; Sadaghiani, A.; Khan, A.; Lindman, B. Lecithin-based microemulsions: phase behavior and microstructure. *The Journal of Physical Chemistry* **1991**, *95*, 989-993, DOI 10.1021/j100155a091.

46. Chen, H.; Guan, Y.; Zhong, Q. Microemulsions based on a sunflower lecithin-Tween 20 blend have high capacity for dissolving peppermint oil and stabilizing coenzyme Q10. *Journal of agricultural and food chemistry* **2015**, *63*, 983-9, DOI 10.1021/jf504146t.

47. Gosenca, M.; Bester-Rogac, M.; Gasperlin, M. Lecithin based lamellar liquid crystals as a physiologically acceptable dermal delivery system for ascorbyl palmitate. *Eur J Pharm Sci* **2013**, *50*, 114-22, DOI 10.1016/j.ejps.2013.04.029.

48. Clayton, J. R., Jr.; Payne, J. R.; Farlow, J. S. Oil Spill Dispersants: Mechanisms of Action and Laboratory Tests; CRC Press, Inc.: Boca Raton, FL, 1993.

49. Fingas, M. F. K., D.A.; Wang, Z.; Handfield, D; Ianuzzi, D.; Ackerman, F. Laboratory effectiveness testing of oil spill dispersants (ASTM STP 1252). In *The Use of Chemicals in Oil Spill Response*, Lane, P., Ed. ASTM International: Philadelphia, PA, 1995.

50. Venosa, A. D.; King, D. W.; Sorial, G. a. The Baffled Flask Test for Dispersant Effectiveness: A Round Robin Evaluation of Reproducibility and Repeatability. *Spill Sci. Technol. B.* **2002**, *7*, 299-308, DOI 10.1016/S1353-2561(02)00072-5.

51. Belore, R. C.; Trudel, B. K.; Lee, K. Correlating Wave Tank Dispersant Effectiveness Tests with at-Sea Trials. *International Oil Spill Conference Proceedings* **2005**, *2005*, 65-70, DOI 10.7901/2169-3358-2005-1-65.

52. Belore, R.; Buist, I.; Trudel, K.; Morrison, J. Wave Tank and Swirling Flask Dispersant Effectiveness Testing on Fresh Mississippi Canyon 252 Oil. *International Oil Spill Conference Proceedings* **2011**, *2011*, abs251, DOI 10.7901/2169-3358-2011-1-251.

53. Lewis, A.; Trudel, B. K.; Belore, R. C.; Mullin, J. V. Large-scale dispersant leaching and effectiveness experiments with oils on calm water. *Mar. Poll. Bull.* **2010**, *60*, 244-254, DOI 10.1016/j.marpolbul.2009.09.019.

54. Riehm, D. A.; McCormick, A. V. The role of dispersants' dynamic interfacial tension in effective crude oil spill dispersion. *Mar. Poll. Bull.* **2014**, *84*, 155-163, DOI 10.1016/j.marpolbul.2014.05.018.

55. Swirling Flask Dispersant Effectiveness Test, Revised Standard Dispersant Toxicity Test, and Bioremediation Agent Effectiveness Test. In *Appendix C to 40CFR300*, 1994; pp 224-246.

56. Alvarez, N. J.; Walker, L. M.; Anna, S. L. A microtensiometer to probe the effect of radius of curvature on surfactant transport to a spherical interface. *Langmuir* **2010**, *26*, 13310-9, DOI 10.1021/la101870m.

57. Adrian, M.; Dubochet, J.; Lepault, J.; McDowall, A. W. Cryo-electron microscopy of viruses. *Nature* **1984**, *308*, 32-36, DOI 10.1038/308032a0.

58. van Staveren, H. J.; Moes, C. J.; van Marie, J.; Prahl, S. A.; van Gemert, M. J. Light scattering in Intralipid-10% in the wavelength range of 400-1100 nm. *Appl Opt* **1991**, *30*, 4507-14, DOI 10.1364/AO.30.004507.

59. Brown, J. C. P., P.N.; Dietz, R. Photon correlation study of polydisperse samples of polystyrene in cyclohexane. *J. Chem. Phys.* **1975**, *62*, 1136-1144, DOI 10.1063/1.430557.

60. Rewick, R. T.; Sabo, K. A.; Smith, J. H. The drop-weight interfacial tension method for predicting dispersant performance. *Industrial and Engineering Chemistry Product Research and Development* **1983**, *22*, 683-688, DOI 10.1021/i300012a032.

61. Knudsen, O. Ø.; Brandvik, P. J.; Lewis, A. In *Treating Oil Spills with W/O Emulsion Inhibitors-A Laboratory Study of Surfactant Leaching from the Oil to the Water Phase*, Seventeenth Arctic and Marine Oilspill Program Technical Seminar, Vancouver, BC, Canada, Environment Canada: Vancouver, BC, Canada, 1994; pp 1023-1034.

62. Knudsen, O.; Hokstad, J. N.; Brandvik, P. J. In *Leaching of surfactants used in oil spill chemicals from the oil to the water phase (DIWO Report no. 26)*, Trondheim, Norway, Trondheim, Norway, 1997.

63. Hokstad, J. N.; Knudsen, B.; Daling, P. S. In *Oil-surfactant interaction and mechanism studies - Part 1: Leaching of surfactants from oil to water. Chemical composition of dispersed oil.*, Trondheim, Norway, Trondheim, Norway, 1996.

64. Reichert, M. D.; Walker, L. M. Interfacial tension dynamics, interfacial mechanics, and response to rapid dilution of bulk surfactant of a model oil-water-dispersant system. *Langmuir* **2013**, *29*, 1857-1867, DOI 10.1021/la4000395.

65. Kirby, S. M.; Anna, S. L.; Walker, L. M. Sequential adsorption of an irreversibly adsorbed nonionic surfactant and an anionic surfactant at an oil/aqueous interface. *Langmuir* **2015**, *31*, 4063-71, DOI 10.1021/la504969v.

66. Kester, D. R.; Duedall, I. W.; Connors, D. N.; Pytkowicz, R. M. Preparation of artificial seawater. *Limnol. Oceanogr.* **1967**, *12*, 176-179, DOI 10.4319/lo.1967.12.1.0176.

67. Aerosol OT Solution 75%; MSDS No. 00409. Fisher Scientific: Fair Lawn, NJ, 2009.

68. Joseph, D. D. A., M.S.; Gillberg, G.; Hu, H.; Hultman, D.; Verdier, C.; Vinagre, T.M. A spinning drop tensioextensometer. *J. Rheol.* **1992**, *36*, 621-662, DOI 10.1122/1.550311.

69. Li, Z.; Lee, K.; King, T.; Boufadel, M. C.; Venosa, A. D. Assessment of chemical dispersant effectiveness in a wave tank under regular non-breaking and breaking wave conditions. *Marine pollution bulletin* **2008**, *56*, 903-912, DOI 10.1016/j.marpolbul.2008.01.031.

70. Mukherjee, B.; Wrenn, B. A. Influence of Dynamic Mixing Energy on Dispersant Performance: Role of Mixing Systems. *Environmental Engineering Science* **2009**, *26*, 1725-1737, DOI 10.1089/ees.2009.0159.

71. Lunel, T. Understanding the Mechanism of Dispersion through Oil Droplet Size Measurements at Sea. In *The Use of Chemicals in Oil Spill Response*, Lane, P., Ed. ASTM International: Philadelphia, PA, 1995.

72. Capdevila, M.; Maestro, A.; Porras, M.; Gutiérrez, J. M. Preparation of Span 80/oil/water highly concentrated emulsions: influence of composition and formation variables and scale-up. *Journal of colloid and interface science* **2010**, *345*, 27-33, DOI 10.1016/j.jcis.2010.01.045.

73. Griffin, W. C. Classification of Surface-Active Agents by "HLB". *Journal of Cosmetic Science* **1954**, *1*, 311-326, DOI.

74. Kundu, K.; Paul, B. K. Physicochemical investigation of mixed surfactant reverse micelles: Water solubilization and conductometric studies. *Colloids and Surfaces A: Physicochemical and Engineering Aspects* **2013**, *433*, 154-165, DOI 10.1016/j.colsurfa.2013.05.009.

75. Ron, E. Z.; Rosenberg, E. Biosurfactants and oil bioremediation. *Current Opinion in Biotechnology* **2002**, *13*, 249-252, DOI 10.1016/s0958-1669(02)00316-6.

76. Zulauf, M.; Eicke, H. F. Inverted micelles and microemulsions in the ternary system water/aerosol-OT/isooctane as studied by photon correlation spectroscopy. *J. Phys. Chem. B* **1979**, *83*, 480-486, DOI 10.1021/j100467a011.

77. Cheng, M. B.; Wang, J. C.; Li, Y. H.; Liu, X. Y.; Zhang, X.; Chen, D. W.; Zhou, S. F.; Zhang, Q. Characterization of water-in-oil microemulsion for oral delivery of earthworm fibrinolytic enzyme. *J. Control Release* **2008**, *129*, 41-8, DOI 10.1016/j.jconrel.2008.03.018.

78. Ayyub, P.; Maitra, A.; Shah, D. O. Microstructure of the CTAB-butanol-octane-water microemulsion system: effect of dissolved salts. *J. Chem. Soc., Faraday Trans.* **1993**, *89*, 3585, DOI 10.1039/ft9938903585.

79. Royal Society of Chemistry. The Merck Index Online. https://www.rsc.org/Merck-Index/monograph/m8973/polysorbates derivative polysorbate.

80. Almela, A.; Elizalde, M. P.; Benito, R. The aggregation of Span 80 in toluene. *J. Solution Chem.* **1993**, *22*, 231-241, DOI 10.1007/BF00649246.

81. Silva, A. E.; Barratt, G.; Cheron, M.; Egito, E. S. Development of oil-in-water microemulsions for the oral delivery of amphotericin B. *Int. J. Pharm.* **2013**, *454*, 641-8, DOI 10.1016/j.ijpharm.2013.05.044.

82. Shukla, A. Characterization of Microemulsions using Small Angle Scattering Techniques. Ph.D. Dissertation, Martin Luther University of Halle-Wittenberg, Halle, Germany, 2003.

83. Liu, D.; Ma, J.; Cheng, H.; Zhao, Z. Investigation on the conductivity and microstructure of AOT/non-ionic surfactants/water/n-heptane mixed reverse micelles. *Colloid. Surface. A* **1998**, *135*, 157-164, DOI 10.1016/s0927-7757(97)00239-2.

84. Nazário, L. M. M.; Hatton, T. A.; Crespo, J. P. S. G. Nonionic Cosurfactants in AOT Reversed Micelles: Effect on Percolation, Size, and Solubilization Site. *Langmuir* **1996**, *12*, 6326-6335, DOI 10.1021/la960687u.

85. Kundu, K.; Paul, B. K. Physicochemical investigation of biocompatible mixed surfactant reverse micelles: II. Dynamics of conductance percolation, energetics of droplet clustering, effect of additives and dynamic light scattering studies. *J. Chem. Thermodyn.* **2013**, *63*, 148-163, DOI 10.1016/j.jct.2013.04.005.

86. Zhang, X.; Chen, Y.; Liu, J.; Zhao, C.; Zhang, H. Investigation on the structure of water/AOT/IPM/alcohols reverse micelles by conductivity, dynamic light scattering, and small angle X-ray scattering. *J. Phys. Chem. B* **2012**, *116*, 3723-3734, DOI 10.1021/jp210902r.

87. Baalousha, M.; Lead, J. R. Rationalizing nanomaterial sizes measured by atomic force microscopy, flow field-flow fractionation, and dynamic light scattering: sample preparation, polydispersity, and particle structure. *Environ. Sci. Technol.* **2012**, *46*, 6134-42, DOI 10.1021/es301167x.

88. Parmar, A. S.; Muschol, M. Hydration and hydrodynamic interactions of lysozyme: effects of chaotropic versus kosmotropic ions. *Biophys. J.* **2009**, *97*, 590-598, DOI 10.1016/j.bpj.2009.04.045.

89. Yudin, I. K.; Anisimov, M. A. Dynamic Light Scattering Monitoring of Asphaltene Aggregation in Crude Oils and Hydrocarbon Solutions. In *Asphaltenes, Heavy Oils, and Petroleomics*, Mullins, O. C.; Sheu, E. Y.; Hammami, A.; Marshall, A. G., Eds. Springer New York: 2007; pp 439-468.

90. Product Safety Summary: Isopar M Fluid 2014. https://www.exxonmobilchemical.com/Chem-English/Files/Resources/isopar-m-fluid-product-safety-summary.pdf (accessed Aug 14, 2015).

91. Koifman, N.; Schnabel-Lubovsky, M.; Talmon, Y. Nanostructure formation in the lecithin/isooctane/water system. *J. Phys. Chem. B* **2013**, *117*, 9558-9567, DOI 10.1021/jp405490q.

92. Steering Committee for the Petroleum in the Marine Environment Update (National Research Council). Oil in the Sea: Inputs, Fates, and Effects; National Academy Press: Washington, DC, 1985.

93. Liu, Z.; Liu, J.; Zhu, Q.; Wu, W. The weathering of oil after theDeepwater Horizonoil spill: insights from the chemical composition of the oil from the sea surface, salt marshes and sediments. *Environ. Res. Lett.* **2012**, *7*, 035302, DOI 10.1088/1748-9326/7/3/035302.

94. Stepto, R. F. T. Dispersity in polymer science (IUPAC Recommendations 2009). *Pure Appl. Chem.* **2009**, *81*, 351-353, DOI 10.1351/pac-rec-08-05-02.

95. Bridié, A. L.; Wanders, T. H.; Zegveld, W.; van der Heijde, H. B. Formation, prevention and breaking of sea water in crude oil emulsions 'chocolate mousses'. *Mar. Poll. Bull.* **1980**, *11*, 343-348, DOI 10.1016/0025-326x(80)90279-9.

96. Hiorns, R. C.; de Bettignies, R.; Leroy, J.; Bailly, S.; Firon, M.; Sentein, C.; Khoukh, A.; Preud'homme, H.; Dagron-Lartigau, C. High Molecular Weights, Polydispersities, and Annealing Temperatures in the Optimization of Bulk-Heterojunction Photovoltaic Cells Based on Poly(3-hexylthiophene) or Poly(3-butylthiophene). *Adv. Funct. Mater.* **2006**, *16*, 2263-2273, DOI 10.1002/adfm.200600005.

97. Coessens, V.; Pintauer, T.; Matyjaszewski, K. Functional polymers by atom transfer radical polymerization. *Prog. Polym. Sci.* **2001**, *26*, 337-377, DOI 10.1016/s0079-6700(01)00003-x.

98. Garti, N.; Wellner, E.; Aserin, A.; Sarig, S. Analysis of sorbitan fatty acid esters by HPLC. *J. Am. Oil Chem. Soc.* **1983**, *60*, 1151-1154, DOI 10.1007/bf02671346.

99. Zhang, R.; Wang, Y.; Tan, L.; Zhang, H. Y.; Yang, M. Analysis of polysorbate 80 and its related compounds by RP-HPLC with ELSD and MS detection. *J. Chromatogr. Sci.* **2012**, *50*, 598-607, DOI 10.1093/chromsci/bms035.

100. Acevedo, S.; Rodríguez, P.; Labrador, H. An Electron Microscopy Study of Crude Oils and Maltenes. *Energ. Fuel.* **2004**, *18*, 1757-1763, DOI 10.1021/ef040044j.

101. Wilson, A.; Fuchs, G.; Scramoncin, C.; Martin, D.; Planche, J. P. Localization of the Polymer Phase in Bitumen/Polymer Blends by Field Emission Cryo-Scanning Electron Microscopy. *Energ. Fuel.* **2000**, *14*, 575-584, DOI 10.1021/ef9902303.

102. Royal Society of Chemistry. The Merck Index Online. https://www.rsc.org/Merck-Index/monograph/m4716/docusate sodium.

103. Fiume, M. Z. Final Report on the Safety Assessment of Lecithin and Hydrogenated Lecithin. *Int. J. Toxicol.* **2001**, *20*, 21-45, DOI 10.1080/109158101750300937.

104. Kaku, V. J.; Boufadel, M. C.; Venosa, A. D. Evaluation of Mixing Energy in Laboratory Flasks Used for Dispersant Effectiveness Testing. *J. Environ. Eng.* **2006**, *132*, 93-101, DOI 10.1061/(ASCE)0733-9372(2006)132:1(93).

105. Sorial, G. A.; Venosa, A. D.; Koran, K. M.; Holder, E.; King, D. W. Oil Spill Dispersant Effectiveness Protocol. I: Impact of Operational Variables. *J. Environ. Eng.* **2004**, *130*, 1073-1084, DOI 10.1061/(ASCE)0733-9372(2004)130:10(1073).

106. Sorial, G. A.; Venosa, A. D.; Koran, K. M.; Holder, E.; King, D. W. Oil Spill Dispersant Effectiveness Protocol. II: Performance of Revised Protocol. *J. Environ. Eng.* **2004**, *130*, 1085-1093, DOI 10.1061/(ASCE)0733-9372(2004)130:10(1085).

107. Venosa, A. D., Holder, E. *Laboratory-Scale Testing of Dispersant Effectiveness of 20 Oils Using the Baffled Flask Test*; 2011. http://www.bsee.gov/Technology-and-Research/Oil-Spill-Response-Research/Reports/600-699/666AA/

108. Srinivasan, R.; Lu, Q.; Sorial, G. A.; Venosa, A. D.; Mullin, J. Dispersant Effectiveness of Heavy Fuel Oils Using Baffled Flask Test. *Environ. Eng. Sci.* **2007**, *24*, 1307-1320, DOI 10.1089/ees.2006.0251.

109. Khelifa, A., Fingas, M.; Hollebone, B.P.; Brown, C.E. Effects of Chemical Dispersants on Oil Physical Properties and Dispersion. In *Thirtieth Arctic and Marine Oil Spill Program Technical Seminar*, Ottawa, Canada, 2007; pp 105-116.

110. Shchipunov, Y. A. Self-organising structures of lecithin. *Russ. Chem. Rev* **1997**, *66*, 301-322, DOI 10.1070/RC1997v066n04ABEH000253.

111. Shchipunov, Y. A. Lecithin organogel: A micellar system with unique properties. *Colloid Surface A* **2001**, *183-185*, 541-554, DOI 10.1016/s0927-7757(01)00511-8.

112. Davies, R.; Graham, D. E.; Vincent, B. Water-cyclohexane-"Span 80"-"Tween 80" systems: Solution properties and water/oil emulsion formation. *J. Colloid Interf. Sci.* **1987**, *116*, 88-99, DOI 10.1016/0021-9797(87)90101-9.

113. Suhaj, B. F., Ed. Lecithins: Sources, Manufacture & Uses; The American Oil Chemists' Society: Champaign, IL, 1989.

114. Coors, E. A.; Seybold, H.; Merk, H. F.; Mahler, V. Polysorbate 80 in medical products and nonimmunologic anaphylactoid reactions. *Ann. Allergy Asthma Immun.* **2005**, *95*, 593-599, DOI 10.1016/s1081-1206(10)61024-1.

115. Shchipunov, Y. A.; Schmiedel, P. Phase Behavior of Lecithin at the Oil/Water Interface. *Langmuir* **1996**, *12*, 6443-6445, DOI 10.1021/la960082y.

116. Rydhag, L.; Wilton, I. The function of phospholipids of soybean lecithin in emulsions. *J. Am. Oil Chem. Soc.* **1981**, *58*, 830-837, DOI 10.1007/bf02665591.

117. Ogino, K.; Onishi, M. Interfacial action of natural surfactants in oil/water systems. *J. Colloid Interface Sci.* **1981**, *83*, 18-25, DOI 10.1016/0021-9797(81)90004-7.

118. Kumar, T. S. Preparation and Characterization of Novel Span 80:Tween 80 Based Organogels for Food and Pharmaceutical Industries. Ph.D. Dissertation, National Institute of Technology-Rourkela, Rourkela, Odisha, 2011.

119. Sagiri, S. S.; Behera, B.; Sudheep, T.; Pal, K. Effect of Composition on the Properties of Tween-80–Span-80-Based Organogels. *Des. Monomers Polym.* **2012**, *15*, 253-273, DOI 10.1163/156855511x615669.

120. Mercuri, A.; Passalacqua, A.; Wickham, M. S.; Faulks, R. M.; Craig, D. Q.; Barker, S. A. The effect of composition and gastric conditions on the self-emulsification process of ibuprofen-loaded self-emulsifying drug delivery systems: a microscopic and dynamic gastric model study. *Pharm. Res.* **2011**, *28*, 1540-51, DOI 10.1007/s11095-011-0387-8.

121. Komaiko, J. S.; McClements, D. J. Formation of Food-Grade Nanoemulsions Using Low-Energy Preparation Methods: A Review of Available Methods. *Compr. Rev. Food Sci. F.* **2016**, *15*, 331-352, DOI 10.1111/1541-4337.12189.

122. Davies, J.; Rideal, E. Interfacial Phenomena, 2nd Ed.; Academic Press: New York, 1963.

123. López-Montilla, J. C.; Herrera-Morales, P. E.; Pandey, S.; Shah, D. O. Spontaneous Emulsification: Mechanisms, Physicochemical Aspects, Modeling, and Applications. *J. Disper. Sci. Technol.* **2002**, *23*, 219-268, DOI 10.1080/01932690208984202.

124. Miller, C. A. Spontaneous Emulsification Produced by Diffusion — A Review. *Colloid. Surface.* **1988**, *29*, 89-102, DOI 10.1016/0166-6622(88)80173-2.

125. Santana-Solano, J.; Quezada, C. M.; Ozuna-Chacón, S.; Arauz-Lara, J. L. Spontaneous emulsification at the water/oil interface. *Colloid. Surface. A* **2012**, *399*, 78-82, DOI 10.1016/j.colsurfa.2012.02.032.

126. Evdokimov, I. N.; Fesan, A. A.; Kronin, A. M.; Losev, A. P. Common Features of "Rag" Layers in Water-in-Crude Oil Emulsions with Different Stability. Possible Presence of Spontaneous Emulsification. *J. Disp. Sci. Technol.* **2015**, *37*, 1535-1543, DOI 10.1080/01932691.2015.1116081.

127. Lee, H. S.; Morrison, E. D.; Frethem, C. D.; Zasadzinski, J. A.; McCormick, A. V. Cryogenic electron microscopy study of nanoemulsion formation from microemulsions. *Langmuir* **2014**, *30*, 10826-10833, DOI 10.1021/la502207f.

128. Riehm, D. A.; Rokke, D. J.; McCormick, A. V. Water-in-Oil Microstructures Formed by Marine Oil Dispersants in a Model Crude Oil. *Langmuir* **2016**, *32*, 3954-62, DOI 10.1021/acs.langmuir.6b00643.

129. Reichert, M. D.; Walker, L. M. Coalescence behavior of oil droplets coated in irreversibly-adsorbed surfactant layers. *J. Colloid Interface Sci.* **2015**, *449*, 480-7, DOI 10.1016/j.jcis.2015.02.032.

130. Daly, K. L. P., U.; Chanton, J.; Hollander, D. Assessing the impacts of oil-associated marine snow formation and sedimentation during and after the Deepwater Horizon oil spill. *Anthropocene* **2016**, *13*, 18-33, DOI j.ancene.2016.01.006.

131. Simon, S.; Subramanian, S.; Gao, B.; Sjöblom, J. Interfacial Shear Rheology of Gels Formed at the Oil/Water Interface by Tetrameric Acid and Calcium Ion: Influence of Tetrameric Acid Structure and Oil Composition. *Industrial & Engineering Chemistry Research* **2015**, *54*, 8713-8722, DOI 10.1021/acs.iecr.5b02165.

132. Riehm, D. A.; Rokke, D. J.; Paul, P. G.; Lee, H. S.; Vizanko, B. S.; McCormick, A. V. Dispersion of oil into water using lecithin-Tween 80 blends: The role of spontaneous emulsification. *J Colloid Interface Sci* **2017**, *487*, 52-59, DOI 10.1016/j.jcis.2016.10.010.

133. Papadopulos, A.; Vehring, S.; Lopez-Montero, I.; Kutschenko, L.; Stockl, M.; Devaux, P. F.; Kozlov, M.; Pomorski, T.; Herrmann, A. Flippase activity detected with unlabeled lipids by shape changes of giant unilamellar vesicles. *J Biol Chem* **2007**, *282*, 15559-68, DOI 10.1074/jbc.M604740200.

134. Fan, T.; Buckley, J. S. Rapid and Accurate SARA Analysis of Medium Gravity Crude Oils. *Energy & Fuels* **2002**, *16*, 1571-1575, DOI 10.1021/ef0201228.

Appendix A: Supporting Information for Chapter 3

A.1 Preparation of Oil Dispersant

The required amount of each dispersant component may be calculated as follows:

1) Determine desired weight fractions of Tween 80, Span 80, and DOSS in the dispersant.
2) Given densities of 1.1 g/cm^3 for AOT-75 (which contains 75 wt% DOSS), 0.99 g/cm^3 for Span 80, and 1.07 g/cm^3 for Tween 80, convert the weight fractions to volume fractions.
    a. **Note:** Use (0.75*1.1 g/cm^3) for the density of DOSS, so that wt% DOSS is converted to vol% AOT-75.
    b. For example, 40 wt% DOSS and 60 wt% Tween 80 convert to:
        i. $\frac{40*(0.75*1.1)}{(0*0.99)+(60*1.07)+(40*(0.75*1.1))}$ = 46.4 vol% AOT-75
        ii. $\frac{60*1.07}{(0*0.99)+(60*1.07)+(40*(0.75*1.1))}$ = 53.6 vol% Tween 80
3) Determine the volume of dispersant to be generated.
    a. Multiply this volume by 20/33 to calculate the amount of solvent (e.g., Isopar M) to be added.
    b. Multiply this volume by 13/33 to calculate to total volume of surfactant to be added.
4) Using the surfactant volume fractions from (2) and the total volume of surfactant from (3)(b), calculate the volumes of Tween 80, Span 80, and AOT-75 to be added.
5) Divide the total volume of AOT-75 by 1.1 g/cm^3 = 1.1 mg/µL to obtain the total mass of AOT-75, and then use the composition of AOT-75 (75 wt% DOSS, 18.5 wt% water, 6.5 wt% ethanol) to calculate the amounts of DOSS, water, and ethanol required for the dispersant.

A.2 Calibration Curves for Effectiveness Test Spectrophotometry

Calibration standards for this curve were prepared according to a method described in the US EPA "Swirling Flask Test" that is designed to simulate a set of samples with known dispersion effectivenesses. A mixture of dispersant solvent (Isopar M) and crude oil at a 1:20 volumetric ratio was prepared, and aliquots of this mixture with volumes (simulated effectivenesses) of 0.945 µL (10%), 2.36 µL (25%), 4.725 µL (50%), and 9.45 µL (100%) were each added to separatory flasks containing 4.5 mL of synthetic seawater. The oil was emulsified by shaking the flasks, and was then extracted from the emulsion with dichloromethane and the extracts' absorbances were measured between 360 and 400 nm, via the same procedure used for characterizing oil-water dispersions described above. Additionally, a 100%-dispersion-standard was prepared, as described above, by adding 9.45 µL of oil directly to 4 mL of dichloromethane, and its absorbance was also measured between 360 and 400 nm.

In Figure A.1(b), expected linear dependences of absorbance on effectiveness at 360 nm (blue), 380 nm (green), and 400 nm (red) are plotted as straight lines between the origin and the observed absorbances (Figure A.1(a)) of the 100%-dispersion-standard at those wavelengths. The absorbances of the calibration standards at those same wavelengths are plotted as markers in Figure A.1(b), and are seen to follow the linear extrapolations from the 100%-dispersion-standard absorbances very well. Thus, approximating dispersant effectiveness as the ratio of the absorbance of an oil-water dispersion sample extract to the absorbance of a 100%-dispersion-standard was determined to be an acceptable substitute for constructing a full calibration curve before every effectiveness test.

(a)

Wavelength (nm)	100%-Dispersion-Standard Absorbance
360	1.94
380	1.385
400	1.049

(b)

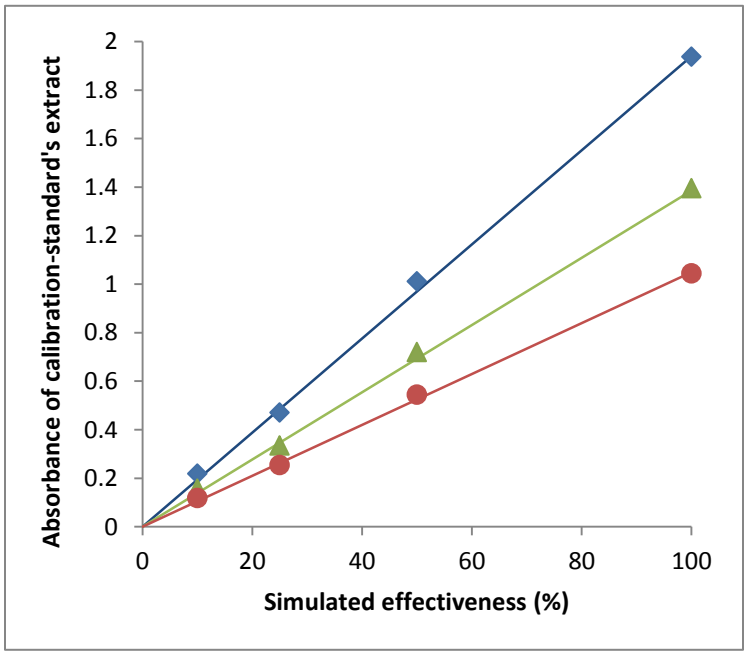

Figure A.1 (a) Absorbances of 100%-dispersion-standard at 360 nm, 380 nm, and 400 nm. (b) Markers indicate absorbances at 360 nm(♦), 380 nm(▲), and 400 nm(●) of oil-dichloromethane mixtures extracted from oil-water dispersions with known, "simulated" dispersion effectivenesses. Lines indicate expected dependence of absorbance on effectiveness based on a linear extrapolation from the measured absorbance of the 100%-dispersion-standard oil-DCM mixture at each wavelength to the origin.

A.3 Droplet Settling in Stirred Flask Test

The 50 mL Pyrex Erlenmeyer flasks used in this work for effectiveness testing, when filled with 50 mL of simulated seawater and the 1-1/2" x 3/8" Fisherbrand Spinbar Octagonal Magnetic Stir Bar, have a total water column height of 4.9 cm. Since the time allowed for droplet settling after the end of agitation and prior to sampling of the oil-in-water dispersion is five minutes, any droplet which rises faster than 0.98 cm/min, or 0.16 mm/s, will settle out. We may approximate the oil droplets as solid rising spheres undergoing Stokes flow (Re << 1) through the water. Then balancing the drag force $F_{drag,\infty}$ at terminal velocity v_∞ given by Stokes' Law, $F_{drag,\infty} = 3\pi\mu_{water}D_{drop}v_\infty$, with the buoyant force on the oil droplets, $F_{buoy} = (\rho_{water} - \rho_{oil}) * g * (\frac{\pi}{6}D_{drop}^3)$, we may solve for the maximum droplet diameter in the dispersion sample $D_{drop} = \sqrt{\frac{6\mu_{water}v_\infty}{g(\rho_{water}-\rho_{oil})}} = \sqrt{\frac{18(0.001\ Pa*s)(0.00016\frac{m}{s})}{(9.8\frac{N}{kg})\left(1017\frac{kg}{m^3}-842\frac{kg}{m^3}\right)}} = 41\ \mu m$, which corresponds to a maximum droplet volume of $V_{drop} = \frac{\pi}{6}D_{drop}^3 = 3.6 * 10^{-5}\mu L$.

A.4 Supplementary Cryo-Electron Microscopy of Dispersant-Treated Oil-Water Interface

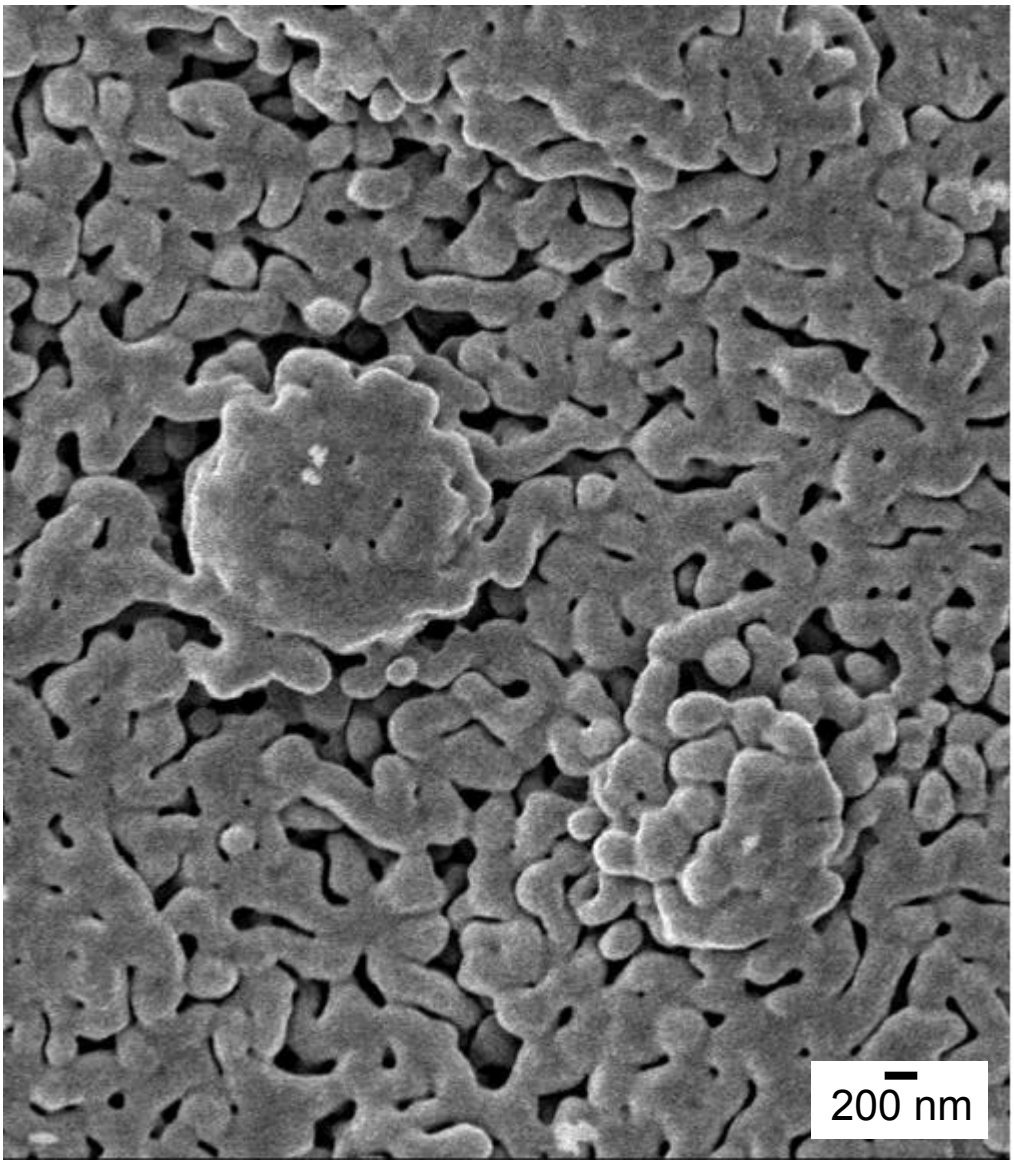

Figure A.2 Cryo-SEM image of crude-oil seawater interface treated with 42:38:20 DOSS:Tween 80:Span 80 (w:w:w) dispersant at a 1:10 volumetric dispersant:oil ratio. Dispersant was prepared as described in Section 3.2.3; cryo-SEM was conducted using a procedure similar to that described in Section 6.2.5.

Appendix B: Supporting Information for Chapter 4

B.1 Calculations of Synthetic Seawater Molar Masses

NaCl synthetic seawater (SSW), as prepared in this work, contains 24.96 g/L NaCl, 5.27 g/L $MgCl_2$, 3.86 g/L Na_2SO_4, and 982.4 g/L distilled H_2O, for an overall density of 1016.5 g/L. The molar masses of these compounds may be used to calculate their molar concentrations in the NaCl SSW: 0.427 mol/L NaCl, 0.0554 mol/L $MgCl_2$, 0.0272 mol/L Na_2SO_4, and 54.5 mol/L H_2O. Since the salts actually dissociate into their constituent ions when they enter aqueous solution, the "overall molar mass" of the NaCl SSW was calculated using the molar concentrations of the ions: (0.427 + 2*0.0272) = 0.481 mol/L Na^+, (0.427 + 2*0.0554) = 0.538 mol/L Cl^-, 0.0554 mol/L Mg^{2+}, and 0.0272 mol/L SO_4^{2-}. Finally, the density of the SSW may be divided by the total number of moles of ions and water per liter of SSW to calculate the "overall molar mass" of the NaCl SSW:

$$NaCl\ SSW\ molar\ mass = \frac{(SSW\ density)}{\sum(molar\ concentrations\ of\ ions\ and\ water\ in\ SSW)}$$

$$= \frac{(1016.5\ {}^{g}/_{L})}{(0.481\ {}^{mol}/_{L}\ Na^{+} + 0.538\ {}^{mol}/_{L}\ Cl^{-} + 0.0554\ {}^{mol}/_{L}\ Mg^{2+} + 0.0272\ {}^{mol}/_{L}\ SO_4^{2-} + 54.5\ {}^{mol}/_{L}}$$

$$= \mathbf{18.28\ g/mol}$$

Substituting CsCl for NaCl in this calculation yields the "overall molar mass" of CsCl SSW:

$$CsCl\ SSW\ molar\ mass = \frac{(SSW\ density)}{\sum(molar\ concentrations\ of\ ions\ and\ water\ in\ SSW)}$$

$$= \frac{(1058\ {}^{g}/_{L})}{(0.427\ {}^{mol}/_{L}\ Cs^{+} + 0.0272\ {}^{mol}/_{L}\ Na^{+} + 0.538\ {}^{mol}/_{L}\ Cl^{-} + 0.0554\ {}^{mol}/_{L}\ Mg^{2+} + 0.0272\ {}^{mol}/$$

$$= \mathbf{19.13\ g/mol}$$

B.2 Supplementary Cryo-TEM Images

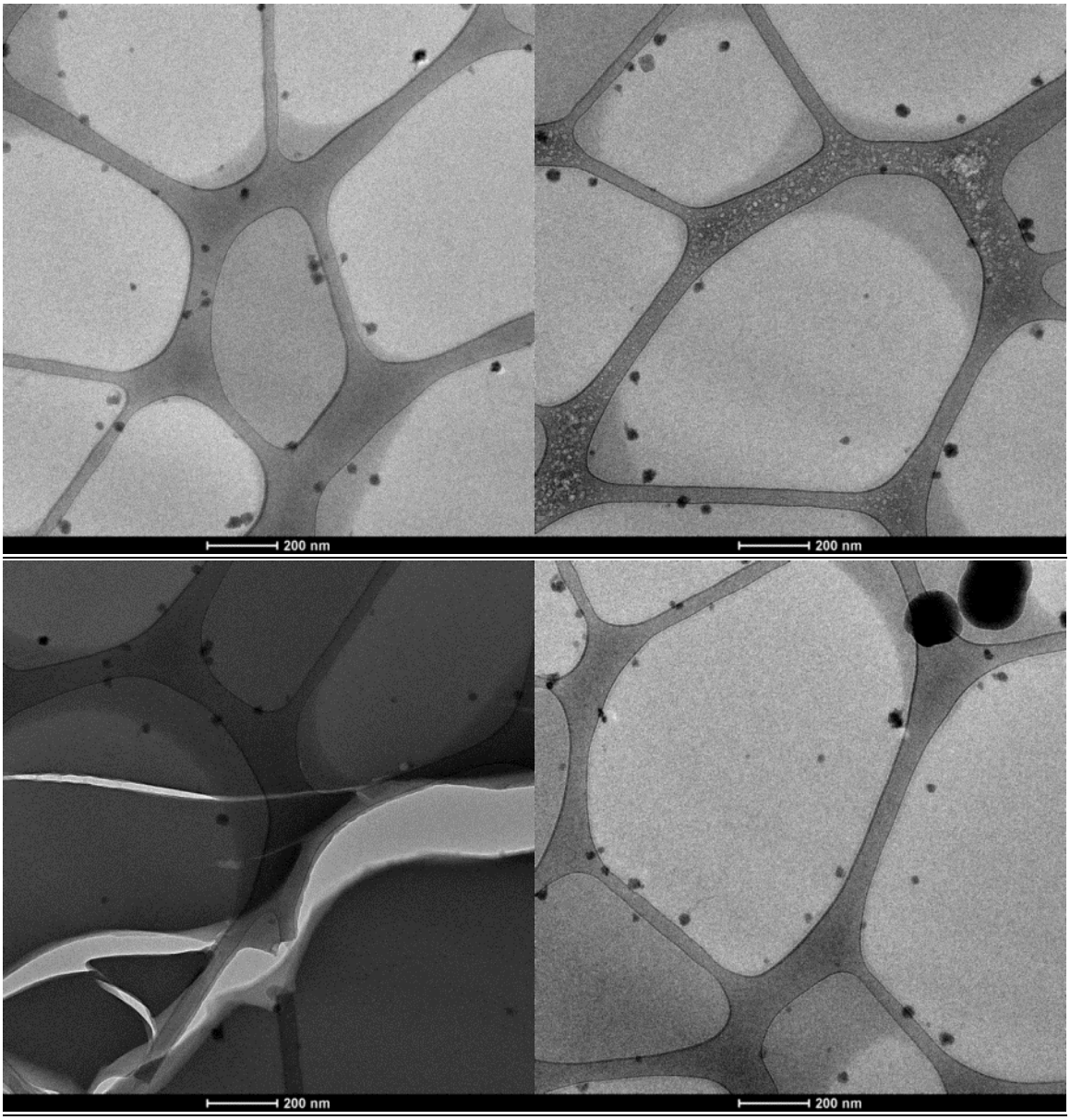

Figure B.1: Additional cryo-TEM images of the 50:50:0 (w:w:w) DOSS:Tween 80:Span 80 sample with a seawater:surfactant molar ratio $\omega = 25$ imaged in the paper.
Top left: Another good image of the water-in-oil microstructures.
Top right: Typical beam damage is visible.
Bottom left: A crack in the frozen sample film, showing clearly that the observed ~20-40 nm ice crystals are embedded in it and are therefore microstructures and not artifacts.
Bottom right: Large ice crystals (upper-right corner) are clearly distinguishable as artifacts by their excessive underfocus, as they are well out of the focal plane and not embedded in the frozen sample film with the microstructures.

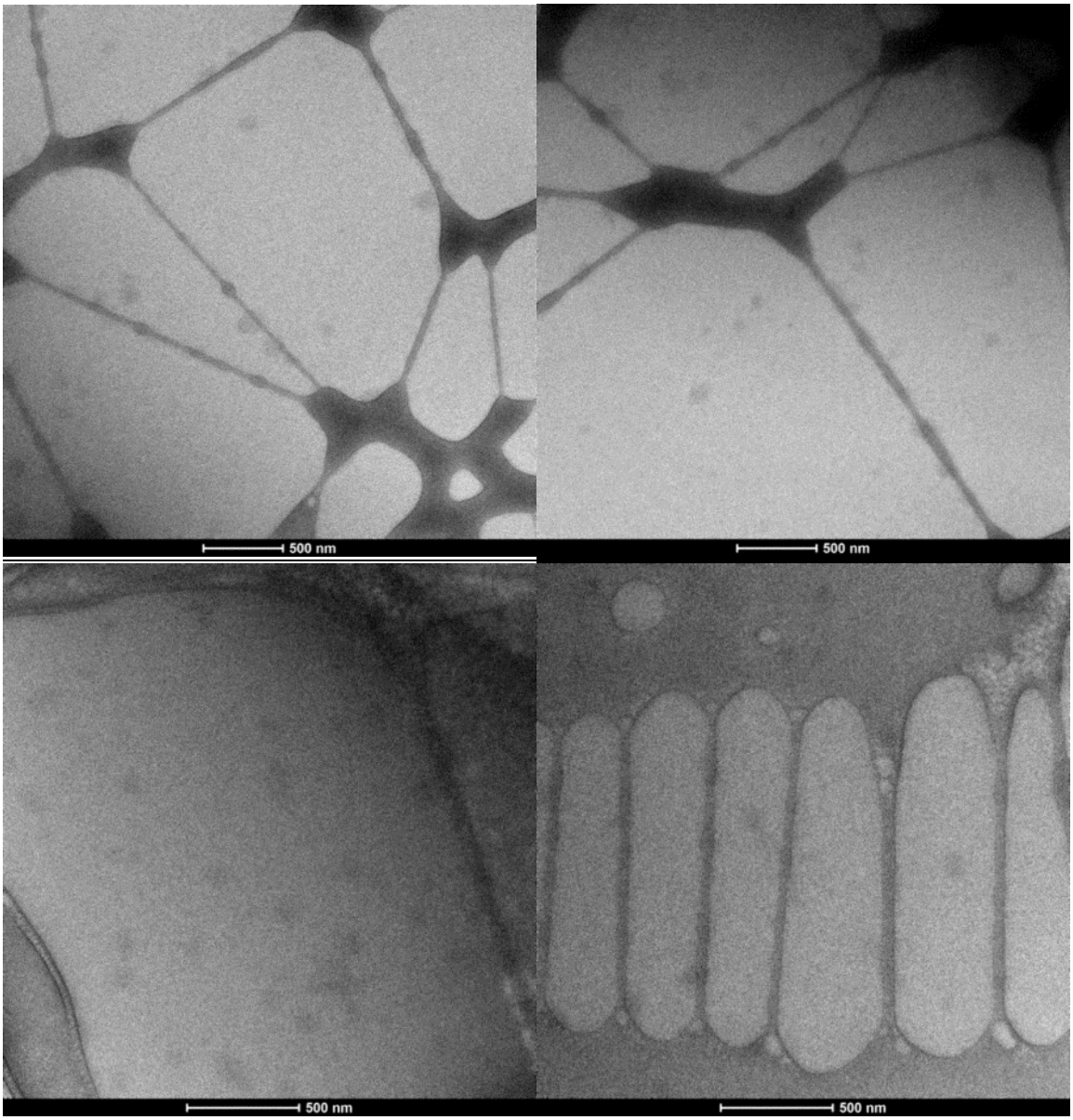

Figure B.2: Additional cryo-TEM images.
Top left, top right: Additional cryo-TEM images of the 0:50:50 (w:w:w) DOSS:Tween 80:Span 80 sample with a seawater:surfactant molar ratio $\omega = 12.5$ imaged in Figure.
Bottom left, bottom right: Cryo-TEM images of a second 0:50:50 (w:w:w) DOSS:Tween 80:Span 80 sample, establishing the reproducibility of these dispersant microstructures' appearance (since they are much paler than the microstructures observed in any of the other imaged surfactant-oil-seawater mixtures).

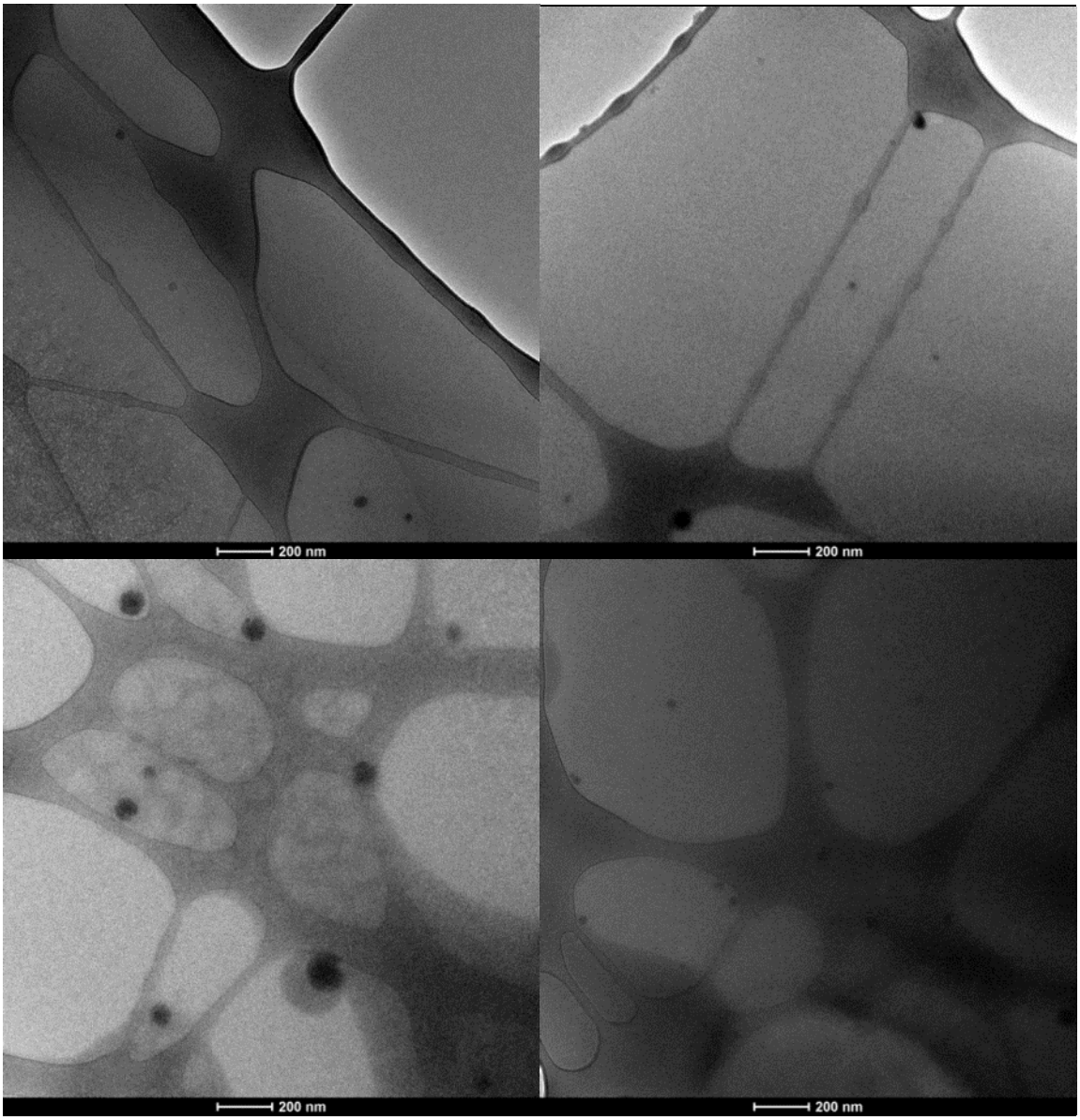

Figure B.3: Additional cryo-TEM images.
Top left, top right: Additional cryo-TEM images of the 30:50:20 (w:w:w) DOSS:Tween 80:Span 80 sample with a seawater:surfactant molar ratio $\omega = 25$ imaged in the paper.
Bottom left, bottom right: Cryo-TEM images of a 50:50:0 (w:w:w) DOSS:Tween 80:Span 80 sample with a seawater:surfactant molar ratio W:S = 40. The bottom left sample was equilibrated for 12 hours before imaging (like other cryo-TEM samples), while the bottom right sample was equilibrated for 60 hours before imaging. The decline in microstructure diameter over time shown in these two images confirms the observation of such a decline via dynamic light scattering in Figures 4.5-4.7, as well as in Figure B.4 on the following page.

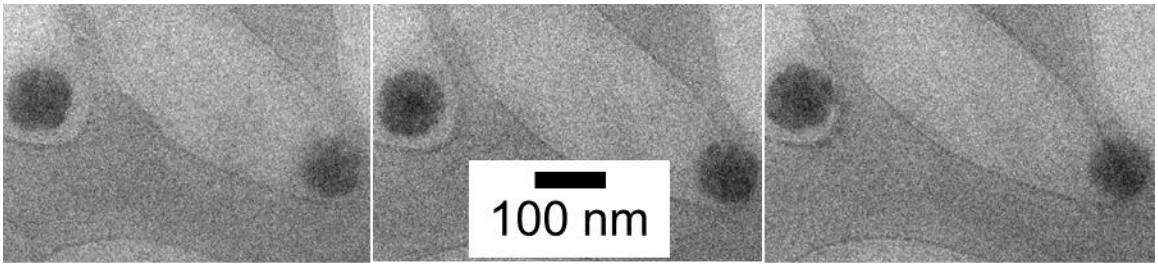

Figure B.4: Cryo-TEM images of a 50:50:0 (w:w:w) DOSS:Tween 80:Span 80 sample. The sample was tilted at angles of 0° (left), 15° (center), and 0° again (right), relative to the plane perpendicular to the electron beam. The darkest areas in the microstructures change as the sample is tilted, indicating that the microstructures are at least partly crystalline.

B.3 Supplementary DLS Data

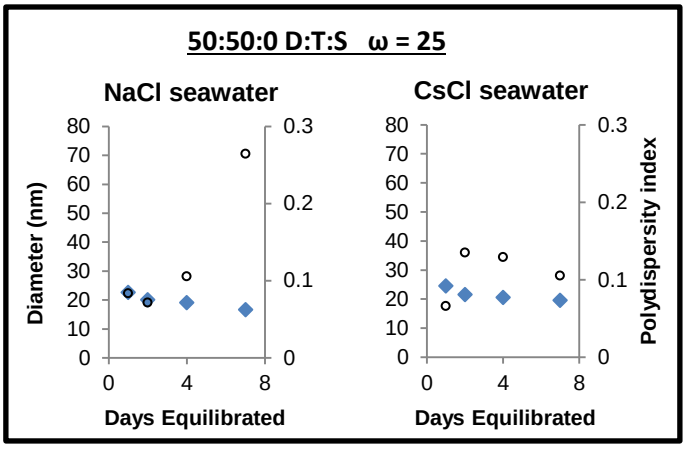

Figure B.5: Diameter (♦) and polydispersity index (o) of W/O microstructures formed by a 50:50:0 DOSS:Tween 80:Span 80 blend in model crude oil at an added seawater:surfactant molar ratio ω = 25, measured via DLS.

The data on the left was collected from a surfactant-oil-seawater mixture in which the synthetic seawater was prepared using NaCl, like all samples characterized via DLS in the main paper. The sample on the right was collected from a surfactant-oil-seawater mixture in which CsCl was substituted for NaCl in the synthetic seawater, as was done for samples characterized via cryo-TEM in the main paper.

The nearly identical diameters of the microstructures in the two samples indicate that substituting CsCl for NaCl in the cryo-TEM imaged samples in order to improve contrast in the cryo-TEM images did not discernibly alter the observed microstructures.

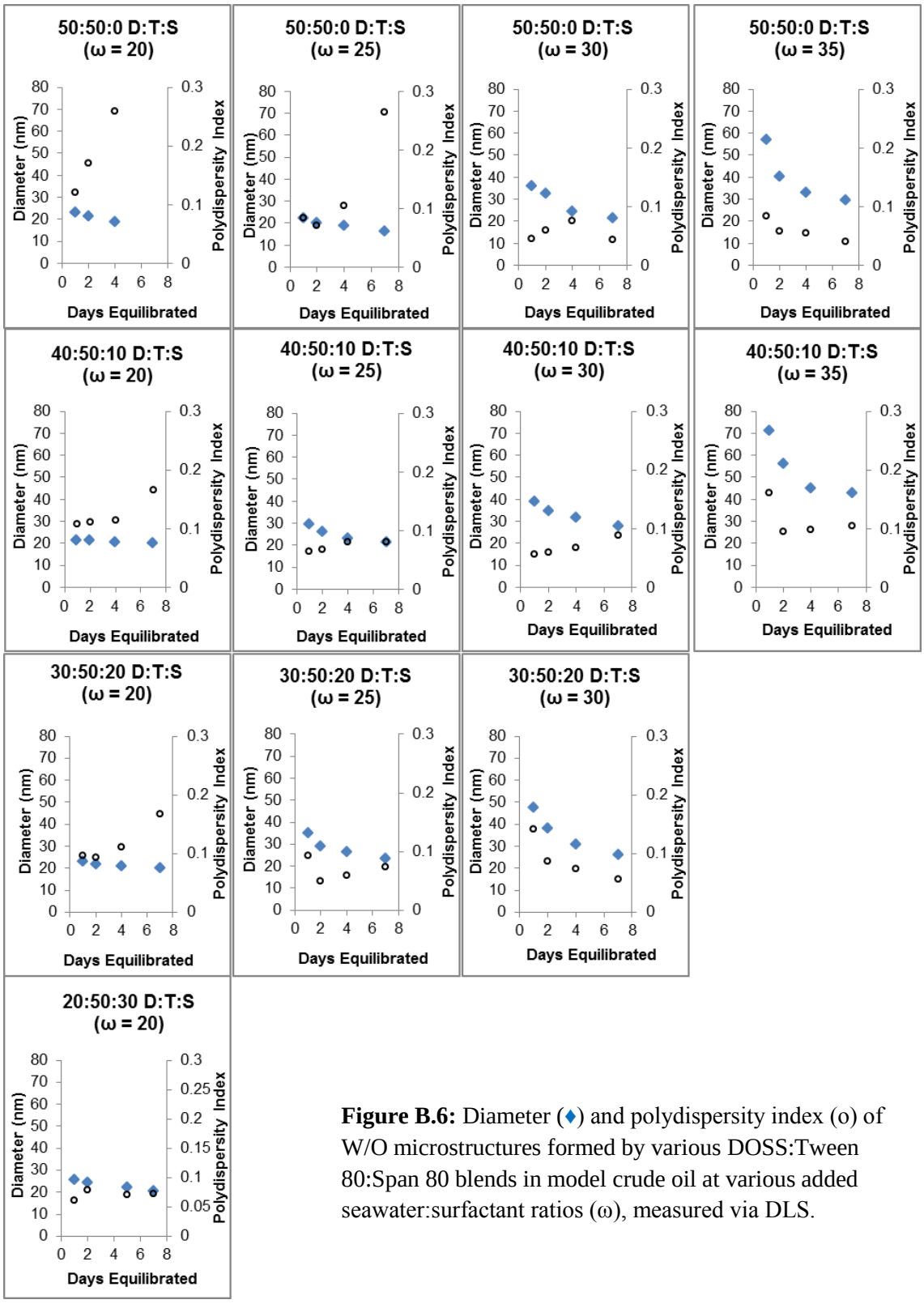

Figure B.6: Diameter (♦) and polydispersity index (o) of W/O microstructures formed by various DOSS:Tween 80:Span 80 blends in model crude oil at various added seawater:surfactant ratios (ω), measured via DLS.

Appendix C: Supporting Information for Chapter 6

C.1 EDS for Figures 5.5-5.6

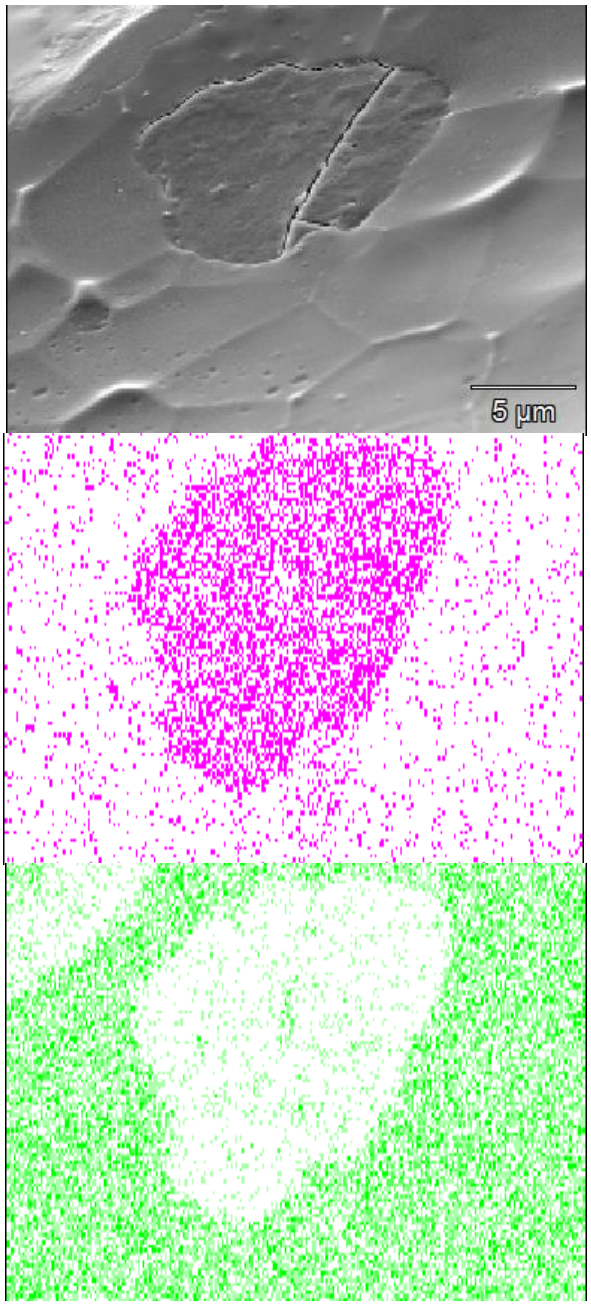

Figure C.1: Cryo-SEM and EDS images associated with Figure 5, 60:40 L:T.
Top, greyscale image: Secondary electron image of the sample, as shown in Figure 5.
Middle, purple image: Carbon (oil) in the imaged area, mapped using EDS.
Bottom, green image: Oxygen (seawater) in the imaged area, mapped using EDS.

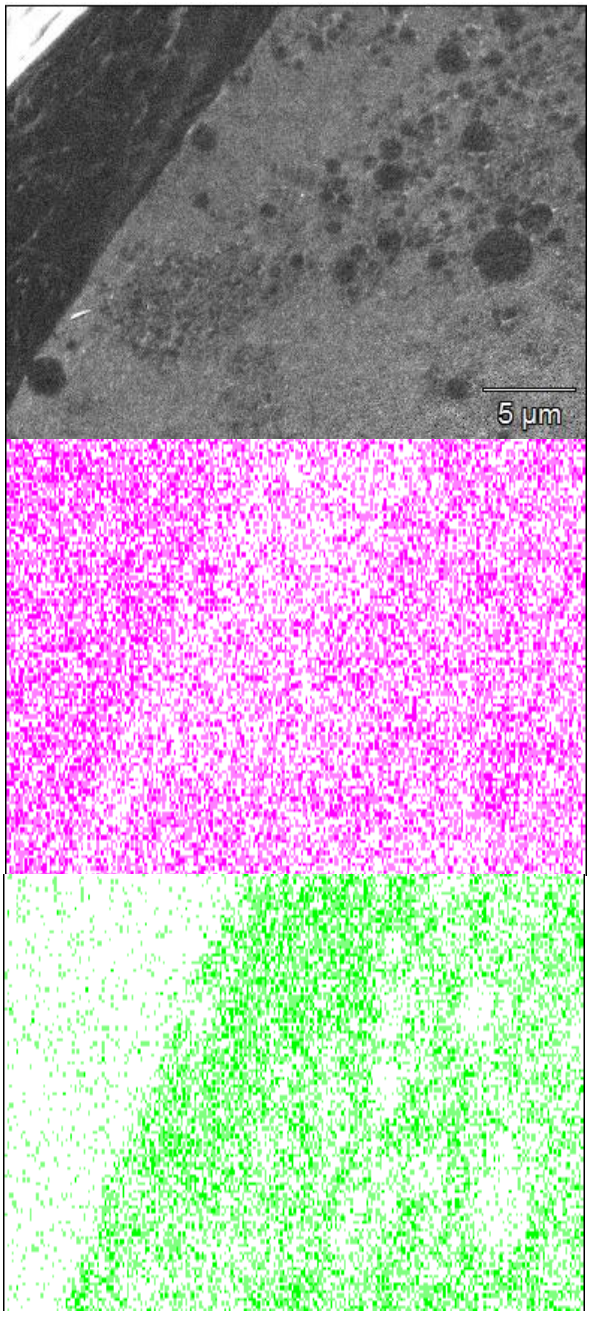

Figure C.2: Cryo-SEM and EDS images associated with Figure 5, 20:80 L:T.
Top, greyscale image: Secondary electron image of the sample, as shown in Figure 5.
Middle, purple image: Carbon (oil) in the imaged area, mapped using EDS.
Bottom, green image: Oxygen (seawater) in the imaged area, mapped using EDS.

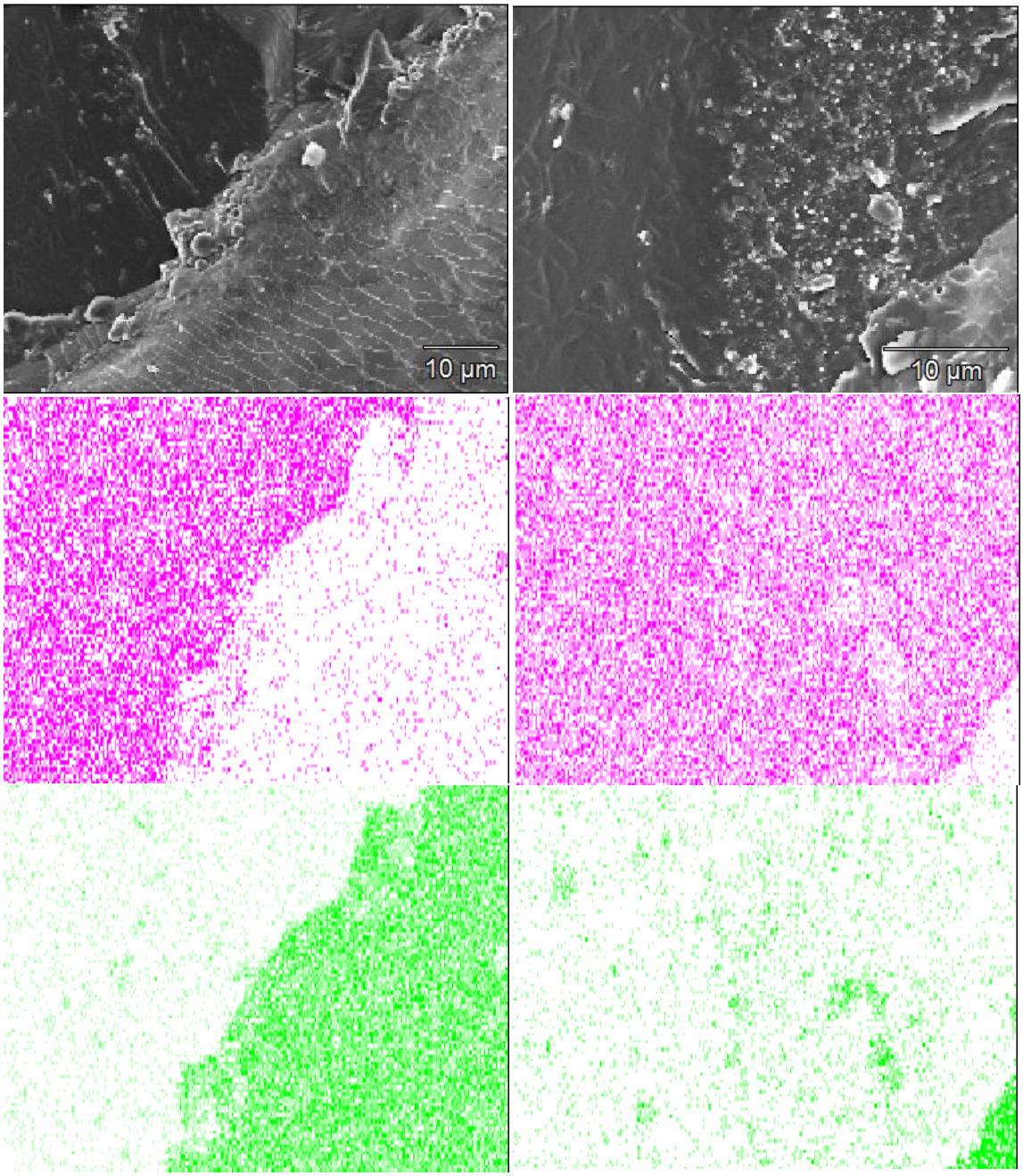

Figure C.3: Cryo-SEM and EDS images associated with Figure 6, 80:20 L:T.
Top, greyscale images: Secondary electron images of the sample, as shown in Figure 6.
Middle, purple images: Carbon (oil) in the imaged areas, mapped using EDS.
Bottom, green images: Oxygen (seawater) in the imaged areas, mapped using EDS.

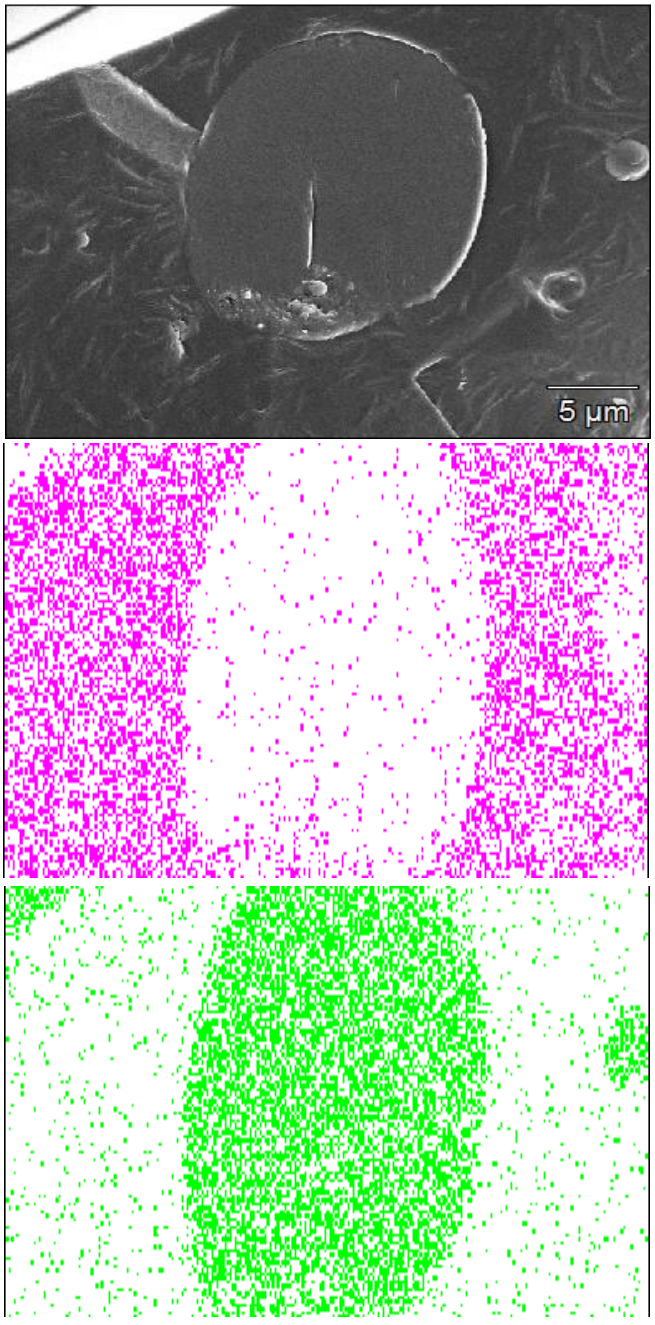

Figure C.4: Cryo-SEM and EDS images associated with Figure 6, 60:40 L:T.
Top, greyscale image: Secondary electron image of the sample, as shown in Figure 6.
Middle, purple image: Carbon (oil) in the imaged area, mapped using EDS.
Bottom, green image: Oxygen (seawater) in the imaged area, mapped using EDS.

C.2 Cryo-SEM Particle Sizing Images (Figure 5.5, 20:80 L:T)

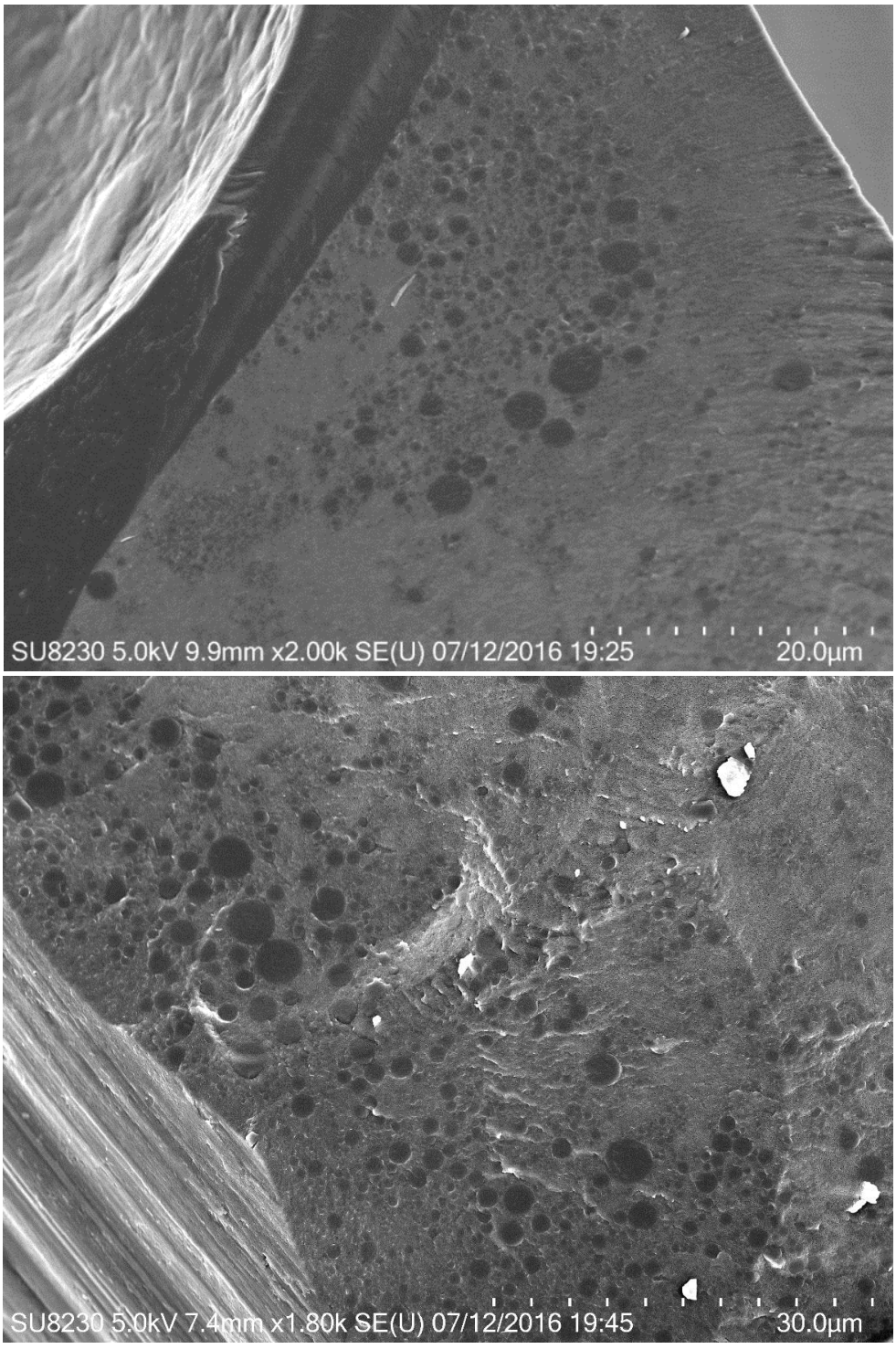

Figure C.5: Cryo-SEM images of droplets of crude oil containing 5 wt% 20:80 L:T dispersant, which were spontaneously emulsified into seawater from the interface depicted in the left half of the upper image. The 20:80 L:T image in Figure 5 is a magnified view of the upper image's lower left corner. Approximately 500 droplets were measured by hand to calculate their median diameter, 0.7 µm

C.3 Supplementary Light Microscopy Images

C.3.1 Oil-into-water Spontaneous Emulsification (100:0, 80:20, and 0:100 L:T)

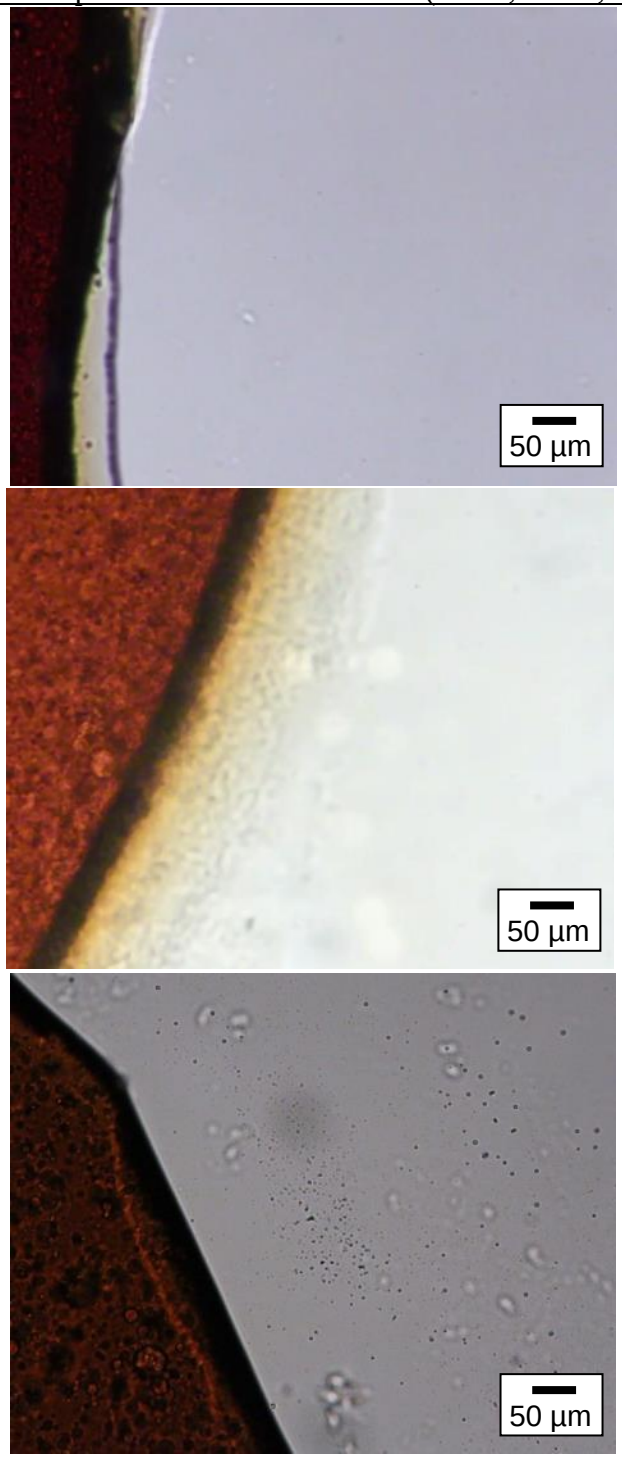

Figure C.6: Light microscopy images of dispersant-crude oil mixtures showing their spontaneous emulsification, or lack thereof, into seawater. Dispersant-oil mixtures contain: (top) 4 wt% 100:0 L:T dispersant; (middle) 5 wt% 80:20 L:T dispersant; (bottom) 5 wt% 0:100 L:T dispersant. Images were taken 10-20 minutes after oil-water contact.

C.3.2 Water-into-oil Spontaneous Emulsification (60:40, 40:60, and 20:80 L:T)

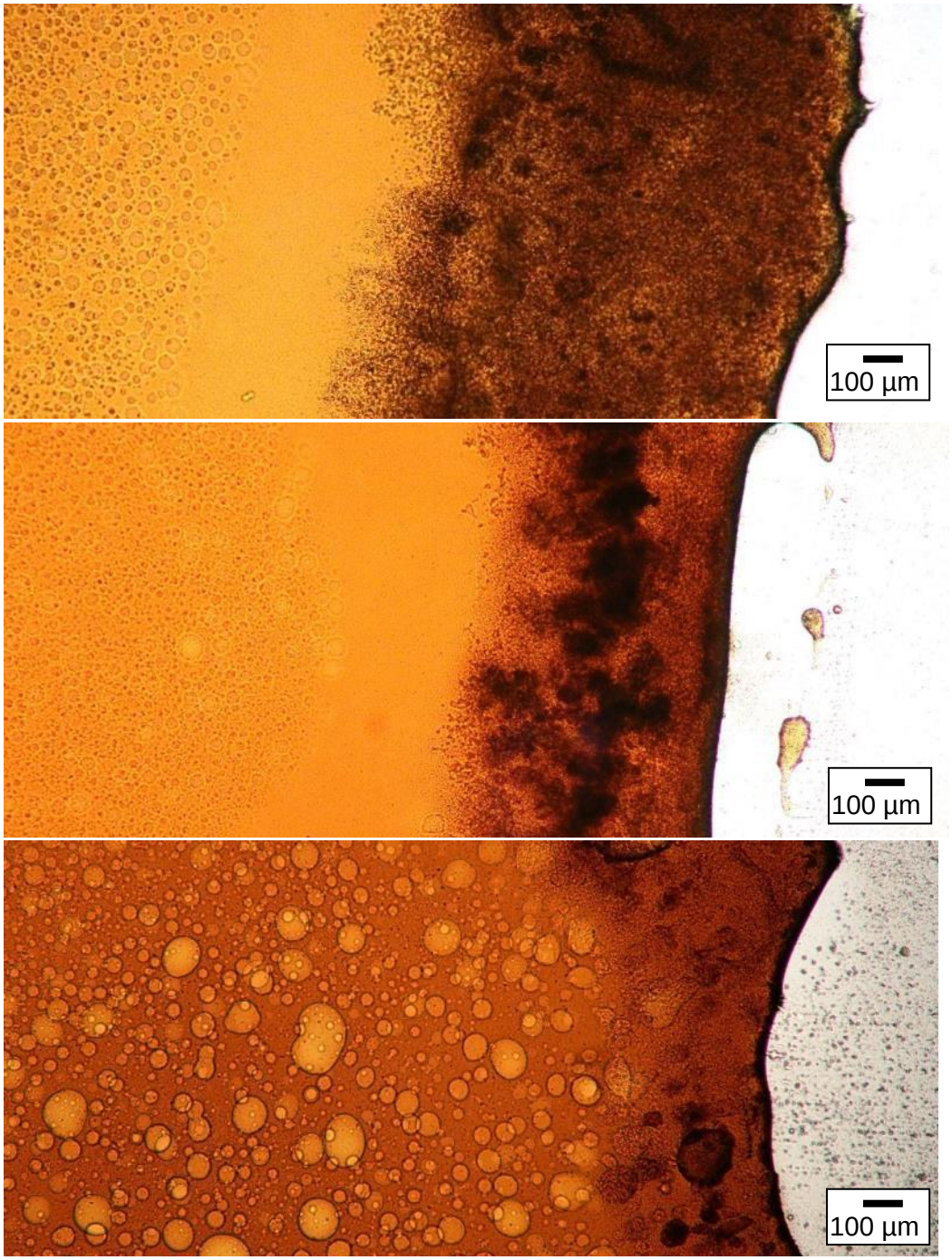

Figure C.7: Light microscopy images of water-into-oil emulsification at dispersant-treated oil-water interfaces, 60 min after oil-water contact. Dispersant-crude oil mixtures contained 10 wt% of the following dispersants: 60:40 L:T (top); 40:60 L:T (middle); 20:80 L:T (bottom). Translucent drops in the oil phase on the left side of each image are believed to be unsolubilized dispersant. These drops were not observed in the 10 wt% dispersant, 80:20 L:T dispersant-oil mixture in Figure 7, perhaps due to its low Tween 80 content, or in dispersant-oil mixtures containing <10 wt% dispersant.

C.4 Penetration of Dispersant-Laden Pendant Drop by Needle

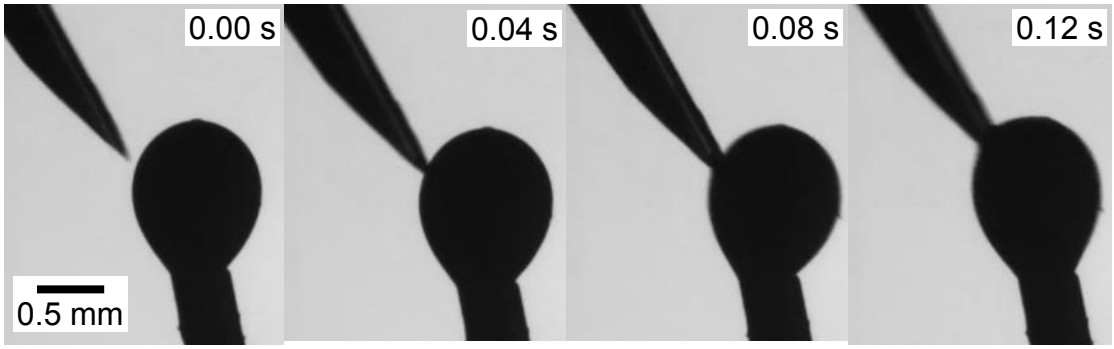

Figure C.8: Clean insertion of a needle into a ~0.25 μL pendant drop of dispersant-oil mixture in ~25 μL seawater, demonstrating the absence of an interfacial film resisting the needle. Images were recorded at 0.04 s intervals (25 frames per second). The droplet was allowed to equilibrate for 12 min after its formation, during which time its IFT continually declined due to ongoing surfactant adsorption at the oil-water interface. The dispersant-oil mixture contained 2.5 wt% dispersant and a 0:100 L:T ratio.